universität wien

MASTERARBEIT / MASTER'S THESIS

Titel der Masterarbeit / Title of the Master's Thesis

„Interfacial Behavior of Ring Polymer Solutions on Planar, Hard Walls“

verfasst von / submitted by

Iurii Chubak, BSc

angestrebter akademischer Grad / in partial fulfilment of the requirements for the degree of

Master of Science (MSc)

Wien, 2017 / Vienna, 2017

Studienkennzahl lt. Studienblatt / degree programme code as it appears on the student record sheet:	A 066 876
Studienrichtung lt. Studienblatt / degree programme as it appears on the student record sheet:	Masterstudium Physik
Betreut von / Supervisor:	Univ.-Prof. Dipl.-Ing. Dr. Christos N. Likos

Abstract

In this thesis, we investigate the depletion interaction between two planar, hard walls immersed in a solution of ring polymers. As a first step, we derived an effective interaction potential between the centers of mass of flexible, unknotted ring polymers and the hard wall. This effective potential approaches the scaling limit for relatively big rings with the degree of polymerization $N > 200$. Moreover, in the scaling regime, it can be modeled as a repulsive Yukawa potential in the region close to the wall and as a Gaussian at a distance greater than the gyration radius of the rings. Adopting the coarse-grained description of ring polymers as ultrasoft, penetrable spheres, we apply the mean-field density functional theory to examine ring polymer solutions in contact with one hard wall and confined between two parallel, hard walls. As a result, we demonstrate that even within the range of applicability of the effective model, the depletion potential between two hard walls features an oscillatory behavior intensifying with increasing concentration of the rings. Finally, the obtained form of the depletion interaction is shown to be qualitatively different in comparison to the linear polymer case.

Deutschsprachiger Abstract

Ziel dieser Masterarbeit ist die Bestimmung der Depletionswechselwirkung zwischen zwei planaren, harten Wänden, die in einer Ringpolymerlösung eingetaucht sind. Am Anfang haben wir das effektive Wechselwirkungspotential zwischen den Massenmittelpunkten der flexiblen, unverknoteten Ringpolymeren und der harten Wand berechnet. Dieses Potential nimmt eine universelle Form im Skalierungslimes für Werte des Polymerisationsgrads der Ringen im Bereich mit $N > 200$ an. Überdies kann es in diesem Limes durch ein Yukawa-Potential in der Nähe der Wand und eine Gaußfunktion für Abstände, die größer als die Gyrationsradius der Ringen sind, beschrieben werden. Danach modellieren wir die ringförmigen Polymeren als weiche, penetrierbare Kugeln und verwenden die Mittelfeld-Dichtefunktionaltheorie, um die Struktur der Ringpolymerlösungen, die in Kontakt mit einer harten Wand sind oder zwischen zwei Wänden eingesperrt sind, zu bestimmen. Als Endergebnis zeigen wir, dass das Depletionspotential zwischen zwei harten Wänden innerhalb des Geltungsbereichs des effekitven Modells über ein oszillierendes Verhalten, welches sich mit erhöhenden Konzentration der Ringen verstärkt, verfügt. Schließlich wird die Depletionswechselwirkung auch im Falle einer Linearpolymerlösung ausgerechnet, um ihren qualitativen Unterschied hervorzuheben.

Contents

Chapter 1

Introduction

A ring polymer is probably one of the simplest and, at the same time, one of the most outstanding examples of a macromolecule with a non-trivial topology [1, 2]. Its structural simplicity often serves as the main reason for using it as a "guinea pig" when investigating the influence of topology on soft condensed matter systems [3, 4, 5]. Besides that, the interest in ring polymer systems is considerably amplified by their biological relevance: many DNA and RNA molecules acquire a ring form when confined within eukaryotes or cells [6, 7]. Moreover, very recently a deficiency of circular RNAs in mammalian brain has been linked to its dysfunction [8].

From the physicists' point of view, ring polymers, in comparison to their linear counterparts, feature a series of distinctive static and dynamic properties [9]:

1) the effective interaction potential between two ring polymers in solution does not follow a Gaussian functional form [10, 11] and for short chains strongly depends on the topology of the rings [12];

2) ring polymer solutions have a different θ-point [13, 14];

3) melts of entangled ring polymers exhibit a power-law stress relaxation [15], which is exponential in the case of linear chains [16].

In this thesis, we will try to answer a different interesting question: *how do flexible ring polymers behave as depleting agents and how does this behavior differ from the linear polymer case?* In order to investigate ring polymer solutions, we will employ the mean-field density functional theory of the coarse-grained models of ring polymers. Although this approach works best in the dilute case, even in this regime, we will observe a dramatically different form of the depletion interactions induced by the rings, as compared to the linear chains. In particular, we will derive the effective interaction potential between the centers

of mass of ring polymers and a planar, hard wall and we will obtain the depletion potential between two hard walls immersed in a "sea" of ring polymers.

The thesis is organized as follows:

- In Chapter 2 and 3 we will consider a general statistical-mechanical theory underlying the coarse-graining approach of mixtures and macromolecules. Moreover, in Section 3.3 and 3.4 we will review the effective interactions of polymers of different architectures on hard walls and the effective interactions between ring polymers, respectively, that have been studied so far.

- In Chapter 4 we will explain how to perform Monte Carlo simulations of ring polymers correctly and how the effective pair potentials can be obtained from these simulations. Finally, the simulation results will be presented in Section 4.2 (in particular, the effective pair potential between the center of mass of the ring polymer and the hard wall as a function of the polymerization degree N).

- Finally, Chapter 5 contains density functional study of the ring and linear polymer solutions. We will consider homogeneous and inhomogeneous (in contact with one and two hard walls) polymer fluids and, as the main result, in both cases, we will obtain the surface tension at the wall-liquid interface and the depletion potential between two hard walls.

Chapter 2

Theoretical Basis of the Coarse-Graining Approach

In this chapter, we will discuss the general formalism underlying a *coarse-grained* description of a classical multi-component system in thermodynamic equilibrium, starting from its full many-body Hamiltonian. Although this procedure can be carried out analytically only in limited cases, a variety of computational techniques can be employed to derive an effective, single-component Hamiltonian which preserves the original thermodynamic properties.

In particular, we will focus on binary mixtures and apply the presented formalism to eliminate a component that evolves on significantly shorter length scales than the other. As a result, we will obtain a series representation for the effective potential, which takes the form of a sum of $n-$body interaction terms. As a specific example, we will consider the Asakura-Oosawa model of the colloid-polymer mixtures.

2.1 Statistical-mechanical considerations

In this section, primarily based on references [1] and [2], we will shortly describe the *bottom-up* strategy of coarse-graining a classical multi-component system, consisting in the elimination of irrelevant microscopic degrees of freedom from the full Hamiltonian of the system.

Let us start with a ν-component mixture comprised of $N = \sum_{\alpha=1}^{\nu} N_\alpha$ particles, whose Hamiltonian has the following form:

$$\mathcal{H} = \sum_{\alpha=1}^{\nu} \sum_{j=1}^{N_\alpha} \frac{\mathbf{p}_{j\alpha}^2}{2m_\alpha} + U\left(\{\mathbf{r}_\alpha\}\right), \tag{2.1}$$

where $\{\mathbf{r}_\alpha\}$ refers to the coordinates $\mathbf{r}_{1\alpha}, \mathbf{r}_{2\alpha}, \dots \mathbf{r}_{N_\alpha\alpha}$ of the particles of type α, $\{\mathbf{p}_\alpha\}$ refers to their momenta $\mathbf{p}_{1\alpha}, \mathbf{p}_{2\alpha}, \dots \mathbf{p}_{N_\alpha\alpha}$, m_α are the masses of each particle species, and $U(\{\mathbf{r}_\alpha\})$ stands for the total potential energy of the mixture. Also, from this point onwards we will denote the volume elements in the coordinate and momentum space as follows:

$$\begin{aligned} d\mathbf{r}_{1\alpha} d\mathbf{r}_{2\alpha} \cdots d\mathbf{r}_{N_\alpha\alpha} &= d\mathbf{r}_\alpha^{N_\alpha}, \quad \alpha = 1, 2, \dots, \nu, \\ d\mathbf{p}_{1\alpha} d\mathbf{p}_{2\alpha} \cdots d\mathbf{p}_{N_\alpha\alpha} &= d\mathbf{p}_\alpha^{N_\alpha}, \quad \alpha = 1, 2, \dots, \nu. \end{aligned} \tag{2.2}$$

First of all, the canonical partition function $Q(\{N_\alpha\}, V, T)$ of the system can be written as

$$Q(\{N_\alpha\}, V, T) = \mathrm{Tr}_1 \, \mathrm{Tr}_2 \cdots \mathrm{Tr}_\nu \left[\exp\left(-\beta \mathcal{H}\right)\right], \tag{2.3}$$

where $\beta = (k_B T)^{-1}$ is the inverse temperature with k_B denoting the Boltzmann's constant and the following shorthand for integrals over the phase space of α-type-particles has been introduced:

$$\mathrm{Tr}_\alpha = \frac{h^{-3N_\alpha}}{N_\alpha!} \int d\mathbf{p}_\alpha^{N_\alpha} \int d\mathbf{r}_\alpha^{N_\alpha}. \tag{2.4}$$

By performing integration in the momentum space, we arrive at the following expression:

$$Q\left(\{N_\alpha\}, V, T\right) = \left(\prod_{\alpha=1}^{\nu} \frac{\left(V \Lambda_\alpha^{-3}\right)^{N_\alpha}}{N_\alpha!} \right) Z\left(\{N_\alpha\}, V, T\right), \tag{2.5}$$

where $\Lambda_\alpha = h/\sqrt{2\pi m_\alpha k_B T}$ is the thermal de Broglie wavelength and $Z\left(\{N_\alpha\}, V, T\right)$ stands for the configuration integral

$$Z\left(\{N_\alpha\}, V, T\right) = \frac{1}{V^N} \int \prod_{\alpha=1}^{\nu} d\mathbf{r}_\alpha^{N_\alpha} \, \exp\left(-\beta U\right). \tag{2.6}$$

In order to coarse-grain the mixture on the given length scale, we might wish to trace out coordinates and momenta of several particle types in the Hamiltonian (2.1), while keeping the thermodynamics of the full system, given by the partition function (2.3), preserved. Let us assume that the main interest lies in the behavior of a particle type γ. In this case, the effective Hamiltonian $\mathcal{H}_{\text{eff}}$ is defined as follows:

$$\exp\left(-\beta \mathcal{H}_{\text{eff}}\right) = \prod_{\alpha \neq \gamma}^{\nu} \mathrm{Tr}_\alpha \, \exp\left(-\beta \mathcal{H}\right). \tag{2.7}$$

As a result, the coarse-grained mixture can be described with the help of the one-component Hamiltonian that depends only on the variables $\{\mathbf{r}_\gamma\}, \{\mathbf{p}_\gamma\}$:

$$\mathcal{H}_{\text{eff}} = \sum_{j=1}^{N_\gamma} \frac{\mathbf{p}_{j\gamma}^2}{2m_\gamma} + \tilde{U}_\gamma\left(\{\mathbf{r}_\gamma\}\right), \tag{2.8}$$

where the effective interaction potential $\tilde{U}_\gamma(\{\mathbf{r}_\gamma\})$ can be computed directly from (2.7) and reads as

$$\exp\left(-\beta\tilde{U}_\gamma(\{\mathbf{r}_\gamma\})\right) = \left(\prod_{\alpha\neq\gamma}^{\nu}\frac{\Lambda_\alpha^{-3N_\alpha}}{N_\alpha!}\right)\int\prod_{\alpha\neq\gamma}^{\nu}d\mathbf{r}_\alpha^{N_\alpha}\,\exp(-\beta U)\,. \tag{2.9}$$

The form of the effective Hamiltonian (2.7) assures that the partition function (2.3) is preserved and now it can be computed in the following way:

$$Q(\{N_\alpha\},V,T)\equiv Q(N_\gamma,V,T) = \frac{\Lambda_\gamma^{-3N_\gamma}}{N_\gamma!}\int d\mathbf{r}_\gamma^{N_\gamma}\,\exp\left(-\beta\tilde{U}_\gamma(\{\mathbf{r}_\gamma\})\right). \tag{2.10}$$

Furthermore, it is obvious that the expectation value of any observable $\mathcal{O}_\gamma$, which depends on the coordinates $\{\mathbf{r}_\gamma\}$ and momenta $\{\mathbf{p}_\gamma\}$ only, is invariant under the elimination of all particle types $\alpha\neq\gamma$:

$$\langle\mathcal{O}_\gamma\rangle = \frac{1}{Q}\prod_{\alpha\neq\gamma}^{\nu}\mathrm{Tr}_\alpha\left[\mathcal{O}_\gamma\exp(-\beta U)\right] = \frac{1}{Q}\,\mathrm{Tr}_\gamma\left[\mathcal{O}_\gamma\exp\left(-\beta\tilde{U}_\gamma\right)\right]. \tag{2.11}$$

So far we have formally defined the effective interaction potential (2.9), despite the fact that its general structure remains unknown. However, later on we will see that the potential $\tilde{U}_\gamma(\{\mathbf{r}_\gamma\})$ depends in general not only on the coordinates $\{\mathbf{r}_\gamma\}$ but also on thermodynamic variables of the eliminated components, which makes it sensitive to the composition of the system and, hence, tunable. On the other hand, having coarse-grained the "small" and "fast" components of the mixture, we landed on the length scales that are directly accessible to experimental observations, which makes the effective potential measurable [1].

Last, it is important to mention that the coarse-graining through (2.9) can rarely be accomplished analytically (otherwise the coarse-graining approach would represent only a redundant step in the calculation of the system's partition function and, therefore, its thermodynamic properties), so one has to employ different computational methods to obtain a decent approximation for the potential.

2.2 Coarse-graining a binary mixture

Without loss of generality we will now switch to studying two-component mixtures, where one of the constituents is considered to evolve on notably different length and time scales than the other. A standard colloidal suspension gives a good example of such kind of system: it contains mesoscopic particles dispersed into solvent molecules of atomic size, whose diffusion times can exceed that of colloids ($\tau_{\mathrm{col}}\sim\mu$s) in more than five orders of magnitude [1].

Let us start with a system composed of N_1 particle of type 1 and N_2 particles of type 2, assuming that particles of the second type are the "small" ones and therefore are to be traced out in the equation (2.7). In addition, the shorthands $\{\mathbf{R}\}, \{\mathbf{P}\}$ and $\{\mathbf{r}\}, \{\mathbf{p}\}$ stand for the sets of coordinates and momenta ($\mathbf{R}_1, \mathbf{R}_2, \ldots, \mathbf{R}_{N_1}$, etc.) of the large and small particles, respectively. With reference to (2.2), we write the volume elements

$$d\mathbf{R}_1 d\mathbf{R}_2 \cdots d\mathbf{R}_{N_1} = d\mathbf{R}^{N_1}, \quad d\mathbf{P}_1 d\mathbf{P}_2 \cdots d\mathbf{P}_{N_1} = d\mathbf{P}^{N_1}, \tag{2.12}$$

and equivalently for the "small" variables. Lastly, the many-body Hamiltonian (2.1) becomes now

$$\mathcal{H} = \sum_{j=1}^{N_1} \frac{\mathbf{P}_j^2}{2m_1} + \sum_{j=1}^{N_2} \frac{\mathbf{p}_j^2}{2m_2} + U_{11}\left(\{\mathbf{R}\}\right) + U_{22}\left(\{\mathbf{r}\}\right) + U_{12}\left(\{\mathbf{R}\}, \{\mathbf{r}\}\right), \tag{2.13}$$

where the intra- and interspecial interaction energies are given as the sums of pair potentials:

$$U_{11}\left(\{\mathbf{R}\}\right) = \sum_{i<j}^{N_1} u_{11}\left(|\mathbf{R}_i - \mathbf{R}_j|\right), \tag{2.14}$$

$$U_{22}\left(\{\mathbf{r}\}\right) = \sum_{i<j}^{N_2} u_{22}\left(|\mathbf{r}_i - \mathbf{r}_j|\right), \tag{2.15}$$

$$U_{12}\left(\{\mathbf{R}\}, \{\mathbf{r}\}\right) = \sum_{i=1}^{N_1} \sum_{j=1}^{N_2} u_{12}\left(|\mathbf{R}_i - \mathbf{r}_j|\right). \tag{2.16}$$

In order to obtain the effective one-component Hamiltonian (2.7), one has to integrate out the interaction energies $U_{22}\left(\{\mathbf{r}\}\right)$ and $U_{12}\left(\{\mathbf{R}\}, \{\mathbf{r}\}\right)$ in the partition function of the system. Dijkstra et al. [17] employed the cluster expansion method to reveal the general structure of the effective potential for arbitrary pair interactions u_{12}, u_{22} and in the following steps we will outline their considerations.

It is known that the cluster expansion is easier to perform in the grand canonical ensemble [18], thus from now onwards we will work in the semi-grand ensemble by fixing the second component's chemical potential μ_2. Furthermore, the semi-grand potential can be immediately written by means of the Legendre transformation

$$\Omega(N_1, \mu_2, V, T) = F(N_1, N_2, V, T) - \mu_2 N_2, \tag{2.17}$$

where $F(N_1, N_2, V, T)$ is the Helmholtz free energy. Most importantly, the partition function of the system $\Xi(N_1, \mu_2, V, T)$ becomes

$$\Xi(N_1, \mu_2, V, T) = \mathrm{Tr}_1 \left[\sum_{N_2=0}^{\infty} \frac{e^{\beta\mu_2 N_2}}{N_2!} \int d\mathbf{p}^{N_2} \int d\mathbf{r}^{N_2} \, \exp\left(-\beta\mathcal{H}\right) \right]. \tag{2.18}$$

Keeping the equation (2.7) in sight, we obtain the following form of the effective Hamiltonian:

$$\mathcal{H}_{\text{eff}} = \sum_{j=1}^{N_1} \frac{\mathbf{P}_j^2}{2m_1} + U_{11}\left(\{\mathbf{R}\}\right) + \tilde{U}_{11}\left(\{\mathbf{R}\}, \mu_2, V, T\right), \tag{2.19}$$

where the additional interaction term $\tilde{U}_{11}\left(\{\mathbf{R}\}, \mu_2, V, T\right)$ stems from the elimination of the small particles and reads as

$$\exp\left(-\beta\tilde{U}_{11}\left(\{\mathbf{R}\}, \mu_2, V, T\right)\right) = \sum_{N_2=0}^{\infty} \frac{z_2^{N_2}}{N_2!} \int d\mathbf{r}^{N_2} \exp\left(-\beta(U_{12} + U_{22})\right) \tag{2.20}$$

with z_2 denoting the fugacity

$$z_2 = \Lambda_2^{-3} \exp\left(\beta\mu_2\right). \tag{2.21}$$

The potential $\tilde{U}_{11}\left(\{\mathbf{R}\}, \mu_2, V, T\right)$ can be calculated explicitly by using the cluster expansion in terms of the Mayer functions f_{ij} and g_{kl}, which are defined as

$$f_{ij} = \exp\left(-\beta u_{12}(|\mathbf{R}_i - \mathbf{r}_j|)\right) - 1, \tag{2.22}$$

$$g_{kl} = \exp\left(-\beta u_{22}(|\mathbf{r}_k - \mathbf{r}_l|)\right) - 1. \tag{2.23}$$

In particular, the Boltzmann factors $\exp\left(-\beta U_{12}\right), \exp\left(-\beta U_{22}\right)$ for high enough temperatures can be expanded as follows:

$$\begin{aligned} \exp\left(-\beta U_{12}\right) &\equiv e^{-\beta\sum_{i,j} u_{12}} = \prod_{i,j}\left(1 + f_{ij}\right) = 1 + \sum_{i,j} f_{ij} + \sum_{i,j,n,m} f_{ij} f_{nm} + \cdots \\ \exp\left(-\beta U_{22}\right) &\equiv e^{-\beta\sum_{k<l} u_{22}} = \prod_{k<l}\left(1 + g_{kl}\right) = 1 + \sum_{k<l} g_{kl} + \sum_{k<l,r<s} g_{kl} g_{rs} + \cdots \end{aligned} \tag{2.24}$$

As a result, it can be shown [17] that $\tilde{U}_{11}$ has a series representation

$$\tilde{U}_{11}\left(\{\mathbf{R}\}, \mu_2, V, T\right) = \sum_{n=0}^{N_1} \tilde{U}_{11}^{(n)} \equiv \tilde{U}_{11}^{(0)} + \tilde{U}_{11}^{(1)} + \tilde{U}_{11}^{(2)} + \cdots + \tilde{U}_{11}^{(N_1)}, \tag{2.25}$$

where the index n denotes the number of many-body interactions between the particles of species 1 and 2.

The first term $\tilde{U}_{11}^{(0)}$ can be obtained directly from (2.20) by switching off the inter-special interaction U_{12}:

$$\exp\left(-\beta\tilde{U}_{11}^{(0)}\right) = \sum_{N_2=0}^{\infty} \frac{z_2^{N_2}}{N_2!} \int d\mathbf{r}^{N_2} \exp\left(-\beta U_{22}\right) \equiv \Xi_2\left(\mu_2, V, T\right), \tag{2.26}$$

where $\Xi_2\left(\mu_2, V, T\right)$ is exactly the grand-partition function of the second species, placed alone in a macroscopic volume V at fixed temperature T and chemical potential μ_2. Therefore, from the definition of the grand potential it follows that

$$\tilde{U}_{11}^{(0)} = -\beta^{-1} \ln\left(\Xi_2\left(\mu_2, V, T\right)\right) \equiv \Omega_2\left(\mu_2, V, T\right) = -V p_2\left(\mu_2, T\right), \tag{2.27}$$

with p_2 being the pressure of the second component under the above-mentioned conditions.

Secondly, the succeeding terms in the expansion (2.25) are connected to the averages of the quantities

$$U_{12}^{(n)}\left(\{\mathbf{R}\},\{\mathbf{r}\}\right)=\sum_{i=1}^{n}\sum_{j=1}^{N_2}u_{12}\left(|\mathbf{R}_i-\mathbf{r}_j|\right) \tag{2.28}$$

with respect to the grand canonical ensemble of the small particles alone. In particular, the one-body term $\tilde{U}_{11}^{(1)}$ can be written as

$$\tilde{U}_{11}^{(1)}=N_1\,\tilde{u}^{(1)}\left(\mu_2,T\right), \tag{2.29}$$

with $\tilde{u}^{(1)}$, in relation to (2.28), given by

$$\exp\left(-\beta\tilde{u}^{(1)}\left(\mu_2,T\right)\right)=\left\langle\exp\left(-\beta U_{12}^{(1)}\right)\right\rangle, \tag{2.30}$$

where the brackets $\langle\cdots\rangle$ denote averaging in the above-described grand-canonical ensemble:

$$\langle\cdots\rangle=\frac{1}{\Xi_2}\sum_{N_2=0}^{\infty}\frac{z_2^{N_2}}{N_2!}\int d\mathbf{r}^{N_2}\,\left(\cdots\right)\exp\left(-\beta U_{22}\right). \tag{2.31}$$

As one can easily see, the sum of the first two expansion terms

$$\tilde{U}_{11}^{(0)}+\tilde{U}_{11}^{(1)}=-Vp_2\left(\mu_2,T\right)+N_1\,\tilde{u}^{(1)}\left(\mu_2,T\right) \tag{2.32}$$

constitutes an extensive constant in the effective Hamiltonian (2.13) and does not depend on the coordinates $\{\mathbf{R}\}$ and momenta $\{\mathbf{P}\}$. Although this constant does not affect any expectation value of some observable $\mathcal{O}\left(\{\mathbf{R}\},\{\mathbf{P}\}\right)$, it cannot be regarded as unimportant. In general, this term contains a non-zero contribution to the system's total free energy that depends on the densities $\rho_1=N_1/V$ and $\rho_2=N_2/V$ and therefore may affect the common tangent construction used by the determination of the phase equilibrium [1].

Thirdly, the two-body term $\tilde{U}_{11}^{(2)}$ can be decomposed into pair interactions of the form

$$\tilde{U}_{11}^{(2)}=\sum_{i<j}^{N_1}\tilde{u}^{(2)}\left(|\mathbf{R}_i-\mathbf{R}_j|,\mu_2,T\right), \tag{2.33}$$

where, according to definitions (2.31) and (2.28),

$$\exp\left(-\beta\tilde{u}^{(2)}\left(|\mathbf{R}_i-\mathbf{R}_j|,\mu_2,T\right)\right)=\left\langle\exp\left(-\beta U_{12}^{(2)}\right)\right\rangle\cdot\left\langle\exp\left(-\beta U_{12}^{(1)}\right)\right\rangle^{-2}. \tag{2.34}$$

Last of all, the remaining sum $\tilde{U}_{11}^{(3)}+\cdots+\tilde{U}_{11}^{(N_1)}$ in the expansion (2.25) consists of triplet- and higher-order interactions, which however will not be included in the discussion, since the pair-potential approximation is assumed to break only at very high concentrations of macroscopic particles.

To sum up, the effective Hamiltonian (2.13) in the pair-potential approximation becomes

$$\mathcal{H}_{\text{eff}} = \mathcal{H}_0 + \sum_{j=1}^{N_1} \frac{\mathbf{P}_j^2}{2m_1} + U_{11}\left(\{\mathbf{R}\}\right) + \sum_{i<j}^{N_1} \tilde{u}^{(2)}\left(|\mathbf{R}_i - \mathbf{R}_j|, \mu_2, T\right), \tag{2.35}$$

with $\mathcal{H}_0$ denoting the extensive constant (2.32). Furthermore, the effective pair potential u_{eff} between the large particles in the coarse-grained description is given as

$$u_{\text{eff}}\left(|\mathbf{R}_i - \mathbf{R}_j|, \mu_2, T\right) = u_{11}\left(|\mathbf{R}_i - \mathbf{R}_j|\right) + \tilde{u}^{(2)}\left(|\mathbf{R}_i - \mathbf{R}_j|, \mu_2, T\right), \tag{2.36}$$

consisting of the direct intraspecial contribution u_{11} and the induced, *depletion* term $\tilde{u}^{(2)}$.

It is worth mentioning that the depletion interactions have a purely entropic origin. Using the equation (2.9) in the canonical ensemble, we write the effective pair potential u_{eff} as follows:

$$u_{\text{eff}}\left(|\mathbf{R}_i - \mathbf{R}_j|, N_2, T\right) = u_{11}\left(|\mathbf{R}_i - \mathbf{R}_j|\right) - \beta^{-1} \ln\left(\frac{Z_2(|\mathbf{R}_i - \mathbf{R}_j|)}{Z_2(\infty)}\right), \tag{2.37}$$

where $Z_2(R)$ denotes the configuration integral (2.6) for a system containing two large particles separated by a distance R that are immersed in a "sea" of N_2 small particles:

$$Z_2(R) = \frac{1}{V^{N_1+N_2}} \int d\mathbf{R}^{N_1} d\mathbf{r}^{N_2} \, \exp\left(-\beta(U_{12} + U_{22})\right) \delta\left(|\mathbf{R}_1 - \mathbf{R}_2| - R\right). \tag{2.38}$$

In other words, $Z_2(R)$ is simply equal to the number of available microstates for the given configuration and, hence, is connected to the entropy of the system with the relation $S_2(R) = k_B \ln Z_2(R)$. Finally, the effective pair potential can be recast as

$$u_{\text{eff}}\left(|\mathbf{R}_i - \mathbf{R}_j|, N_2, T\right) = u_{11}\left(|\mathbf{R}_i - \mathbf{R}_j|\right) - T\left(S_2(|\mathbf{R}_i - \mathbf{R}_j|) - S_2(\infty)\right), \tag{2.39}$$

which clearly emphasizes the entropic origin of the depletion term $\tilde{u}^{(2)}$.

2.3 The Asakura-Oosawa model

Nevertheless, the equations above provide only a formal structure of the effective Hamiltonian (2.13): in order to obtain the explicit form of the depletion potential $\tilde{u}^{(2)}$, one has to evaluate statistical averages (2.27), (2.34) with specific pair potentials u_{22}, u_{12}.

For instance, Dijkstra et al. [19] used this method to calculate the depletion interaction in the colloid-polymer mixture by means of the Asakura-Oosawa model. More specifically, the colloids interact via the hard sphere pair potential

$$u_{11}\left(|\mathbf{R}_i - \mathbf{R}_j|\right) = \begin{cases} \infty, & \text{for } |\mathbf{R}_i - \mathbf{R}_j| < \sigma_c, \\ 0, & \text{otherwise}, \end{cases} \tag{2.40}$$

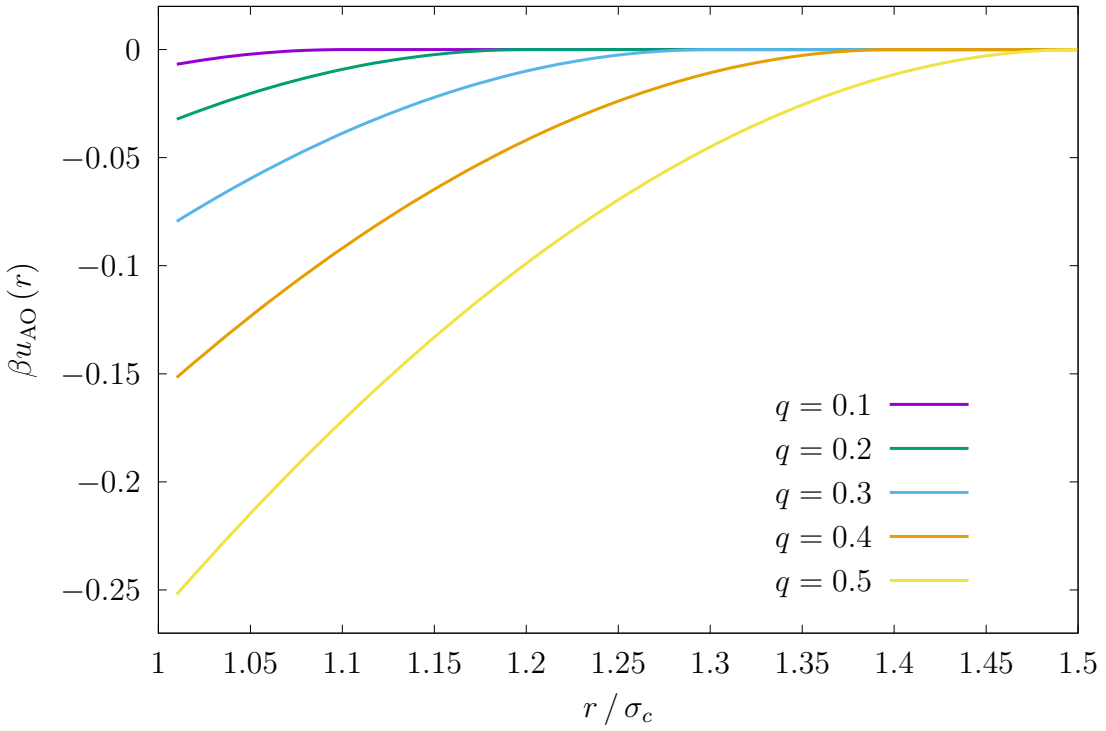

Figure 2.1: The polymer-colloid depletion potential in the Asakura-Oosawa model for various size ratios q with $z_2\sigma_c^3 = 1$.

where σ_c is the diameter of the colloids. On the other hand, the non-adsorbing polymer coils are modelled as non-interacting particles

$$u_{22}\left(|\mathbf{r}_i - \mathbf{r}_j|\right) = 0 \tag{2.41}$$

that are excluded from the colloids through

$$u_{12}\left(|\mathbf{R}_i - \mathbf{r}_j|\right) = \begin{cases} \infty, & \text{for } |\mathbf{R}_i - \mathbf{r}_j| < \frac{1}{2}(\sigma_c + \sigma_p), \\ 0, & \text{otherwise.} \end{cases} \tag{2.42}$$

where the diameter of the coil equals $\sigma_p = 2R_g$ with R_g denoting the gyration radius of the polymers.

As a result, the extensive constant $\mathcal{H}_0$ in the effective Hamiltonian (2.35) becomes

$$\mathcal{H}_0 = -\beta^{-1} z_2 \left(1 - \eta_1 (1+q)^3\right) V, \tag{2.43}$$

where $\eta_1 = (\pi/6)\,\sigma_c^3\, N_1/V$ stands for the colloid packing fraction, $q = \sigma_p/\sigma_c$ is the size ratio, and $z_2 = \Lambda_2^{-3} \exp(\beta\mu_2)$ denotes the fugacity of the polymers as if they did not interact with the colloid particles.

Most importantly, the depletion interaction in this model can be described exactly by the Asakura-Oosawa pair potential [20], which diverges for $r \leq \sigma_c$ and for $r > \sigma_c$ is given

by the following expression:

$$u_{\mathrm{AO}}\left(|\mathbf{R}_i-\mathbf{R}_j|\right)=\begin{cases}-\frac{\pi}{6}\,\beta^{-1}\sigma_p^3 z_2\,(1+q^{-1})^3\times & \\ \quad\times\left(1-\frac{3|\mathbf{R}_i-\mathbf{R}_j|}{2(1+q)\sigma_c}+\frac{|\mathbf{R}_i-\mathbf{R}_j|^3}{2(1+q)^3\sigma_c^3}\right), & \text{for } \sigma_c<|\mathbf{R}_i-\mathbf{R}_j|<\sigma_c+\sigma_p,\\ 0, & \text{for } |\mathbf{R}_i-\mathbf{R}_j|\geq\sigma_c+\sigma_p,\end{cases}$$

which is shown in Figure 2.1. Therefore, the effective pair potential between the colloids in this system is a sum of the hard-spheres and the Asakura-Oosawa interactions:

$$u_{\mathrm{eff}}\left(|\mathbf{R}_i-\mathbf{R}_j|,\mu_2,T\right)=u_{11}\left(|\mathbf{R}_i-\mathbf{R}_j|\right)+u_{\mathrm{AO}}\left(|\mathbf{R}_i-\mathbf{R}_j|,\mu_2,T\right). \tag{2.44}$$

In addition, let us note that the depletion term explicitly depends on the thermodynamic variables of the system: it is linear in temperature T and fugacity z_2. The quantity $\mathcal{H}_0/V$ is also linear in the colloid density ρ_1 and therefore affects the pressure of the colloid-polymer mixture, albeit leaving the phase equilibria unchanged [19].

Chapter 3

Coarse-Graining of Macromolecules

In this chapter, we will apply the general method of coarse-graining, developed in Chapter 2, for an entirely different purpose: instead of eliminating a whole particle species from the multicomponent Hamiltonian (2.1), we will average out most of the degrees of freedom of a single macromolecule in order to describe it with a much smaller number of effective coordinates. Most importantly, we aim to establish statistical relations that can be directly used in computer simulations. In what follows, we will use this approach to describe the effective interaction between a flexible ring polymer and a planar, hard wall, as a function of the distance of the center of mass of the polymer from the wall.

Last of all, in Section 3.3 we will provide a short review of the effective polymer-wall potentials that have been studied so far and in Section 3.4 we will review the effective interactions between the ring polymers.

3.1 Macromolecules subject to external fields

Let us consider a flexible, unknotted ring polymer containing N monomers, whose positions and momenta are given by the set of vectors $\{\mathbf{r}\} = \mathbf{r}_1, \mathbf{r}_2, \ldots \mathbf{r}_N$ and $\{\mathbf{p}\} = \mathbf{p}_1, \mathbf{p}_2, \ldots \mathbf{p}_N$, respectively, in the presence of a hard wall placed at $z = 0$.

The canonical partition function of this system can be expressed as

$$Q\left(N, V, T\right) = \frac{h^{-N}}{N!} \int d\mathbf{p}^N d\mathbf{r}^N \, \exp\left(-\beta \mathcal{H}\right), \tag{3.1}$$

where by default we assume that Q is topologically faithful. In other words, Q sums only over those configurations that correspond to the unknotted ring topology. Formally, it can be achieved by writing the Hamiltonian of this system $\mathcal{H}$ as follows:

$$\mathcal{H} = \sum_{i=1}^{N} \frac{\mathbf{p}_i^2}{2m} + U_{\mathrm{mm}}\left(\{\mathbf{r}\}\right) + U_{\mathrm{top}}\left(\{\mathbf{r}\}\right) + \sum_{i=1}^{N} U_{\mathrm{ext}}(\mathbf{r}_i), \tag{3.2}$$

where $U_{\mathrm{mm}}(\{\mathbf{r}\})$ denotes the monomer-monomer potential energy comprised of the bond and excluded volume interactions, $U_{\mathrm{top}}(\{\mathbf{r}\})$ stands for the formal "topological" potential

$$U_{\mathrm{top}}(\{\mathbf{r}\}) = \begin{cases} 0, & \text{for unknotted rings,} \\ +\infty, & \text{otherwise.} \end{cases} \tag{3.3}$$

Moreover, the monomer-wall interactions are set to

$$U_{\mathrm{ext}}(\mathbf{r}_i) = \begin{cases} +\infty, & \text{for } z_i \leq 0, \\ 0, & \text{otherwise.} \end{cases} \tag{3.4}$$

Finally, it should be noted that the system under consideration is already treated on a coarse-grained level: we assume that the ring polymers are immersed in a solvent which acts as a thermal bath and whose quality may have a direct influence on the inter-monomer interactions. Consequently, the solvent is included implicitly by adjusting the excluded volume part of the U_{mm} potential, which is purely repulsive in the case of a good solvent [21].

Now, by carrying out integrals in the momentum space, the partition function (3.1) can be recast as:

$$Q(N,V,T) = \frac{\left(V\Lambda^{-3}\right)^N}{N!} Z(N,V,T), \tag{3.5}$$

where Z is the configuration integral

$$Z(N,V,T) = \frac{1}{V^N} \int d\mathbf{r}_1 d\mathbf{r}_2 \cdots d\mathbf{r}_N \, \exp\left(-\beta U(\mathbf{r}_1, \mathbf{r}_2, \ldots, \mathbf{r}_N)\right) \tag{3.6}$$

and $U(\mathbf{r}_1, \mathbf{r}_2, \ldots, \mathbf{r}_N)$ denotes the total potential energy of our system.

The configuration integral Z is the key quantity in establishing a practical relation that can be directly utilized in Monte Carlo (MC) simulations. In order to eliminate all the degrees of freedom of a polymer except the position of its center of mass, let us consider its configuration integral with $\mathbf{r}_{\mathrm{cm}}$ fixed at a position $\mathbf{s}$:

$$Z(s_z) = \frac{1}{V^N} \int d\mathbf{r}^N \, \exp\left(-\beta U(\{\mathbf{r}\})\right) \delta\left(\mathbf{s} - \frac{1}{N}\sum_{i=1}^{N} \mathbf{r}_i\right), \tag{3.7}$$

where the expression above explicitly depends only on the s_z coordinate due to the symmetry of our problem (indeed, U_{ext} is a function of the $z_1, \cdots, z_N$ coordinates only, thereby breaking translational symmetry of the system in the $z-$direction). Moreover, additional dependence of (3.7) on thermodynamic variables has been omitted to facilitate writing.

Therefore, the probability density $p(z)$ of observing the polymer's center of mass at the distance z away from the wall by its construction is directly proportional to $Z(z)$ (to

avoid possible confusion, we again stress that in our case p depends on the z-component of the center of mass position only):

$$p(z) \;\propto\; Z(z). \tag{3.8}$$

Consequently, the effective interaction potential between the polymer and the wall can be defined as the work needed to move its center of mass from infinite separation to the distance z in front of the wall (equivalently, as the 'potential of mean force' [22]):

$$U_{\text{eff}}(z) = \int_{+\infty}^{z} d\mathbf{s} \cdot \Big\langle \nabla_{\mathbf{s}} U \Big\rangle, \tag{3.9}$$

where we average over those configurations that correspond to the $\mathbf{r}_{\text{cm}} = \frac{1}{N}\sum_{i=1}^{N} \mathbf{r}_i$ fixed at $\mathbf{s}$. To obtain $U_{\text{eff}}(z)$, let us consider the averaged force acting on the center of mass:

$$-\Big\langle \nabla_{\mathbf{s}} U \Big\rangle = -\frac{\displaystyle\int d\mathbf{r}^N \, \exp\left(-\beta U\right) \delta\left(\mathbf{s} - \tfrac{1}{N}\textstyle\sum_{i=1}^{N} \mathbf{r}_i\right) \Big(\nabla_{\mathbf{s}} U\Big)}{\displaystyle\int d\mathbf{r}^N \, \exp\left(-\beta U\right) \delta\left(\mathbf{s} - \tfrac{1}{N}\textstyle\sum_{i=1}^{N} \mathbf{r}_i\right)}. \tag{3.10}$$

Now, using the property of the Dirac delta function that

$$\nabla_{\mathbf{s}}\, \delta(\mathbf{s} - \mathbf{a}) = -\nabla_{\mathbf{a}}\, \delta(\mathbf{s} - \mathbf{a}) \tag{3.11}$$

and integrating by parts, it can be shown that the gradient $\nabla_{\mathbf{s}}$ can be pulled out of the integral in the numerator of the expression (3.10). Indeed,

$$\begin{aligned}
&\nabla_{\mathbf{s}} \int d\mathbf{r}^N \, \exp\left(-\beta U\right) \delta\left(\mathbf{s} - \frac{1}{N}\textstyle\sum_{i=1}^{N} \mathbf{r}_i\right) \\
&= \int d\mathbf{r}^N \, \exp\left(-\beta U\right) \left[\nabla_{\mathbf{s}} \delta\left(\mathbf{s} - \frac{1}{N}\textstyle\sum_{i=1}^{N} \mathbf{r}_i\right)\right] \\
&= \int d\mathbf{r}^N \, \left[\left(\frac{1}{N}\textstyle\sum_{i=1}^{N} \nabla_i\right) \exp\left(-\beta U\right)\right] \delta\left(\mathbf{s} - \frac{1}{N}\textstyle\sum_{i=1}^{N} \mathbf{r}_i\right) \\
&= \int d\mathbf{r}^N \, \left(-\beta \nabla_{\mathbf{s}} U\right) \exp\left(-\beta U\right) \delta\left(\mathbf{s} - \frac{1}{N}\textstyle\sum_{i=1}^{N} \mathbf{r}_i\right).
\end{aligned} \tag{3.12}$$

Thus,

$$\begin{aligned}
-\Big\langle \nabla_{\mathbf{s}} U \Big\rangle &= \beta^{-1} \nabla_{\mathbf{s}} \ln \left[\int d\mathbf{r}^N \, \exp\left(-\beta U\right) \delta\left(\mathbf{s} - \frac{1}{N}\sum_{i=1}^{N} \mathbf{r}_i\right)\right] \\
&= \beta^{-1} \nabla_{\mathbf{s}} \ln \Big[V^N Z(s_z)\Big],
\end{aligned} \tag{3.13}$$

where in the last step we use the definition of $Z(s_z)$ (3.7). Therefore, the effective potential (3.9) becomes

$$U_{\text{eff}}(z) = -\beta^{-1} \int_{+\infty}^{z} ds_z \left(\frac{\partial}{\partial s_z} \ln \Big[V^N Z(s_z)\Big]\right) = -\beta^{-1} \ln\left(\frac{Z(z)}{Z(z \to \infty)}\right), \tag{3.14}$$

where $Z(z \to \infty)$ stands for the configuration integral of the polymer in the absence of the hard wall. Finally, the distribution function $P_{\text{wall}}(z)$ can be defined as the ratio:

$$P_{\text{wall}}(z) = \frac{Z(z)}{Z(z \to \infty)} \equiv \frac{p(z)}{p_{\text{id}}(z)}, \tag{3.15}$$

with $p(z)$ and $p_{\text{id}}(z)$ denoting the probability densities of observing the ring centered at z in the presence and absence of the wall. Moreover, according to definition (3.15), we see that $P_{\text{wall}}(z)$ in normalized in the following way:

$$P_{\text{wall}}(z \to \infty) = 1. \tag{3.16}$$

It is worth emphasizing that the distribution function $P_{\text{wall}}(z; \beta, \rho)$ depends in general on the inverse temperature β and the density $\rho = N/V$. More precisely, the definitions above are valid only for an infinitely diluted system (only one molecule subject to an external field), thus

$$\exp\left(-\beta U_{\text{eff}}(z)\right) = \lim_{\rho \to 0} P_{\text{wall}}(z; \beta, \rho), \tag{3.17}$$

Obviously, the aforementioned approximation is valid up to some density ρ^* of the system. Beyond that point, discrepancies between the coarse-grained and the full description of the system are too significant to be neglected.

To sum up, the equation (3.17) provides a direct method of obtaining effective potentials using MC simulations: first, we measure the probability of finding the center of mass of the ring at a distance z away from the wall, then we normalize it (3.16) to get the distribution function $P_{\text{wall}}(z; \rho \to 0)$, whose logarithm is proportional to $U_{\text{eff}}(z)$.

3.2 Effective pair potentials between two molecular aggregates

Up to this point, we have examined a complex system interacting with an external field and, in order to coarse-grain it, the field has been coupled only to certain 'effective' degrees of freedom of this system. The presence of external fields breaks translational symmetry of the system and conditions its inhomogeneity. More precisely, the single-particle density defined as

$$\rho^{(1)}(\mathbf{r}) = \left\langle \sum_{i=1}^{N} \delta(\mathbf{r} - \mathbf{r}_i) \right\rangle \neq \text{const} \tag{3.18}$$

is not constant (averaging in the equation above is performed in the canonical ensemble) and the distribution functions of type (3.15), as a consequence, also vary in space.

Furthermore, with a small modification, the method described in this section can be applied to homogeneous systems (that is, in the absence of any external fields) with

$$\rho^{(1)}(\mathbf{r}) = \left\langle \sum_{i=1}^{N} \delta(\mathbf{r} - \mathbf{r}_i) \right\rangle = \frac{N}{V} = \text{const.} \tag{3.19}$$

For instance, such a situation occurs when one aims to calculate effective pair potentials between two complex sub-parts of the whole system (e.g., between two ring polymers). In this case, the effective pair potential $u_{\text{eff}}(r)$ can be defined as follows [2]:

$$u_{\text{eff}}(r) = -\beta^{-1} \ln \left(\frac{Z_2(r)}{Z_2(r \to \infty)} \right) = -\beta^{-1} \ln \left(\frac{Z_2(r)}{Z_1^2} \right), \tag{3.20}$$

where $Z_2(r)$ denotes the configuration integral for two molecular aggregates with centers separated by a distance r, which in the limit $r \to \infty$ gives $Z_2(r \to \infty) = Z_1^2$ with Z_1 yielding the configuration integral of a single free object centered at some fixed point in space. Therefore, with respect to (3.15), we obtain that

$$\exp\left(-\beta u_{\text{eff}}(r)\right) = \frac{p(\mathbf{r})}{p_{\text{id}}(\mathbf{r})} \equiv g(r), \tag{3.21}$$

where $g(r)$ is nothing else as the radial distribution function of the centers of only two molecular objects in some fixed volume V. Moreover, $p(\mathbf{r})$ denotes the probability density of finding these centers separated by $\mathbf{r}$ and $p_{\text{id}}(\mathbf{r})$ stands for the probability density of finding a single free molecule centered at the point $\mathbf{r}$. Therefore, it holds that

$$g(r \to \infty) = 1. \tag{3.22}$$

In addition, we emphasize the dependence of $g(r; \beta, \rho)$ on the inverse temperature β and density $\rho = N/V$ and note that the approximations made are valid only in the infinitely diluted limit (only two objects in the system interact with each other) up to some density ρ^* of the system:

$$\exp\left(-\beta u_{\text{eff}}(r)\right) = \lim_{\rho \to 0} g(r; \beta, \rho). \tag{3.23}$$

3.3 Effective interactions of polymers on hard walls: a review

We present a short review of the effective interactions of polymers of different architectures on hard walls. This problem naturally arises in the coarse-grained description of the colloid-polymer mixtures, since the effective potential between the center of mass (CM)

of the polymer (or any other chosen effective coordinate) and the hard wall approximates with good precision the effective interaction of polymers on hard, spherical colloids in the limit of small size ratios

$$q = \sigma_p \,/\, \sigma_c, \qquad (\text{typically, } q = 0.1 \div 0.5)\,, \tag{3.24}$$

where $\sigma_p = 2R_g$ and R_g here and in the following stands for the gyration radius of the polymers at infinite dilution. In general, the effective polymer-wall potential allows to model polymer fluids in complex geometries given that the curvature is not much larger than R_g^{-1}.

Louis et al. [23] studied the effective wall-linear polymer CM interaction $\beta U(z)$ as well as the effective pair potential $\beta u(r)$ between the centers of mass of two linear polymers for finite concentrations (in the dilute and semidilute regimes) employing the self-avoiding walks model (SAW) for polymers in good solvent conditions. In particular, the pair distribution function $g(r)$ of the center of mass was measured for different bulk densities ρ and the effective pair potential $\beta u(r)$ was obtained from the hypernetted-chain (HNC) approximation closure relation:

$$g(r) = \exp\left(-\beta u(r) + g(r) - c(r) - 1\right), \tag{3.25}$$

where the direct pair correlation function $c(r)$ can be calculated from $g(r)$ using the Ornstein-Zernike (OZ) relation [24]:

$$h(r) = c(r) + \rho \int d\mathbf{r}'\, h(r')c\left(|\mathbf{r} - \mathbf{r}'|\right), \tag{3.26}$$

with $h(r) = g(r) - 1$. As a result, they confirmed that the effective pair potential between the centers of mass of two linear polymers follows the well-known Gaussian curve $\beta u(r) \sim \exp\left(-\alpha(r/R_g)^2\right)$. Moreover, they found that the effective potentials computed for various polymer densities in the system do not differ strongly and therefore the approximation for the potential in the $\rho \to 0$ limit is reasonable at finite concentrations.

Consequently, the effective chain-wall potential $\beta U(z)$ was computed in a similar way using

$$\beta U(z) = -\ln\left(\rho(z)/\rho\right) + \int d\mathbf{r}'\, \left(\rho(z) - \rho\right)c\left(|\mathbf{r} - \mathbf{r}'|\right), \tag{3.27}$$

where $\rho(z)$ is the density profile of the system in the presence of the hard wall, ρ denotes the bulk density of the polymers, and $c(r)$ is exactly the bulk direct correlation function between the centers of mass of the polymers. Note that the first term in (3.27) is the potential of the mean force corresponding to the $\rho \to 0$ limit, while the second one stems from the additional correlations between polymers close to the wall. Finally, they found

that $\beta U(z)$ is more sensitive to the polymer concentration in comparison to $\beta u(r)$ and that its range increases with increasing concentration. Further studies [25], [26] suggested the Yukawa form for the effective chain-wall potential:

$$\beta U_{\mathrm{cw}}(z) = \begin{cases} \infty, & \text{for } z \leq 0, \\ A \dfrac{\exp\left(-z/R_g\right)}{z/R_g}, & \text{for } z > 0. \end{cases} \tag{3.28}$$

The effective interaction of star polymers in a good solvent on hard walls was investigated by Jusufi et al. [27]. Particularly, using the radial dependence of the osmotic pressure within a star, they found the effective star-wall potential as a function of the distance z from the center of the star to the wall:

$$\beta U_{\mathrm{sw}}(z) = \Lambda f^{3/2} \begin{cases} -\ln\left(z/R_s\right) - \left(z^2/R_s^2 - 1\right)\left(\xi - 1/2\right) + \zeta, & \text{for } z \leq R_s, \\ \zeta \mathrm{erfc}(\kappa z)/\mathrm{erfc}(\kappa R_s), & \text{for } z > R_s. \end{cases} \tag{3.29}$$

where f denotes star functionality, R_s stands for its corona radius (i.e., the distance from the center up to which the monomer density profile $\rho(s)$ scales according to the Daoud-Cotton theory of multiarm stars [28]: $\rho(s) \sim \sigma^{-3}(s/\sigma)^{-4/3}(v/\sigma^3)^{-1/3} f^{2/3}$ with σ being the monomer size and v standing for the excluded volume parameter). Furthermore, Λ is a constant of order unity, κ is another constant of the order of R_g^{-1}, and ξ, ζ are given by the following expressions:

$$\xi = \frac{1}{1 + 2\kappa^2 R_s^2}, \quad \zeta = \frac{\sqrt{\pi}\xi}{\kappa R_s} \mathrm{erfc}(\kappa R_s) e^{\kappa^2 R_s^2}, \tag{3.30}$$

where $\mathrm{erfc}(x) = 1 - \mathrm{erf}(x)$ is the complementary error function and the error function is defined as $\mathrm{erf}(x) = 2/\sqrt{\pi} \int_0^x e^{-t^2} dt$.

Also, an analytic expression for the effective potential between a star and a hard, colloidal particle was found by integrating the osmotic pressure exerted by the star on the colloid [27]. Moreover, the validity of the effective star-colloid, as well as the star-wall (3.30) potentials, was confirmed with the help of molecular dynamics simulations [27].

Finally, it is worthwhile to note that the potential (3.30) in the case with $f = 2$ describes the effective chain-wall interaction. This example illustrates the consequence of the choice of the effective coordinate in the coarse-graining procedure: if z stands for the distance between the *center* of the linear polymer and the wall, then the effective potential $\beta U_{\mathrm{cw}}(z)$ scales as $\sim \ln\left(z^{-1}\right)$ for small distances z (3.30). On the other hand, if z is the distance between the *center of mass* of the chain and the wall, then $\beta U_{\mathrm{cw}}(z) \sim z^{-1}$ for small z. Therefore, the form of the effective potential, as well as its complexity, depends on the chosen 'effective' coordinate and may be simplified by a suitable choice of the latter one.

3.4 Effective interactions of ring polymers: a review

Here, we provide a short review of the effective interaction between ring polymers in solution compared to their linear counterparts.

First of all, we remind that the effective pair potential between two linear polymers in solution under very good (athermal) solvent conditions has the Gaussian functional form

$$\beta u(r) = \epsilon \exp\left(-\left(r/\sigma\right)^2\right), \tag{3.31}$$

where r denotes the distance between the centers of mass of two linear chains, ϵ sets the interaction strength and was found to be $\epsilon \equiv \beta u(r=0) \cong 2.4$ (for two polymers with $N = 100$) in off-lattice models [11], σ sets the length scale of the system and is of the order of R_g. Moreover, such form of the potential (3.31) was confirmed by numerous computer simulations [11, 29, 23, 27, 30, 31], as well as by renormalization-group calculations [32].

In contrast, there are two striking features that distinguish the effective interaction between the centers of mass of two ring polymers in solution under good solvent conditions [14, 12, 9, 33]:

(1) $\beta u(r)$ follows a non-Gaussian profile, which has a 'plateau' at short center-of-mass separations in the scaling regime.

(2) $\beta u(r)$ between two ring polymers strongly depends on their topology for smaller degrees of polymerization N. Furthermore, for knotted (e.g., with trefoil or pentafoil topology) rings it seems to attain a universal functional form for much larger values of N in comparison to unknotted rings.

In particular, the effective interaction between unknotted ring polymers, as well as between rings with trefoil and pentafoil topology, has been recently studied by Narros et al. [11]. It has been shown that the pair potential between the centers of mass of two unknotted ring reaches a universal shape already for $N \gtrsim 70$. This potential has a flat region for $r \lesssim 0.5R_g$ (even attains a minimum at $r = 0$ for smaller polymerization degrees $N \lesssim 70$) with characteristic value $\beta u(r=0) \cong 6$ and for $r \gtrsim 0.5R_g$ decays to zero, which is located at about $r \cong 3R_g$. The effective pair potentials between knotted rings $\beta u(r;\, \tau_1, N_1, \tau_2, N_2)$ (index $\tau = 0_1, 3_1, 5_1$, etc. denotes the ring's topology in the Conway notation) have been found to have not only larger amplitudes, but also distinct shapes in comparison to unknotted rings. However, the pair potential $\beta u(r;\, 0_1, N_1, 3_1, N_2)$ has been shown to converge to a functional form very similar to that of unknotted ring already for $N_1 = N_2 = 100$ [9]. Moreover, the effective interaction between two trefoil rings $\beta u(r;\, 3_1, N_1, 3_1, N_2)$ seems to approach the same above-mentioned shape for $N_1, N_2 > 200$

[12]. Seemingly, all of the effective potentials $\beta u(r;\, \tau_1, N_1, \tau_2, N_2)$ converge to a universal curve for large enough values of the polymerization degrees N_1, N_2.

The following mechanism underlies the effective interaction between the centers of mass of two rings at small inter-center distances [11, 9]: one of the rings enlarges, whereas the other one becomes smaller and penetrates the first, thereby approaching its center of mass closer. Therefore, the conformations of rings in such configuration is very different from those in the free case. Moreover, both rings can be represented as fully penetrable ultrasoft particles with radii $R_> = R_1/R_g$, $R_< = R_2/R_g$, where $R_1 > R_2$, and one can even formulate a mean-field theory of the effective interaction between them in the scaling limit [9]. Particularly, the effective pair potential with correct scaling behavior can be written (neglecting the prefactors of order unity that scale as N^0) as follows [9]:

$$\beta u(r) \propto (f_> * f_<)(r), \tag{3.32}$$

where '$*$' denotes the convolution operation and $f_>$, $f_<$ are dimensionless shape functions, corresponding to the ring with larger and smaller size, respectively (in the case of linear chains, f is a Gaussian function). Narros et al. [9] have modeled the shape profiles as step functions of the following form:

$$f_\gamma(r) = \frac{3}{4\pi}\,\theta\left(1 - \frac{r/R_g}{R_\gamma}\right), \tag{3.33}$$

where γ is $>$ or $<$. The resulting effective potential accurately describes the simulation data and reads as (in the following, r is given in units of R_g)

$$\beta u(r) = U_0 \begin{cases} \frac{4\pi}{3} R_<^3, & \text{for } 0 \le r < R_-, \\ \frac{\pi}{12r}(r^2 + 2R_+ r - 3R_-^2)(R_+ - r)^2, & \text{for } R_- \le r < R_+, \\ 0, & \text{for } r \ge R_+, \end{cases} \tag{3.34}$$

where $R_\pm = R_> \pm R_<$ and all of the parameters in the expression (3.34) have the following numeric values:

$$U_0 = 1.434, \quad R_> = 1.419, \quad R_< = 1.000, \quad R_+ = 2.419, \quad R_- = 0.419. \tag{3.35}$$

In the forthcoming Chapter 4, we will employ density functional theory (DFT) to study ring polymer solutions in contact with planar, hard walls using the above-described picture of ring polymers as 'ultrasoft colloids' interacting via (3.34). Therefore, it is important to understand the limit of applicability of the coarse-grained model. Narros et al. [11] have performed the comparison between the radial distribution function $g(r)$ obtained from the coarse-grained and the monomer-resolved simulations at different bulk densities

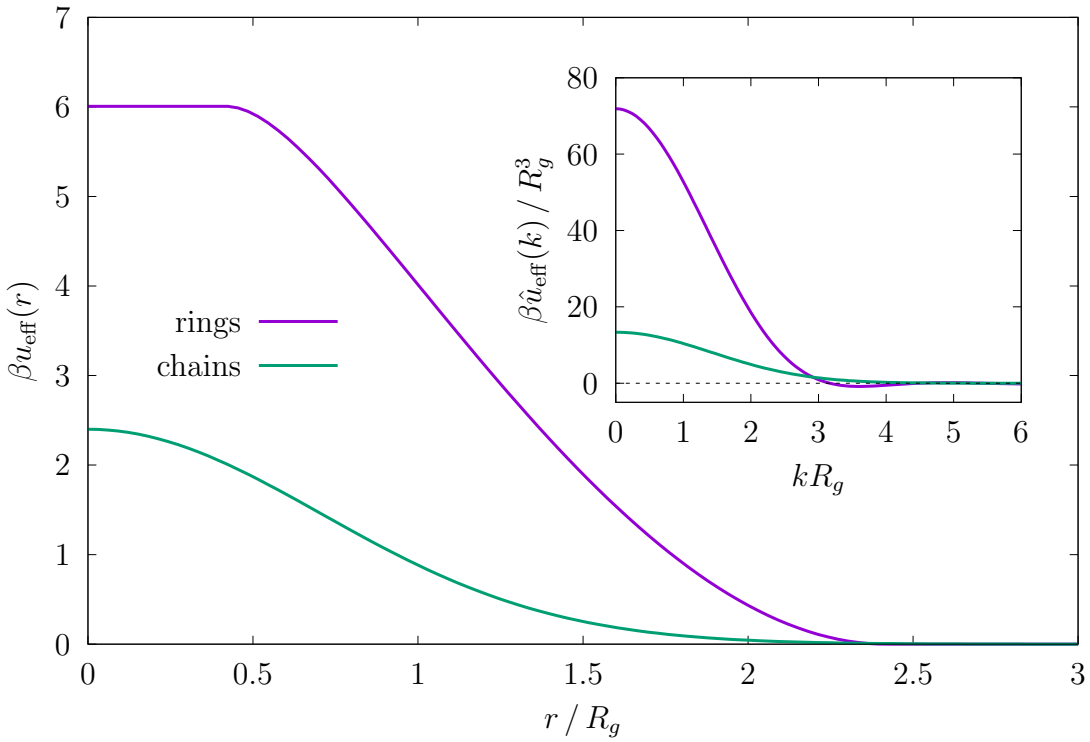

Figure 3.1: The effective pair potentials between polymers of different architecture in the scaling regime. Inset: the Fourier transforms $\beta\hat{u}(k)$ of the potentials. In the case of ring polymers, the Fourier transform of the effective potential attains a minimal negative value $\beta\hat{u}_{\rm min} \approx -0.84R_g^3$.

ρ. As a result, they have found that the approximation (3.34) is in good agreement with the monomer-resolved simulation up to the bulk density

$$\rho^\star R_{g,0}^3 \approx 0.2, \tag{3.36}$$

where we explicitly emphasize the value of the gyration radius in the $\rho \to 0$ limit.

Last of all, it is worth mentioning some consequences of the form of the effective pair potential (3.4) between ring polymers for the thermodynamic properties of ring polymer solutions. More specifically, the Fourier transform of $\beta u(r; \rho \to 0)$ (3.34) contains negative components (as shown in Figure 3.1), which causes the formation of clusters at high enough densities [34] of the ring polymer fluid. However, the clustering scenario has not been reproduced in the monomer-resolved simulations of flexible ring polymers at semidilute concentrations [11] due to growing many-body effects leading to substantial deviations of the effective pair potential $\beta u(r; \rho)$ from the expression (3.4) $\beta u(r; \rho \to 0)$ at infinite dilution.

This fact has encouraged the study of *semiflexible* ring polymers [35, 36, 37], which have an additional stiffness that prevents from shrinking of molecules at higher densities. The interring stiffness can be introduced using a bending potential of the following form

[35]:

$$U_{\text{bend}}(\theta) = \epsilon\kappa_{\text{bend}}(1 - \cos\theta)^2, \tag{3.37}$$

where θ is the angle between two neighboring bonds and κ_{bend} is the bending constant (typically, $\kappa_{\text{bend}} = 30$). Interestingly, the effective pair potentials between semiflexible rings also have a flat region for small center-of-mass separations, although their amplitude is smaller in comparison to flexible rings (e.g., $\beta u(r = 0) \leq 2$ for $N = 100$). Moreover, the Fourier transform of $\beta u_{\text{eff}}(r)$ between semiflexible ring also contains negative components and therefore leads to cluster formation at high enough densities. Finally, this phenomenon has been confirmed with the coarse-grained, as well as with the monomer-resolved simulations [35].

Chapter 4

Coarse-Graining of Ring Polymers on Planar, Hard Walls

We study, by means of Monte Carlo simulations, the effective interaction between flexible, unknotted ring polymers and planar, hard walls. More specifically, the effective potential is calculated from a distribution function $P_{\text{wall}}(z)$ which yields a properly normalized probability of finding the center of mass of the ring polymer at a distance z away from the wall placed at $z = 0$. A detailed description of the employed numerical methods will be provided in Section 4.1. The obtained results will be presented and discussed in Section 4.2.

4.1 Simulation details

In this section, we will present a detailed description of the employed simulation model. Furthermore, conservation of the topology of ring polymers in MC simulations 4.1.2 and crankshaft MC moves 4.1.3 will be discussed in depth.

4.1.1 The monomer-resolved model

To begin with, we perform a standard off-lattice Monte Carlo simulation of ring polymers in the presence of a planar, hard wall in the 'zero-density' limit $\rho \to 0$.

The excluded volume interactions of the monomers are modeled through the truncated and shifted Lennard-Jones (LJ) potential:

$$u_{\text{mm}}(r) = \begin{cases} 4\epsilon \left[\left(\frac{\sigma}{r}\right)^{12} - \left(\frac{\sigma}{r}\right)^{6} + \frac{1}{4} \right], & \text{for } r \leq 2^{1/6}\sigma, \\ 0, & \text{for } r > 2^{1/6}\sigma. \end{cases} \tag{4.1}$$

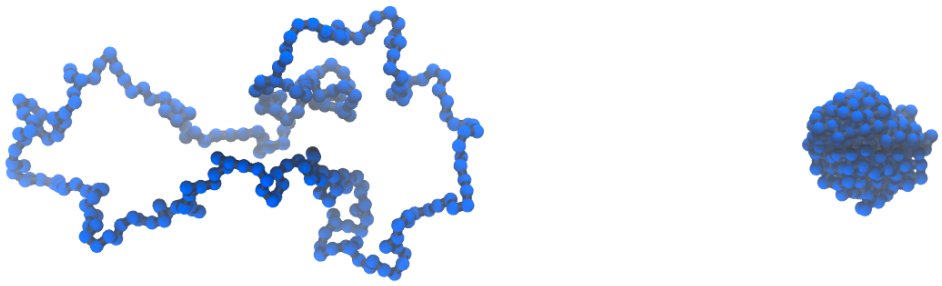

(a) Good solvent conditions (b) Poor solvent conditions

Figure 4.1: The ring with $N = 250$ monomers subject to different solvent conditions. In Subfigure 4.1a, the cutoff $r_{\text{cut}} = 2^{1/6}\sigma$ for the LJ-potential is set. As a result, the excluded volume interactions are purely repulsive, and we observe an expanded coil. On the contrary, in Subfigure 4.1b, $r_{\text{cut}} = 2.5\sigma$ and because of the predominating attraction between monomers the whole ring collapses into a globular state. In both cases, 10^6 MD steps were performed to equilibrate the polymer.

where σ denotes the diameter of the monomers, a positive constant ϵ sets the interaction strength, and $r_{\text{cut}} = 2^{1/6}\sigma \simeq 1.122\sigma$ stands for the minimum of the original LJ-potential, i.e. the point of truncation. As first reported by Grest et al. [21], such form of the LJ-potential ensures that the excluded volume interactions are purely repulsive and therefore resemble good solvent conditions [38]. Effects of the solvent are illustrated in Figure 4.1.

Additionally, the bond energies between the nearest neighbors in a ring are given by the finite extensible nonlinear elastic (FENE) potential:

$$u_{\text{FENE}}(r) = \begin{cases} -\frac{\kappa}{2}\left(\frac{R_0}{\sigma}\right)^2 \ln\left[1 - \left(\frac{r}{R_0}\right)^2\right], & \text{for } r \leq R_0, \\ +\infty, & \text{for } r > R_0, \end{cases} \tag{4.2}$$

with $R_0 = 1.5\sigma$ being the chosen bond length, κ denotes the bond strength and is set to 30ϵ [39]. Obviously, $\sigma \equiv \sigma_{\text{LJ}}$.

Consequently, the total potential energy of a ring with N monomers can be written as follows:

$$U_{\text{ring}}(\{\mathbf{r}\}) = \sum_{i=1}^{N} u_{\text{FENE}}(|\mathbf{r}_i - \mathbf{r}_{i+1}|) + \sum_{i<j=1}^{N} u_{\text{mm}}(|\mathbf{r}_i - \mathbf{r}_j|) + \sum_{i=1}^{N} U_{\text{wall}}(\mathbf{r}_i), \tag{4.3}$$

where $\mathbf{r}_{N+1} \equiv \mathbf{r}_1$ and the monomer-wall potential is given by the expression (3.4).

Furthermore, as a basic set of units, we choose the parameters σ, ϵ of the LJ-potential (4.1) and the monomer's mass m. Thus, the used system of reduced units reads as:

$$r^* = \frac{r}{\sigma}, \quad E^* = \frac{E}{\epsilon}, \quad t^* = t\sigma\left(\frac{\epsilon}{m}\right)^{1/2}, \quad F^* = \frac{F\sigma}{\epsilon}, \quad \rho^* = \rho\sigma^3, \tag{4.4}$$

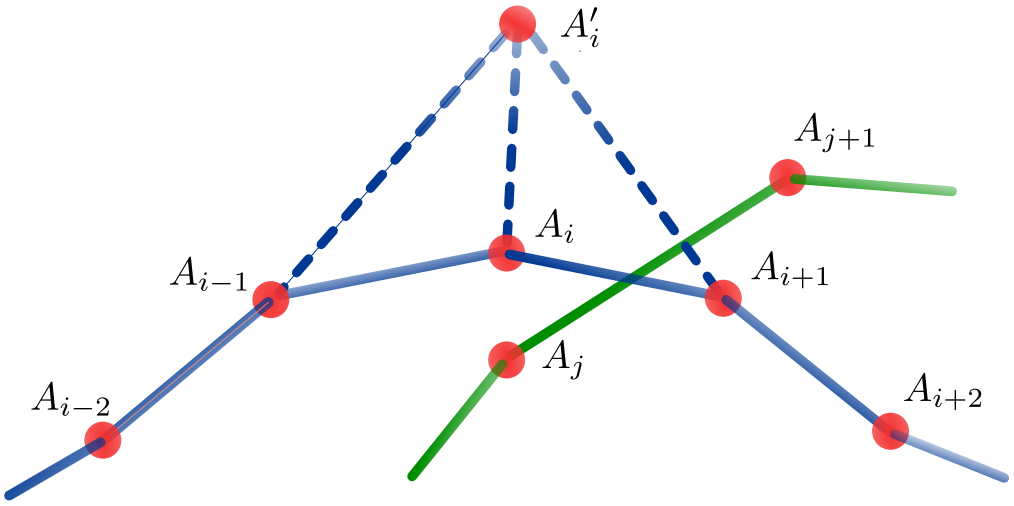

Figure 4.2: The geometry of the bond positions described in the text: an $i-$th monomer has been displaced from an old position A_i to an attempted new position A'_i, the neighboring monomers are placed at A_{i-1}, A_{i+1}. In this particular drawing, bond-crossing has taken place.

with r, E, t, F, ρ standing for the dimensional length, energy, time, force, and density units, respectively. The reduced temperature of the system T^* is set to

$$T^* \equiv \frac{k_B T}{\epsilon} = 1. \tag{4.5}$$

4.1.2 Conservation of the ring polymer's topology

Based on the considerations of Narros et al. [14], we present an algorithm that prevents from unwanted changes of topology in MC simulations of ring polymers. In particular, for each MC move, we check, whether no bond-crossings occur, thereby ensuring the conservation of the topology of the unknotted rings.

Firstly, let us consider a simple translational MC move of a single monomer. More specifically, we assume that the $i-$th monomer is initially placed at the position A_i and is attempted to be displaced to a new position A'_i. Furthermore, the nearest neighbors are located at the points A_{i-1} and A_{i+1} with $A_{i-1}A_i$, A_iA_{i+1} denoting the bonds connecting two sequential beads in the old configuration and $A_{i-1}A'_i$, A'_iA_{i+1} in the attempted new one, respectively. Finally, we are going to check, whether any other bond A_jA_{j+1} ($j \geq i+1$, $j \leq i-2$) crosses the bonds associated with the $i-$th monomer during the above-described MC displacement. Figure 4.2 illustrates the geometry of this situation.

In order to achieve this, we consider two triangles $\triangle A_{i-1}A_iA'_i$ and $\triangle A_{i+1}A_iA'_i$ formed by the monomer positions in the old and new configurations. Therefore, only if these triangles are intersected by other bonds in the ring A_jA_{j+1} ($j \geq i+1$, $j \leq i-2$) does the bond-crossing occur. In the forthcoming discussion, we consider an algorithm that

can be used to determine, if a line segment B_0B_1 intersects a triangle $\triangle A_0A_1A_2$ [40], [41] Furthermore, italic letters A denote points in space and bold letters $\mathbf{A}$ represent vectors pointing to them.

In general, an arbitrary point A on a plane $\mathcal{P}$ containing three points A_0, A_1 and A_2 can be represented with the help of a vector $\mathbf{w}$ parametrized as follows:

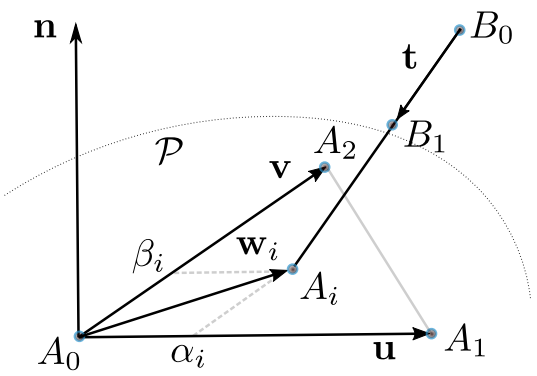

Figure 4.3: Finding the point of intersection A_i between a segment B_0B_1 and a triangle $\triangle A_0A_1A_2$.

$$\mathbf{w}(\alpha, \beta) = \alpha\mathbf{u} + \beta\mathbf{v}, \tag{4.6}$$

with α, β being real numbers and the vectors $\mathbf{w}, \mathbf{u}, \mathbf{v}$ defined as

$$\mathbf{w}(\alpha, \beta) = \mathbf{A}(\alpha, \beta) - \mathbf{A}_0, \tag{4.7}$$

$$\mathbf{u} = \mathbf{A}_1 - \mathbf{A}_0, \tag{4.8}$$

$$\mathbf{v} = \mathbf{A}_2 - \mathbf{A}_0. \tag{4.9}$$

Therefore, a point $A(\alpha, \beta)$ lies inside the triangle $\triangle A_0A_1A_2$ only if

$$\alpha \geq 0, \quad \beta \geq 0, \quad \alpha + \beta \leq 1. \tag{4.10}$$

Moreover, the edges of the triangle are given by the equations $\alpha = 0$, $\beta = 0$, $\alpha + \beta = 1$ and its three vertices are located at the positions $\mathbf{A}_0 = \mathbf{A}(0, 0)$, $\mathbf{A}_1 = \mathbf{A}(1, 0)$ and $\mathbf{A}_2 = \mathbf{A}(0, 1)$.

Next, the line passing through the points B_0 and B_1 has the following parametric form:

$$\mathbf{s}(\gamma) = \gamma\mathbf{t}, \tag{4.11}$$

$$\mathbf{s}(\gamma) = \mathbf{B}(\gamma) - \mathbf{B}_0, \tag{4.12}$$

$$\mathbf{t} = \mathbf{B}_1 - \mathbf{B}_0, \tag{4.13}$$

with the values $0 \leq \gamma \leq 1$ corresponding to the segment B_0B_1. Now, let us shortly describe the conditions under which this segments intersects the triangle $\triangle A_0A_1A_2$, that is the conditions corresponding to the violation of topology during an MC move. Successively, they can be summarized as follows (further geometric details are shown in Figure 4.3):

(1) First of all, we have to check whether the line $\mathcal{L}$ containing B_0B_1 and the plane $\mathcal{P}$ are not parallel, that is

$$\mathbf{n} \cdot \mathbf{t} \equiv \mathbf{n} \cdot (\mathbf{B}_1 - \mathbf{B}_0) \neq 0, \tag{4.14}$$

where $\mathbf{n}$ stands for the plane normal

$$\mathbf{n} = \mathbf{u} \times \mathbf{v} \tag{4.15}$$

and $\mathbf{t}, \mathbf{u}, \mathbf{v}$ are defined as in (4.11), (4.13). If the condition (4.14) holds, then the line $\mathcal{L}$ intersects the plane $\mathcal{P}$, and we proceed to the next step.

(2) Secondly, at the point of intersection between $\mathcal{L}$ and $\mathcal{P}$, the vector $\mathbf{B}(\gamma_i) - \mathbf{A}_0$ is orthogonal to $\mathbf{n}$, and the corresponding parameter γ_i can be found as

$$\gamma_i = \frac{\mathbf{n} \cdot (\mathbf{A}_0 - \mathbf{B}_0)}{\mathbf{n} \cdot \mathbf{t}} \equiv \frac{\mathbf{n} \cdot (\mathbf{A}_0 - \mathbf{B}_0)}{\mathbf{n} \cdot (\mathbf{B}_1 - \mathbf{B}_0)}. \tag{4.16}$$

If $0 \leq \gamma_i \leq 1$, then the segment B_0B_1 intersects the plane $\mathcal{P}$ and we have to find out, whether the intersection point $B(\gamma_i)$ lies inside the triangle $\triangle A_0A_1A_2$. Additionally, let us note that the construction of the line equation (4.11) ensures that $0 \leq \gamma_i \leq 1$ for an arbitrary segment intersecting the plane $\mathcal{P}$, no matter how its initial point is chosen (i.e., with respect to the interchange $\mathbf{B_0} \longleftrightarrow \mathbf{B_1}$).

(3) Thirdly, the point of intersection between the segment B_0B_1 and the plane $\mathcal{P}$ can be obtained from the vector equation

$$\mathbf{w}_i(\alpha_i, \beta_i) \equiv \alpha_i \mathbf{u} + \beta_i \mathbf{v} = (\mathbf{B}_0 - \mathbf{A}_0) + \gamma_i \, (\mathbf{B}_1 - \mathbf{B}_0) \tag{4.17}$$

with γ_i given by (4.16) and the explicit expressions for α_i and β_i read as

$$\alpha_i = \frac{(\mathbf{u} \cdot \mathbf{v}) \, (\mathbf{w}_i \cdot \mathbf{v}) - (\mathbf{v} \cdot \mathbf{v}) \, (\mathbf{w}_i \cdot \mathbf{u})}{(\mathbf{u} \cdot \mathbf{v})^2 - (\mathbf{u} \cdot \mathbf{u}) \, (\mathbf{v} \cdot \mathbf{v})}, \tag{4.18}$$

$$\beta_i = \frac{(\mathbf{u} \cdot \mathbf{v}) \, (\mathbf{w}_i \cdot \mathbf{u}) - (\mathbf{u} \cdot \mathbf{u}) \, (\mathbf{w}_i \cdot \mathbf{v})}{(\mathbf{u} \cdot \mathbf{v})^2 - (\mathbf{u} \cdot \mathbf{u}) \, (\mathbf{v} \cdot \mathbf{v})}, \tag{4.19}$$

where $\mathbf{w}_i = (\mathbf{B}_0 - \mathbf{A}_0) + \gamma_i \, (\mathbf{B}_1 - \mathbf{B}_0)$. Besides, it is worth mentioning that (4.18) and (4.19) contain only five different dot products and share a common denominator. Therefore, these expressions should be computed only once. Finally, only if

$$\alpha_i \geq 0, \qquad \beta_i \geq 0, \qquad \alpha_i + \beta_i \leq 1 \tag{4.20}$$

does the segment B_0B_1 intersect the triangle $\triangle A_0A_1A_2$.

In summary, a simple translational MC move of a monomer in a ring together with the additional topology tests consists of the following steps (in the following, an implementation of the cell list with a cutoff radius r_c is assumed):

(1) Choose a random monomer with index i, $(i = 1, 2, \ldots, N)$ and calculate its energy in the old configuration:

$$U_{\text{old}} = u_{\text{FENE}}(|\mathbf{r}_i - \mathbf{r}_{i+1}|) + u_{\text{FENE}}(|\mathbf{r}_{i-1} - \mathbf{r}_i|) + \sum_j u_{\text{mm}}(|\mathbf{r}_i - \mathbf{r}_j|), \tag{4.21}$$

where the sum $\sum_j$ runs over the neighboring particles in the cell list only.

(2) Randomly displace the $i-$th particle:

$$x_i' = x_i + d_{\max}\left(\xi_x - 0.5\right), \tag{4.22}$$

$$y_i' = y_i + d_{\max}\left(\xi_y - 0.5\right), \tag{4.23}$$

$$z_i' = z_i + d_{\max}\left(\xi_z - 0.5\right), \tag{4.24}$$

where $d_{\max} < 2r_c$ is a maximal allowed displacement and $\xi_x, \xi_y, \xi_z \in [0,1]$ are uncorrelated, random numbers.

(3) Calculate the energy U_{new} in the new configuration and accept the move, if

$$\Delta U = U_{\text{new}} - U_{\text{old}} < 0. \tag{4.25}$$

Otherwise ($\Delta U > 0$), generate a random number $0 < \eta < 1$ and accept the move, if

$$\eta < \exp(-\beta \Delta U). \tag{4.26}$$

(4) If the Metropolis condition is satisfied, perform the topology checks according to the algorithm 4.1.2. Practically, it means that it has to be verified that no bond crosses the triangles $\triangle A_{i-1}A_iA_i'$ and $\triangle A_i'A_iA_{i+1}$. We have observed that only $\sim$5% of moves suffer from the topology violations and therefore the Metropolis criterion should always be computed in the first place.

4.1.3 Description of crankshaft MC moves

In this section, we consider crankshaft MC moves for ring polymers [33] (moreover, these moves can be straightforwardly implemented in the case of other polymer topologies) and a suitable generalization of the algorithm 4.1.2 employed to verify that no bond-crossings occur during a collective displacement. These moves sample the phase space much more efficient than ordinary trial displacements and therefore significantly improve sampling, albeit being computationally more demanding.

A typical crankshaft MC move consists of the following steps (the geometry of the bond positions is pictured in Figure 4.4):

(1) Choose a random monomer with index i, ($i = 1, 2, \ldots, N$). Next, randomly select the second monomer with index j such that

$$2 < |i - j| < N/3. \tag{4.27}$$

In other words, at least 2 monomers are rotated during each crankshaft move.

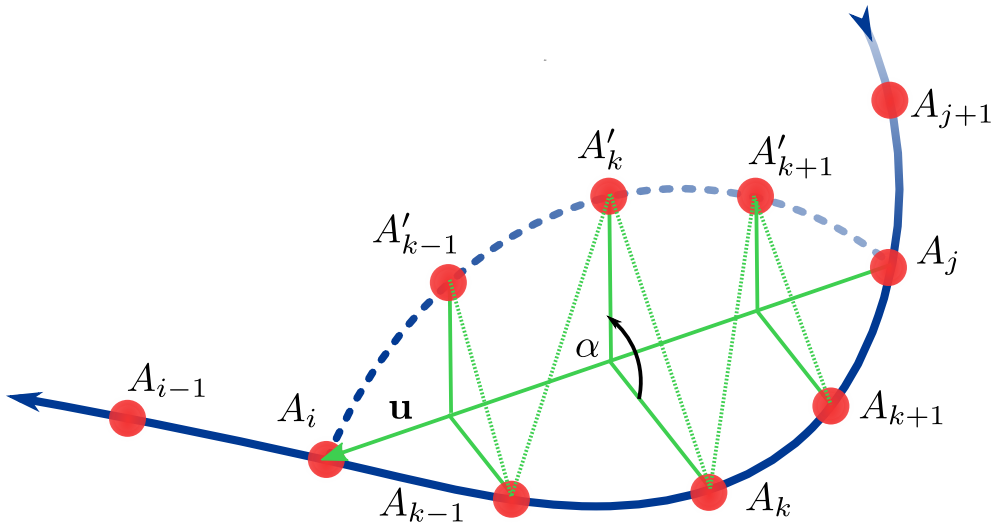

Figure 4.4: The geometry of the bond positions for a simple crankshaft move described in the main text: the monomers with index $i < k < j$ have been rotated from the old positions A_k to the attempted new A'_k around the unit axis $\mathbf{u}$ by an angle α. Triangles built on the bonds in the old and new configurations (dotted green lines) are used to determine, whether no bond-crossings have occurred.

(2) Calculate the unit vector $\mathbf{u}$, which defines the rotation axis, as follows:

$$\mathbf{u} = \frac{\mathbf{r}_i - \mathbf{r}_j}{|\mathbf{r}_i - \mathbf{r}_j|}, \tag{4.28}$$

where $\mathbf{r}_i, \mathbf{r}_j$ are the positions of the i-th and j-th monomers, respectively.

(3) Randomly select an angle $\alpha \in [-\alpha_{\max}, \alpha_{\max}]$, where $\alpha_{\max}$ is chosen under the condition that the maximal displacement among all the monomers during the rotation around $\mathbf{u}$ equals a certain value Δ set to be $\Delta = 10\sigma$.

(4) Rotate all the monomers $k = i+1, \ldots, j-1$ around the axis $\mathbf{u}$ by the chosen angle α (in the following, the Rodrigues' rotation formula is employed):

$$\mathbf{r}_k^{\perp\prime} = \mathbf{r}_k^{\perp} \cos\alpha + \left(\mathbf{u} \times \mathbf{r}_k^{\perp}\right) \sin\alpha + \mathbf{u}\left(\mathbf{u} \cdot \mathbf{r}_k^{\perp}\right)(1 - \cos\alpha)\,, \tag{4.29}$$

where the vectors $\mathbf{r}_k^{\perp}$ denote a component of the vector $\mathbf{r}_k$ which is orthogonal to the rotation axis $\mathbf{u}$:

$$\mathbf{r}_k^{\perp} = (\mathbf{r}_k - \mathbf{r}_j) - \mathbf{u}\left((\mathbf{r}_k - \mathbf{r}_j) \cdot \mathbf{u}\right) \equiv \mathbf{r}_k - \mathbf{r}_k^{\parallel}, \tag{4.30}$$

with $\mathbf{r}_k^{\parallel} = \mathbf{r}_j + \mathbf{u}\left((\mathbf{r}_k - \mathbf{r}_j) \cdot \mathbf{u}\right)$ being a parallel to $\mathbf{u}$ component of $\mathbf{r}_k$ that remains unaffected in the course of the rotation. Therefore, the new positions $\mathbf{r}'_k$ are given by:

$$\mathbf{r}'_k = \mathbf{r}_k^{\perp\prime} + \mathbf{r}_j + \mathbf{u}\left((\mathbf{r}_k - \mathbf{r}_j) \cdot \mathbf{u}\right) \equiv \mathbf{r}_k^{\perp\prime} + \mathbf{r}_k^{\parallel}. \tag{4.31}$$

(5) Accept the move according to the Metropolis Monte Carlo rule, i.e., based on the energy difference $\Delta U = U' - U$ between the new and old configurations.

(a) If, at this point, the move is accepted, proceed to the topology tests.

(b) Otherwise, go to step (1).

(6) In order to verify that no bond-crossing have occurred, employ the algorithm 4.1.2 for the triangles built on the bonds in the old and new configurations:

$$\triangle A_i A_{i+1} A'_{i+1}, \quad \ldots, \triangle A_{k-1} A_k A'_k, , \quad \ldots, \triangle A_{j-1} A'_{j-1} A_j. \tag{4.32}$$

(a) If all of the checks have been successfully passed (that is, none of the bonds $A_r A_{r+1}$, $(r \geq j,\ r \leq i-1)$ has crossed the aforementioned triangles), accept the move by updating the configuration of the polymer and its total energy.

(b) In the opposite case, start from the beginning.

Obviously, the above-described crankshaft moves can be applied to any polymeric chain with N monomers. However, in that case we don't have to perform exhaustive topology tests, since any bead-arrangement is accessible from an arbitrary starting configuration.

4.1.4 The MC method for calculating effective potentials

Let us discuss thoroughly the MC method for calculating effective potentials. Our starting point is the equation (3.20), which allows us to connect the effective potential $U_{\text{eff}}(z)$ with the distribution function $P_{\text{wall}}(z; \rho \to 0)$. The condition $\rho \to 0$ can be satisfied by choosing a large enough simulation box with just one ring polymer in the presence of the hard wall such that the impact of (periodic) boundary conditions is negligible. In addition, let us note that the discussion below applies to homogeneous systems also, that is when the radial distribution function $g(r; \rho \to 0)$ is desired.

Unless otherwise stated, we perform a standard Metropolis Monte Carlo [42] simulation under the condition that the topology of the ring is preserved [14]. The latter can be achieved as follows: for instance, while performing a simple translational MC move of an $i-$th monomer from an old position A_i to an attempted new position A'_i, one gets two triangles $\triangle A_{i-1} A_i A'_i$ and $\triangle A_{i+1} A_i A'_i$, where A_{i-1}, A_{i+1} denote positions of the two neighboring monomers. Now, the topology of the ring has been violated, if any other bond $A_j A_{j+1}$ $(j \geq i+1,\ j \leq i-2)$ has crossed the above-defined triangles. Therefore, the original problem is equivalent to the question, whether a line segment intersects a triangle. Further details have been explored in the previous section. Moreover, this simple method can be applied in the case of more complicated collective MC moves [33] (e.g., crankshaft moves described in 4.1.3).

After a sufficiently large number of equilibration steps, we start sampling a histogram $H(z)$ of the center-of-mass positions, which in the end can be properly normalized and yields the distribution function $P(z;\rho \to 0)$. However, the biggest problem is yet to come: in a naïve MC simulation, the ring could end up trapped within a local minimum of the effective potential. In the occurrence of such event, it would need to overcome an energy barrier in order to continue the exploration of the phase space. This, on the other hand, happens after a very long series of MC steps depending on the depth of the local minimum.

In order to address this issue, we employ the umbrella sampling technique [43], [2]: the whole sampling interval $z \in [z_{\min}, z_{\max}]$ is divided into 'windows' of width Δz_j centered at z_j, where the effective potential does not vary more than a few $k_B T$. It is important to note that the neighboring windows must overlap, so that they could be joined afterwards. Furthermore, one has to include an additional local bias potential $U_{\text{bias}}(z)$ to assure that the ring remains within the preset window. Particularly, in our MC simulations we utilize the local infinite well bias potential [44]:

$$U_{\text{bias}}^{(j)}(z) = \begin{cases} \infty, & \text{for } z < z_j - \frac{\Delta z_j}{2}, \\ 0, & \text{for } z \in \left[z_j - \frac{\Delta z_j}{2}, z_j + \frac{\Delta z_j}{2} \right], \\ \infty, & \text{for } z > z_j + \frac{\Delta z_j}{2}. \end{cases} \tag{4.33}$$

In other words, an MC move is rejected, if the center of mass of the polymer crosses the boundaries of the current window. Alternatively, a harmonic bias potential [2] might be used:

$$U_{\text{bias}}^{(j)}(z) = \frac{k_j}{2}(z - z_j)^2, \tag{4.34}$$

if, for example, a differentiable function is needed.

As a result, we obtain the modified distribution functions $\tilde{P}^{(j)}(z)$ that, in turn, are related to the total potential energy in each window:

$$U_{\text{eff}}^{(j)}(z) + U_{\text{bias}}^{(j)}(z) = -k_B T \ln \tilde{P}^{(j)}(z). \tag{4.35}$$

In order to get a smooth curve for the modified distribution function $\tilde{P}(z)$ from the set of all histograms $H_j(z)$, the following method is used [2]: we start with a histogram $H_1(z) = H(z)$ in the first window ($H(z)$ denotes the total histogram) and link it together with all the following histograms $H_2(z), H_3(z), \ldots$ by means of a least square method. In particular, to add $H_j(z)$ to the total histogram $H(z)$, we multiply $H(z)$ by a factor

$$c_{j,j+1} = \frac{\sum_k z_{k;\,j}^2}{\sum_k z_{k;\,j} z_{k;\,j+1}}, \tag{4.36}$$

where the sum above runs over the overlap points between the two subsequent windows. The resulting total histogram $H(z)$ yields, up to the normalization constant, the distribution function $\tilde{P}(z)$. The unknown constant can be determined from the condition that

$$\lim_{z\to\infty} \tilde{P}(z) = 1. \tag{4.37}$$

Therefore, the effective potential $U_{\text{eff}}(z)$ is given by

$$U_{\text{eff}}(z) = -k_B T \ln \tilde{P}(z) - U_{\text{bias}}(z). \tag{4.38}$$

Alternatively, the effective potential can calculated from the total histogram $H(z)$ directly:

$$U_{\text{eff}}(z) = -k_B T \ln H(z) - U_{\text{bias}}(z) + U_0, \tag{4.39}$$

where the shifting constant U_0 is obtained from the constraint that

$$\lim_{z\to\infty} U_{\text{eff}}(z) = 0. \tag{4.40}$$

Let us discuss the validity of the above-described approach by considering two particles interacting via the GEM-4 pair potential [45]:

$$u(r) = \epsilon \exp\left[-(r/\sigma)^4\right]. \tag{4.41}$$

In particular, we run a MC simulation with two particles interacting via the predefined potential (4.41) and we aim to retrieve the form of this potential by means of the umbrella sampling technique, as if it was unknown. Therefore, we measure the radial distribution function $g(r)$ by fixing the position of the first particle and by sampling the histograms of the interparticle distances for the second one in the interval $[0, 2.2\sigma]$. In this case. we use $N_w = 21$ sampling windows of width $\Delta r_j = 0.2\sigma$, centered at $r_j = j \cdot 0.1\sigma$ with $j = 1, 2, \ldots, N_w$. As one can see, we have a substantial overlap between the neighboring windows, which equals 0.1σ. All the obtained histograms and the corresponding total $H(r)$ are shown in Figure 4.5.

Finally, using (4.39) we calculate the interparticle interaction potential. Comparison of the exact expression and the sampled potential is given in Figure 4.6. As one can easily see, the obtained potential is in excellent agreement with the exact function (4.41), which proves the consistency of our method.

4.1.5 Outline of other simulation techniques

In the present section, we shortly outline other possible methods of obtaining effective potentials based on the calculation of the distribution functions (3.17).

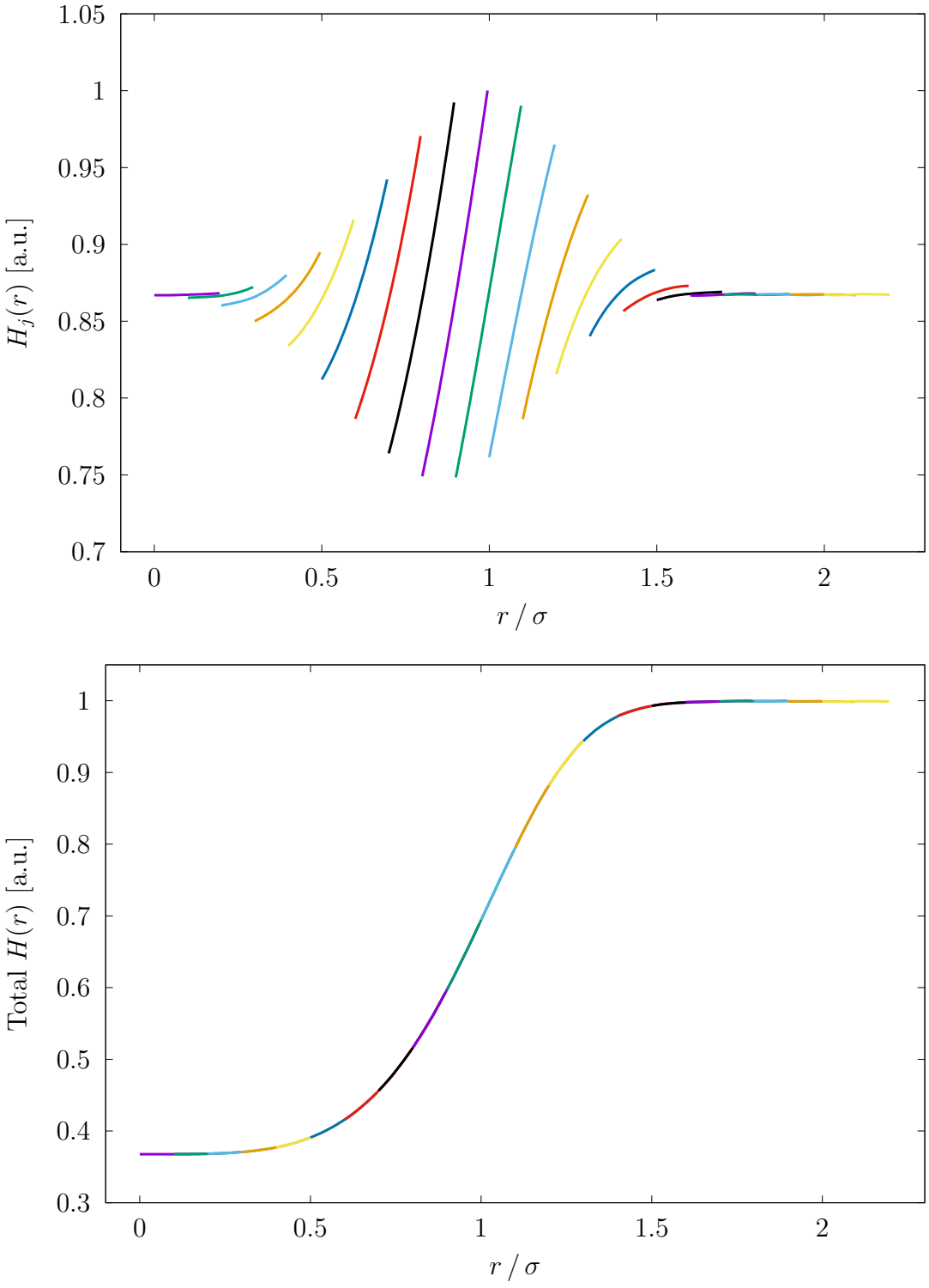

Figure 4.5: Top: interparticle distance histograms obtained for two particles interacting via the GEM-4 pair potential. Bottom: the corresponding total histogram, which is proportional to the modified radial distribution function $\tilde{g}(r)$. The y-axis has an arbitrary scale unit.

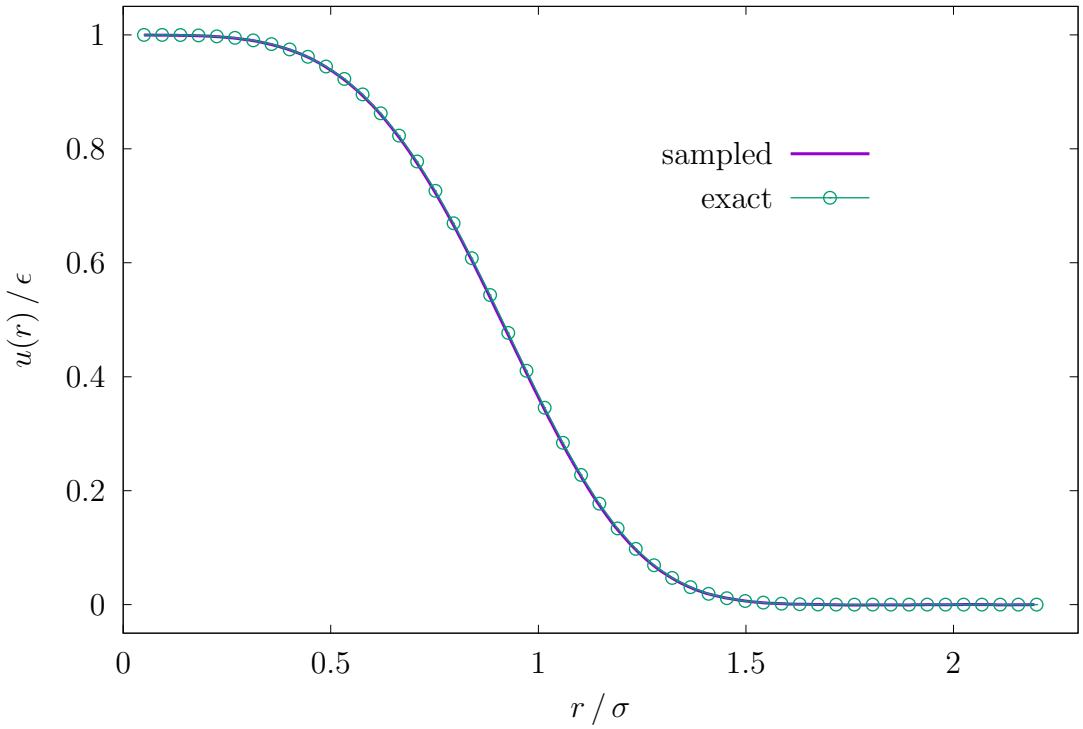

Figure 4.6: Comparison between the exact expression for the GEM-4 potential and the one obtained through the sampling technique described in the main text.

In order to measure the distribution function $P_{\text{wall}}(z)$, we could alternatively employ a standard molecular dynamics (MD) simulation as the replacement for the MC method described in the previous section. The procedure of obtaining histograms of the center-of-mass positions is practically identical to that in the MC case, albeit there are two major points we must care about:

(1) Firstly, the simple form of the monomer-wall interaction potential (3.4) suitable for the MC approach must be replaced with a differentiable expression. For example, the following function suggested by Poier et al. [46] can be used:

$$U_{\text{wall}}(z) = \begin{cases} \epsilon \left(\frac{2}{15} \left(\frac{\sigma}{z} \right)^9 - \left(\frac{\sigma}{z} \right)^3 + \frac{\sqrt{10}}{3} \right), & \text{for } z < \left(\frac{2}{5} \right)^{1/6} \sigma, \\ 0, & \text{for } z \geq \left(\frac{2}{5} \right)^{1/6} \sigma, \end{cases} \tag{4.42}$$

which yields an interaction potential between a monomer located at a distance z away from the wall and the Lennard-Jones particles filling the half-space $z < 0$ with density $\pi\rho\sigma^3/6 = 1$. Moreover, additional cutoff at $z_{\text{cut}} = \left(\frac{2}{5} \right)^{1/6} \sigma$ ensures a purely repulsive character of this potential.

(2) Secondly, due to the same reason as mentioned above, the harmonic bias potential in

each sampling window can be employed:

$$U_{\text{bias}}^{(j)}(z) = \frac{k_j}{2}(z - z_j)^2. \tag{4.43}$$

In all the MD simulations mentioned in this thesis, we perform standard Langevin dynamics, in which the equations of motion of the i-th monomer read as:

$$m\mathbf{a}_i(t) = \mathbf{F}_i(t) - m\gamma\mathbf{v}_i(t) + \mathbf{R}_i(t), \tag{4.44}$$

where we assume that all monomers have the same mass m and are subject to the dissipation force $-m\gamma\mathbf{v}_i(t)$ with the same friction coefficient γ. $\mathbf{F}_i(t)$ denotes the total force exerted on the $i-$th particle by other monomers (and, if included in the simulation, force due to the hard wall, bias force, etc.) at the time t. Finally, $\mathbf{R}_i(t)$ is a stochastic force modeling the heat bath. It is assumed to follow a Gaussian distribution with zero-mean

$$\langle \mathbf{R}_i(t) \rangle = \mathbf{0}, \tag{4.45}$$

and variance, according to the fluctuation-dissipation theorem [47], satisfying

$$\langle \mathbf{R}_i(t) \cdot \mathbf{R}_j(t') \rangle = (6m\gamma k_B T)\, \delta_{ij}\delta(t - t'), \tag{4.46}$$

where T denotes the absolute temperature of the heat bath. In other words, random Langevin noise produces the right amount of fluctuations to hold the system in thermal equilibrium.

In order to integrate the equation of motion (4.44), the modified Velocity-Verlet algorithm [48] is implemented:

$$\mathbf{v}_i\left(t + \tfrac{1}{2}\Delta t\right) = \mathbf{v}_i(t)\left[1 - \tfrac{\gamma\Delta t}{2}\right] + \tfrac{\Delta t}{2m}\left[\mathbf{F}_i(t) + \mathbf{R}_i(t)\right], \tag{4.47}$$

$$\mathbf{x}_i(t + \Delta t) = \mathbf{x}_i(t) + \mathbf{v}_i\left(t + \tfrac{1}{2}\Delta t\right)\Delta t, \tag{4.48}$$

$$\mathbf{v}_i(t + \Delta t) = \left(1 + \tfrac{\gamma\Delta t}{2}\right)^{-1}\left(\mathbf{v}_i\left(t + \tfrac{1}{2}\Delta t\right) + \tfrac{\Delta t}{2m}\left[\mathbf{F}_i(t + \Delta t) + \mathbf{R}_i(t + \Delta t)\right]\right). \tag{4.49}$$

For practical purposes, the components $R_{i,\alpha}$, $(\alpha = x, y, z)$ of the random force $\mathbf{R}_i$ on the time interval $[t, t + \Delta t]$ are approximated as follows:

$$R_{i,\alpha}(t) = \sigma\xi_\alpha, \qquad \sigma = \sqrt{2m\gamma k_B T/\Delta t}, \tag{4.50}$$

where Δt stands for the integration time-step and ξ_α is a Gaussian pseudo-random variable whose mean is equal to zero and variance equal to one:

$$\langle \xi_\alpha \rangle = 0, \qquad \langle \xi_\alpha \xi_\beta \rangle = \delta_{\alpha\beta}. \tag{4.51}$$

In comparison to the MC simulations of rings polymers, there is an advantage of using MD methods, especially relevant for large-size rings: there is no need to perform exhaustive topology checks, since typical choice of parameters in the monomer-resolved model (4.1.1) prevents from unphysical bond-crossings (fluctuations in the system are not large enough to overcome the energy barrier between these two configurations [2], [21]). However, as we will see later on, the effective ring-wall interaction approaches the scaling behavior for $N_{\mathrm{mon}} \gtrsim 200$ and therefore we will deal with rather small rings. This allows to sample better statistics in less computational time using MC simulations and collective moves.

Last of all, it is worthwhile to outline a generalized Widom insertion method [49] for obtaining effective potentials between two molecular aggregates, which is based directly on the equation (3.20):

$$U_{\mathrm{eff}}(r) = -\beta^{-1} \ln \left(\frac{Z_2(r)}{Z_1^2} \right). \tag{4.52}$$

The expression above can be easily rewritten as follows [2]:

$$\exp\left(-\beta U_{\mathrm{eff}}(r)\right) = \Big\langle \exp\Big(-\beta U_{12}\left(\mathbf{0}, \mathbf{r}\right) \Big) \Big\rangle' \equiv g(r), \tag{4.53}$$

where $U_{12}\left(\mathbf{0}, \mathbf{r}\right)$ denotes the interaction energy between two molecules under the condition that the center of one of them is placed at the position $\mathbf{0}$ and of the other at $\mathbf{r}$. Moreover, the averaging $\langle \cdots \rangle'$ is performed in the ensemble of two non-interacting objects:

$$\langle \cdots \rangle' = \frac{\displaystyle\int d\mathbf{r}_1^{N_1} d\mathbf{r}_2^{N_2} \, \exp\Big(-\beta \left(U_{11} + U_{22}\right) \Big) \left(\cdots \right)}{\displaystyle\int d\mathbf{r}_1^{N_1} d\mathbf{r}_2^{N_2} \, \exp\Big(-\beta \left(U_{11} + U_{22}\right) \Big)}, \tag{4.54}$$

with U_{11} and U_{22} denoting the intramolecular potential energies. Calculation of the effective potential proceeds in the following way: first, a large number $(10^4 - 10^6)$ of uncorrelated, equilibrated configurations of a single, free object are generated, secondly, the average (4.53) is calculated by randomly inserting two molecules with centers separated by a distance r. Thus,

$$\exp\left(-\beta U_{\mathrm{eff}}(r)\right) \equiv g(r) = \Big\langle \exp(-\beta \Delta U(r)) \Big\rangle_{N_{\mathrm{trials}}}, \tag{4.55}$$

where $\Delta U(r)$ denotes the energy difference between the free and interacting configurations of two objects, N_{trials} is the number of trial insertions. For instance, this method has been successfully employed to study effective ring-ring interactions [33] (for this problem, no-concatenation of polymers must be taken into account). Nevertheless, this method cannot be applied in the case of effective ring-wall interactions, since the equilibrated configurations of a ring close to the planar, hard wall significantly differ from those in the free case.

4.2 Results

This section is organized as follows: first of all, in (4.2.1), we will consider the equilibration of ring polymers and will test the scaling behavior of their radius of gyration at infinite dilution. Then, in 4.2.2, we will present the effective ring-wall potentials and will move on with their scaling limit discussed in 4.2.3.

4.2.1 Scaling exponents

In order to obtain ensemble configurations of the gyration radius

$$R_g^2 = \frac{1}{N}\sum_{k=1}^{N}\left(\mathbf{r}_k - \mathbf{r}_{\mathrm{cm}}\right)^2 \tag{4.56}$$

and to check its scaling behavior, we employed MC simulations (in the NVT-ensemble) of a single, unknotted ring with various degree of polymerization (N = 20, 40, 60, 80, 100, 150, 200, 200, 250).

In summary, for each N we generated no less that 10^5 data points, separated by $2 \cdot 10^4$ MC steps (such choice ensures that the sampled data in completely uncorrelated, typical autocorrelation function is shown in Figure 4.7), where one MC step was defined as a combination of N single monomer translations and one crankshaft move (all these moves were supplemented with topology checks described in 4.1.2). Initially, the monomers in a ring were placed around a circle with radius $R = N\sigma/2\pi$ and equilibrated for 10^6 MC steps. Figure 4.8 displays the distribution functions $p(R_g)$ of the sampled data.

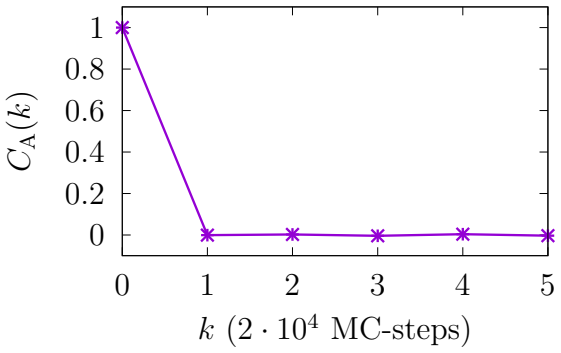

Figure 4.7: Typical autocorrelation function for the R_g-data points. This particular plot displays $C_A(k)$ for $N = 250$.

In order to verify the scaling behavior of the gyration radius, we employ the following fitting function:

$$\langle R_g \rangle = \sigma A N^{\nu}\left(1 + BN^{-\Delta}\right), \tag{4.57}$$

where the term $N^{-\Delta}$ explicitly encompasses the next-to-leading order effects, which are important in our case of rather small polymers ($N \leq 250$), σ sets the length-scale of the system and A, B are model-dependent, numeric constants. The scaling exponents ν, Δ are universal (that is, do not depend on the monomer-resolved model employed) and can be estimated from the renormalization group calculations in the case of linear polymers

Table 4.1: Fit parameters for different values of Δ.

Δ	ν	σ_ν	A	σ_A	B	σ_B	χ^2
∞	0.6116	0.0002	0.325	0.001	—	—	$2.55 \cdot 10^{-5}$
0.400	0.5841	0.0041	0.398	0.012	-0.46	0.06	$6.54 \cdot 10^{-6}$
0.478	0.5881	0.0036	0.383	0.009	-0.49	0.07	$6.49 \cdot 10^{-6}$
0.500	0.5891	0.0034	0.379	0.009	-0.50	0.07	$6.47 \cdot 10^{-6}$
1.000	0.5999	0.0018	0.348	0.004	-1.55	0.22	$6.17 \cdot 10^{-6}$

in good solvent conditions [50]:

$$\nu_{3d} = 0.5882 \pm 0.0011, \qquad \Delta_{3d} = 0.478 \pm 0.010, \tag{4.58}$$

where the subscripts explicitly indicate that the values above are valid in 3 spatial dimensions only. These values have been successfully confirmed numerically, for example, in self-avoiding random walks (resemble linear polymers in good solvent conditions) [51]. Moreover, the Flory exponent $\nu_{3d} = 0.588$ has been found in off-lattice simulations of ring polymers [33].

Table 4.1 contains fit parameters for the model (4.57) with different fixed values of Δ (a general four-parameter fit was unable to converge), where σ's denote standard errors. Moreover, $\Delta = \infty$ stands for the fit $\langle R_g \rangle = AN^\nu$. The fits were performed for $N = 80 \div 250$ and to control their accuracy we additionally provide the values of

$$\chi^2 = \sum_{i=1}^{n_{\text{data}}} \frac{\left(R_g^{(i)} - f(N^{(i)})\right)^2}{f(N^{(i)})}, \tag{4.59}$$

where the sum above runs over the data points used in the fitting procedure.

As one can see from (4.1), in comparison to the large-N limit $\langle R_g \rangle \sim N^\nu$, fits with $\Delta \approx 0.5$ give a really good estimate for the exponent ν, which is very close to the numeric value 0.588 that has been confirmed for rings with much larger $N \lesssim 10^4$ [33]. On the other hand, the obtained results hint that the theoretical estimate of the universal exponent Δ_{3d} for chains in good solvent conditions (4.58) is also valid for rings.

4.2.2 Effective wall-ring CM potentials

We have obtained, by means of MC simulations with the umbrella sampling method described in 4.1.4, the effective interaction potential $U_{\text{eff}}(z)$ between the centers of mass of flexible, unknotted ring polymers with different polymerization index N ($N = 20 \div 250$) and planar, hard walls.

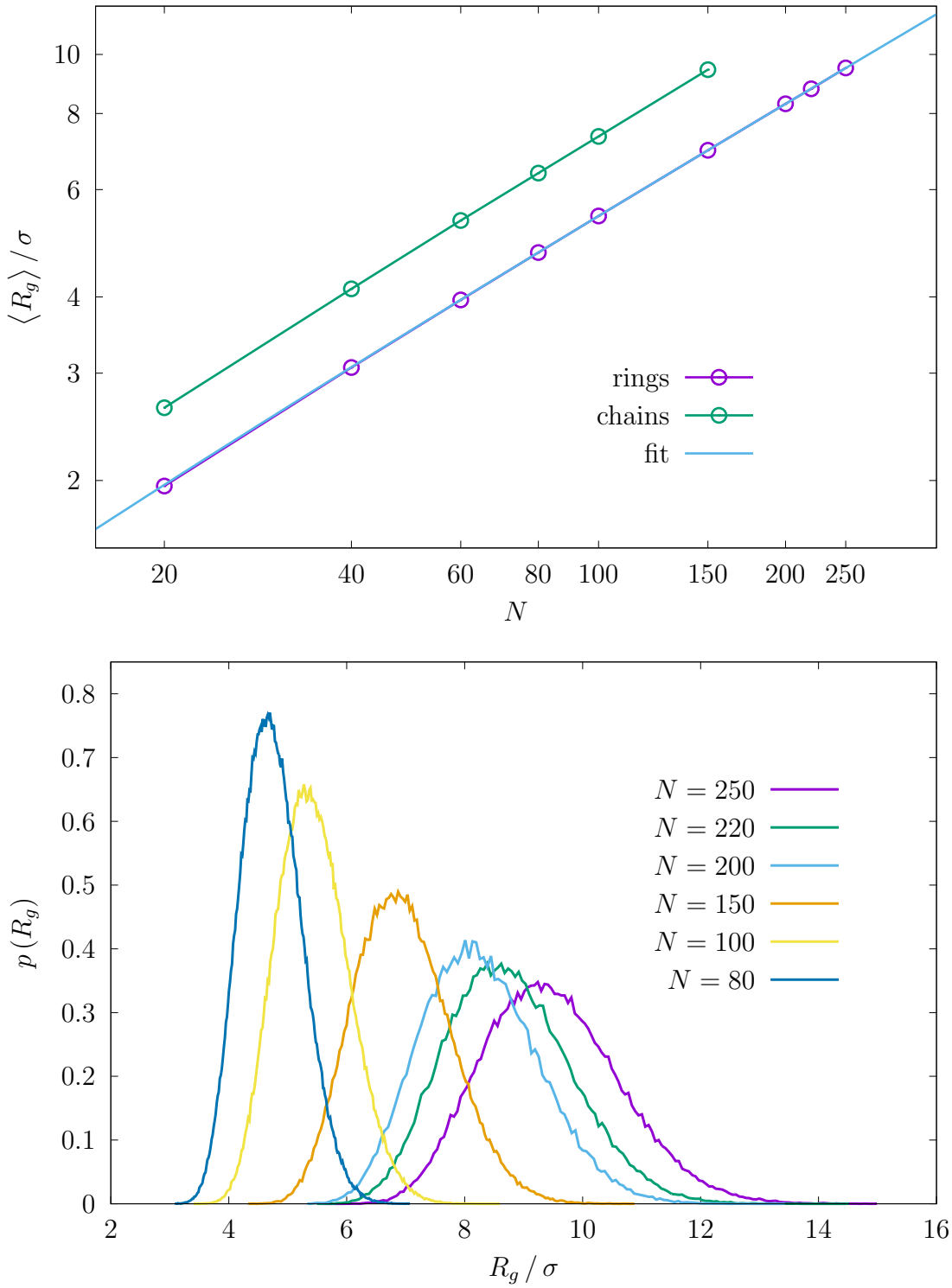

Figure 4.8: Top: a log-log plot of the gyration radius $\langle R_g \rangle$ as a function of the degree of polymerization N for the ring and linear molecules. In addition, we display a fit $\langle R_g \rangle = AN^{\nu} \left(1 + BN^{-0.478}\right)$ for the ring polymers. The obtained $\langle R_g \rangle$-data points for different N are shown with open circles, the corresponding errors are $O\left(10^{-3}\sigma\right)$ and therefore cannot be seen on the plot. Bottom: the distribution functions $p(R_g)$ of the gyration radius for various N in the obtained configuration ensembles.

Separate MC simulations were employed in each sampling window in order to collect histograms of separations between the center of mass of the polymer and the wall. Initially, we equilibrated the rings in every window for 10^6 MC steps (here, we define one MC step as a series of N trial single monomer displacements) and then started collecting data separated by $\sim 10^2$ steps. Occasionally, we used crankshaft and rotational moves to explore the phase space efficiently. Statistics gathered over $10^8 - 10^9$ MC steps already yields good results. Typical histograms and the corresponding sampling parameters are shown in Figure 4.9.

Figure 4.10 displays the final result for the effective potentials $U_{\text{eff}}(z)$, where the effective center-of-mass coordinate z is scaled with σ and the gyration radius of the polymer R_g at infinite dilution. Evidently, $U_{\text{eff}}(z)$ converges to a universal functional form for $N > 200$.

Interestingly, the effective potential of linear chains on hard walls, in comparison to the ring polymers, seems to reach the scaling limit already for $N > 100$ 4.11. At least qualitatively, this effect can be understood as follows: on dimensional grounds, we can express the effective polymer-wall potential $U_{\text{eff}}(z)$ in terms of the fundamental energy and length scales of the system, that is

$$\beta U_{\text{eff}}(z) = \phi(z,\, \sigma,\, R_g), \tag{4.60}$$

where ϕ is some dimensionless function, $k_B T$ determines the energy scale of the system, σ and R_g set the length scale on the monomer-resolved and the coarse-grained level, respectively. Consequently, on the coarse-grained level we have

$$\beta U_{\text{eff}}(z) = \phi\left(z/R_g,\, \sigma/R_g\right) = \phi_0\left(z/R_g\right) + \left(\frac{\sigma}{R_g}\right) \phi_1\left(z/R_g\right) + O\left(\frac{\sigma}{R_g}\right)^2, \tag{4.61}$$

where we use σ/R_g as an expansion parameter whose leading contribution scales with N as $\alpha N^{-\nu}$, $\nu = 0.588$. Most importantly, the numeric constant α that depends on the architecture of the polymer is, as can be seen in Figure 4.8, generally larger for rings in comparison to linear chains and therefore the contribution arising from the term $(\sigma/R_g)\ \phi_1\left(z/R_g\right)$ becomes negligible only for the rings with larger polymerization index N. Finally, in the scaling limit, i.e. for a large enough N, $\beta U_{\text{eff}}(z)$ attains a universal (although, architecture-dependent) functional form $\phi_0(z/R_g)$.

Furthermore, it is interesting to compare typical energies of rings and chains in the presence of the hard wall. In the following, we consider the ring with $N = 250$ and the chain with $N = 100$ monomers, i.e. in the apparent scaling limit. As can be seen in Figure 4.11, the energy of rings not only considerably exceeds that of chains, but also increases steeper with smaller z. For instance, we observe that $\beta U_{\text{rw}}(z = 1R_g) \simeq 0.8$ and

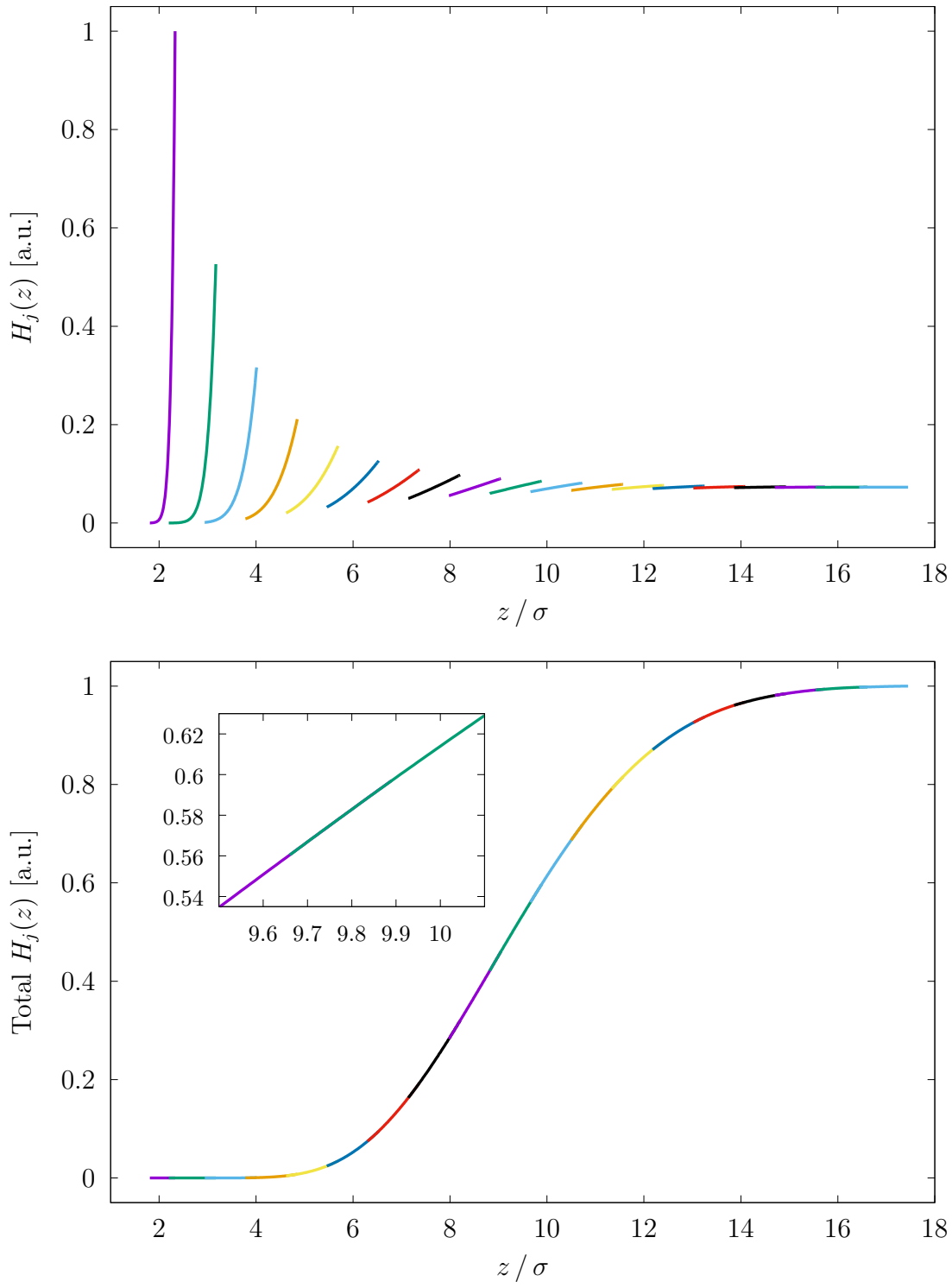

Figure 4.9: Top: the ring-wall distance histograms obtained for the ring with $N = 220$ monomers. In this particular case, we used $N_w = 19$ sampling windows of width $\Delta r_j = 1.08\sigma$, centered at $r_j = (0.12 + j \cdot 0.84)\sigma$ with $j = 1, 2, \ldots, N_w$. The overlap between two neighboring windows equals 0.2σ. Bottom: the corresponding total histogram (proportional to the modified distribution function $\tilde{P}(z)$) The zoomed in subgraph demonstrates the overlap region between two neighboring windows after the joining procedure. The y-axis has an arbitrary scale unit.

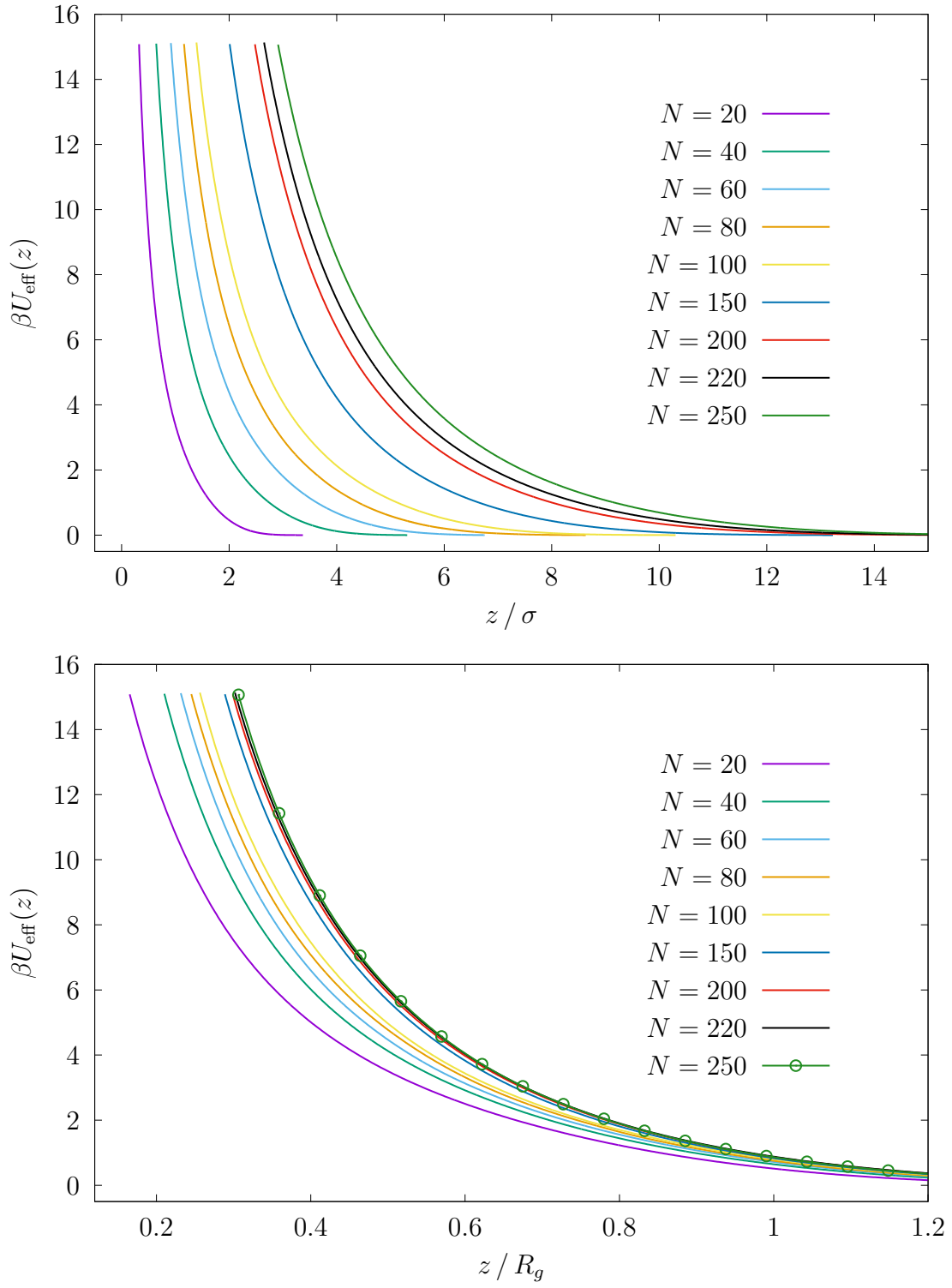

Figure 4.10: Main result: the effective potentials of flexible, unknotted ring polymers on planar, hard walls scaled with LJ-unit σ (top) and with the gyration radius of the polymers R_g at infinite dilution (bottom) calculated for increasing degree of polymerization N. Scaling of the effective potential $U_{\text{eff}}(z)$ becomes evident for $N > 200$.

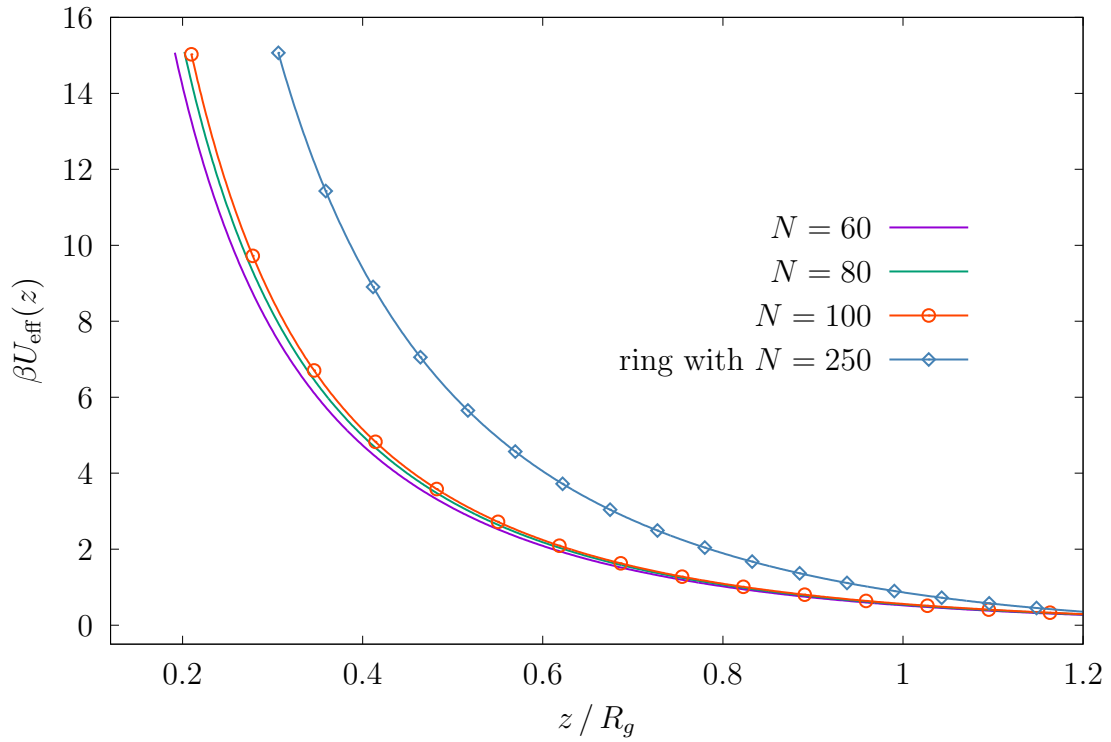

Figure 4.11: The effective potentials of linear polymers on planar, hard walls scaled with the gyration radius R_g at infinite dilution. Seemingly, the effective potential $U_{\text{eff}}(z)$ for linear chains reaches the scaling limit already for $N > 100$.

$\beta U_{\text{cw}}(z = 1R_g) \simeq 0.5$, whereas at $z = 0.5R_g$ we have that $\beta U_{\text{rw}}(z = 0.5R_g) \simeq 6$ and $\beta U_{\text{cw}}(z = 0.5R_g) \simeq 3.3$. We note that the configurations of rings close to the wall are extremely improbable compared to the free polymer case: rings elongate along the wall 4.12 to approach it closer, thereby increasing their size (typical values of R_g) and thus their own energy.

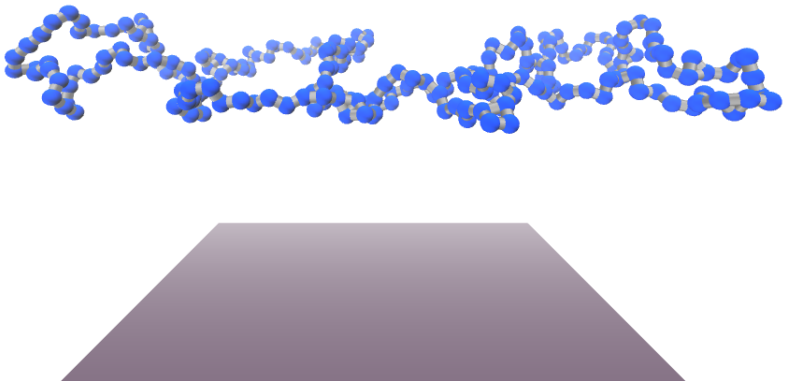

Figure 4.12: Typical conformation of ring polymers with z_{cm} fixed close to the planar, hard wall: ring elongates along the axis parallel to the wall and shrinks in the two other directions.

4.2.3 Effective wall-ring CM potential in the scaling limit

In this section, we provide an analytic expression (data fit) for the effective wall-ring CM potential in the scaling regime that can accurately describe the simulation data. For this purpose, we use the ring with $N = 220$ monomers, for which we sampled the best statistics.

First of all, from a log-log plot of the effective wall-ring CM potential 4.13 we conclude that in the region with $z < 0.5R_g$ the function $\beta U_{\text{eff}}(z)$ predominantly behaves as z^{-1}. This is exactly the same situation as observed for the effective wall-linear polymer CM potential [23].

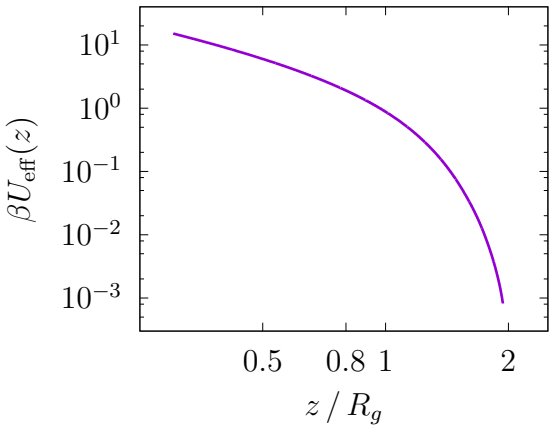

Figure 4.13: A log-log plot of the effective ring-wall potential for the ring with $N = 220$ monomers.

Moreover, for $z < 0.8R_g$ the functional form of $\beta U_{\text{eff}}(z)$ can be accurately modeled using the repulsive Yukawa potential

$$\beta U_{\text{Yukawa}}(z) = g\,\frac{\exp\left(-\kappa z/R_g\right)}{z/R_g}, \quad (4.62)$$

whereas in the region with $z > 0.8R_g$ the potential decays faster than the expression (4.62) and therefore we employ a Gaussian fit function:

$$\beta U_{\text{Gauss}}(z) = A\,\exp\left(-\left(\frac{z-b}{wR_g}\right)^2\right), \quad (4.63)$$

which can describe the simulation data correctly.

In summary, the effective wall-ring CM potential can be written as follows:

$$\beta U_{\text{eff}}(z) = (1-\chi(z))\cdot\beta U_{\text{Yukawa}}(z) + \chi(z)\cdot\beta U_{\text{Gauss}}(z), \quad (4.64)$$

where $\chi(z)$ is a mixing function used to join the two aforementioned regions. It has the following form:

$$\chi(z) = \frac{1}{2}\Big[\tanh\left(\delta\left(z-z_0\right)/R_g\right)+1\Big]. \quad (4.65)$$

Table 4.2: Fit parameters

	βU_{Yukawa}		βU_{Gauss}			χ	
	g	κ	A	bR_g^{-1}	w	δ	$z_0R_g^{-1}$
value	8.700	2.161	2.96	0.337	0.598	11.4	0.887
std. error	0.004	0.001	0.01	0.002	0.001	0.3	0.002

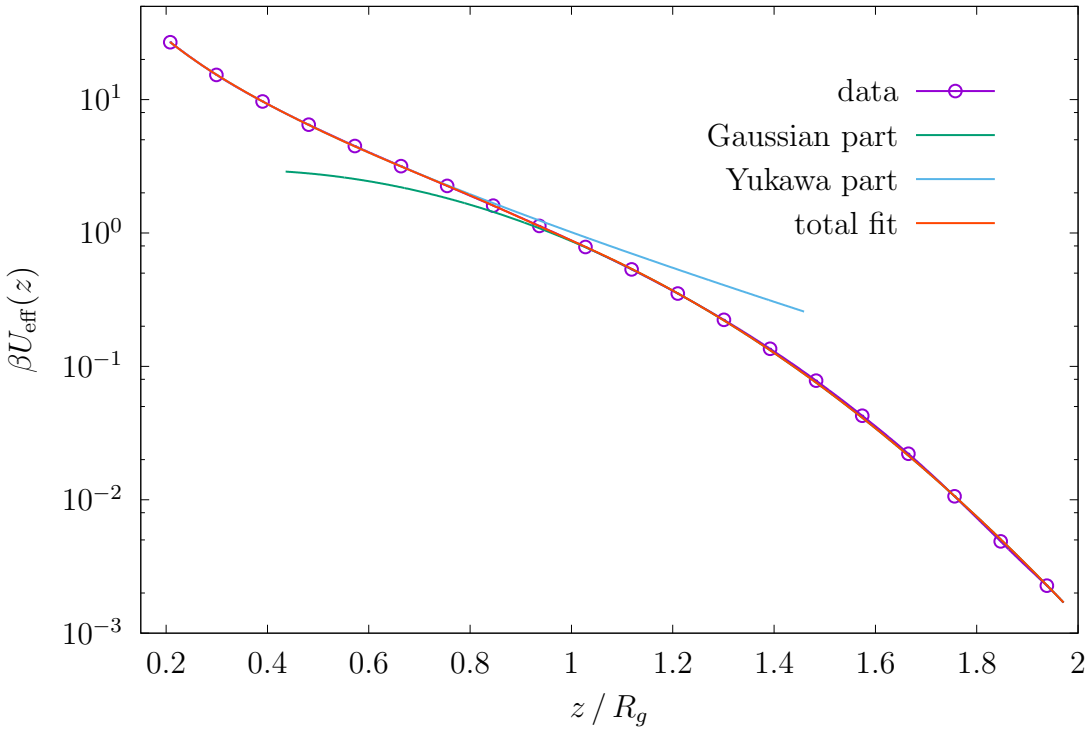

Figure 4.14: Comparison between the measured potential $\beta U_{\text{eff}}(z)$ and the employed fit model (4.64).

All the numeric parameters in the expressions (4.62), (4.63), and (4.65) are obtained by means of a standard fitting procedure and are listed in Table 4.2. Finally, comparison between the obtained data and the fit (4.64) is displayed in Figure 4.14.

Chapter 5

Density Functional Study of Ring Polymer Solutions

In this chapter, we will study the structure of fluids containing ring polymers modeled as ultrasoft colloids interacting via the effective pair potential (3.34).

To begin with, in Section 5.1 we will consider homogeneous ring polymer fluids and we will obtain their radial distribution functions and the corresponding structure factors at various bulk densities. Next, in Section 5.2 and in Section 5.3 we will study inhomogeneous ring polymer solutions in contact with one and two hard walls, respectively, employing the methods of density functional theory (DFT). As a result, we will obtain the inhomogeneous density profiles, which, on the other hand, allow to compute the surface tension at the wall-liquid interface in the single wall case and the depletion potential between two hard walls immersed in a "sea" of ring polymers.

In order to show differences in behavior of ring and linear polymer solutions, for all of the problems considered we will compute the corresponding quantities for linear chains modeled as repulsive Gaussian particles interacting via (3.31).

5.1 Structure of homogeneous ring polymer solutions

Let us consider homogeneous ring and linear polymer solutions. Because of the translational invariance of the Hamiltonian of a homogeneous fluid, its single-particle density attains a constant value:

$$\rho^{(1)}(\mathbf{r}) = \left\langle \sum_{i=1}^{N} \delta(\mathbf{r} - \mathbf{r}_i) \right\rangle = \rho_b, \tag{5.1}$$

whereas its two particle density $\rho^{(2)}(\mathbf{r},\mathbf{r}')$ defined as

$$\rho^{(2)}(\mathbf{r},\mathbf{r}') = \left\langle \sum_{i=1}^{N} \delta(\mathbf{r}-\mathbf{r}_i) \sum_{j=1}^{N} \delta(\mathbf{r}'-\mathbf{r}_j) - \sum_{i=1}^{N} \delta(\mathbf{r}-\mathbf{r}_i)\delta(\mathbf{r}'-\mathbf{r}_i) \right\rangle \tag{5.2}$$

depends on the magnitude of the vector $\mathbf{r}'-\mathbf{r}$ only: $\rho^{(2)}(\mathbf{r},\mathbf{r}') = \rho^{(2)}(|\mathbf{r}-\mathbf{r}'|)$. For the determination of the pair structure of a classical fluid, our main interest lies in the radial distribution function $g(|\mathbf{r}-\mathbf{r}'|)$, which can be defined through the two particle density:

$$\rho^{(2)}(|\mathbf{r}-\mathbf{r}'|) = \rho_b^2\, g(|\mathbf{r}-\mathbf{r}'|) \tag{5.3}$$

and which is proportional to the probability density of finding a particle at $\mathbf{r}'$ under the condition that another is placed at $\mathbf{r}$.

The radial distribution function of a fluid is related to its structure factor $S(k)$, which can be computed as the Fourier transform of the total correlation function $h(r) = g(r)-1$:

$$S(k) = 1 + \rho_b \int d\mathbf{r}\, e^{-i\mathbf{k}\cdot\mathbf{r}} h(r). \tag{5.4}$$

Radial symmetry of the total correlation function $h(r)$ implies that the structure factor $S(k)$ depends on the magnitude of the wavevector $\mathbf{k}$ only. Furthermore, the integrals involving angles in the expression (5.4) can be easily carried out and $S(k)$ reduces to the following form:

$$S(k) = 1 + \frac{4\pi\rho_b}{k} \int_0^{+\infty} dr\, r \sin(kr) h(r). \tag{5.5}$$

In the limit $k \to 0$, the structure factor is proportional to the isothermal compressibility χ_T of the system [24] and we immediately obtain that

$$S(0) = \rho_b k_B T \chi_T = 1 + 4\pi\rho_b \int_0^{+\infty} dr\, r^2 h(r). \tag{5.6}$$

Lastly, $S(k)$ is an important measurable quantity [24] (proportional to the total scattering intensity of a particle beam from a fluid sample), which provides a direct way of testing theoretical predictions for the radial distribution function g.

Therefore, our main goal in this section is to compute the radial distribution function $g(r)$ and the structure factor $S(k)$ for the effective models of ring and linear polymer solutions. In order to address this problem, we will employ integral equation theories based on the exact Ornstein-Zernike relation [24, 1]:

$$h(r) = c(r) + \rho \int d\mathbf{r}'\, h(r') c\left(|\mathbf{r}-\mathbf{r}'|\right), \tag{5.7}$$

which introduces the direct correlation function $c(r)$. Obviously, we need a functional form of $c(r)$ or a relation between $c(r)$ and $h(r)$ to be able to solve the integral equation

(5.7). This ingredient is unknown in general and defines our approximation. Without going into much detail, for all purposes in this section we will use the hypernetted chain closure (HNC) that delivers accurate results for long-range, soft potentials [1]:

$$h(r) = \exp\left(-\beta u(r) + h(r) - c(r)\right) - 1, \tag{5.8}$$

where $u(r)$ is the interparticle pair potential. Other closure relations and their range of applicability can be found, for instance, in references [1] and [24]. Finally, let us note that the equation (5.7) can be solved numerically employing an iterative scheme. The convolution term $\int d\mathbf{r}'\, h(r')c\left(|\mathbf{r} - \mathbf{r}'|\right)$ in the equation (5.7) can be computed efficiently in the Fourier space, since $c(r)$ and $h(r)$ are radially symmetric functions, whose Fourier transforms can be reduced to one-dimensional integrals.

Before focusing on ring polymers, let us consider linear polymer solutions. The interaction between linear chains is modeled by means of the effective Gaussian pair potential, which yields an excellent approximation in the case of an athermal solvent:

$$\beta u(r) = \epsilon \exp\left(-\left(r/\sigma\right)^2\right), \tag{5.9}$$

where $\epsilon \approx 2$ and σ defines the length scale of the system. The obtained for increasing bulk density ρ_b radial distribution functions $g(r)$ and the corresponding structure factors $S(k)$ are shown in Figure 5.1. It is worth emphasizing some representative properties of this model [1]. First of all, at the considered reduced temperature $T^* = k_B T/\epsilon = 0.5$, $g(r)$ has a finite non-zero value at $r = 0$, which means that particles at any density are allowed to fully overlap each other. Secondly, $g(r)$ approaches unity at high densities, i.e. the system becomes ideal. Thirdly, the main peak of the structure factor $S(k)$ lies far below the empirical Hansen-Verlet value [52, 53] 2.85, which signals that the system is far from crystallization.

Next, let us consider the structure of ring polymer solutions. The interaction between ring polymers is given by the following pair potential (r is given in units of R_g):

$$\beta u(r) = U_0 \begin{cases} \frac{4\pi}{3} R_<^3, & \text{for } 0 \le r < R_-, \\ \frac{\pi}{12r}(r^2 + 2R_+ r - 3R_-^2)(R_+ - r)^2, & \text{for } R_- \le r < R_+, \\ 0, & \text{for } r \ge R_+, \end{cases} \tag{5.10}$$

with $U_0 = 1.434, R_> = 1.419, R_< = 1.000, R_+ = 2.419$, and $R_- = 0.419$. The effective potential (5.10) provides a very good approximation up to the bulk density $\rho^\star R_g^3 \approx 0.2$ and, therefore, we will only consider values of ρ_b that do not exceed it significantly. The resulting radial distribution functions $g(r)$ and structure factors $S(k)$ are shown in Figure

5.1 and we can clearly see their qualitative difference in comparison to the linear polymer case. In particular, a local maximum of $g(r)$ forms at $r = 0$ and rises for increasing ρ_b, which corresponds to the formation of clusters, as mentioned in Section 3.4.

This property of the effective model of ring polymer fluids hinges on the form of the effective interaction potential (5.10). More specifically, it belongs to the $k^{\pm}$-class of nonattractive potentials, whose Fourier transforms contain negative components [54, 34]. In contrast, pair potentials with exclusively positive Fourier components (e.g., the Gaussian pair potential (5.9)) belong to the k^{+}-class and their characteristic feature is the formation of a local minimum of the radial distribution function $g(r)$ at $r = 0$. This is exactly the behavior that can be observed for the Gaussian core model in Figure 5.1.

Now, in the mean-field approximation (MFA) which is exact in the limit of high temperature and/or density, the direct correlation function $c(r)$ of the system is given by

$$c(r) = -\beta v(r) \tag{5.11}$$

and, therefore, its structure factor $S(k)$ can be explicitly written using (5.7) as follows:

$$S(k) = \frac{1}{1 + \rho\beta\hat{u}(k)}. \tag{5.12}$$

It can be easily seen from the denominator of the equation (5.12) that for the $k^{\pm}$-potentials $S(k)$ attains its maximum value at the wavevector k^* where $\hat{u}(k)$ has a minimum. This is precisely what happens in our effective model of ring polymers, as well as in the GEM-4 model with the pair potential $\beta u(r) = \epsilon \exp\left(-(r/\sigma)^4\right)$, correlation functions and structure factors of which are shown in Figure 5.3 [34]. In fact, all of the pair potentials of the form $\beta u(r) = \epsilon \exp\left(-(r/\sigma)^m\right)$ with $m > 2$ belong to the $k^{\pm}$-class [34].

Furthermore, this maximum diverges for the set of points $(\rho_\lambda,\ T_\lambda)$ satisfying

$$\rho_\lambda \beta_\lambda = -1/\hat{u}_{\text{eff}}(k_*). \tag{5.13}$$

The equation (5.13) defines a λ-line [34, 55]. According to the MFA, the fluid is absolutely unstable for densities $\rho \geq \rho_\lambda$ on the $(\rho,\ T)$-plane and, therefore, it has to undergo a phase transition to a crystalline state.

Moreover, by inspecting the Fourier transform of the effective pair potential (5.10) between ring polymers shown in Figure 3.1, we obtain the following value of ρ_λ:

$$\rho_\lambda R_g^3 \approx 1.19. \tag{5.14}$$

Finally, it should be noted that the coarse-grained model (5.10) does not describe adequately the behavior of ring polymer solutions for densities much higher than the value $\rho^\star R_g^3 \approx 0.2$, since the clustering scenario cannot be reproduced in the full monomer-resolved simulations.

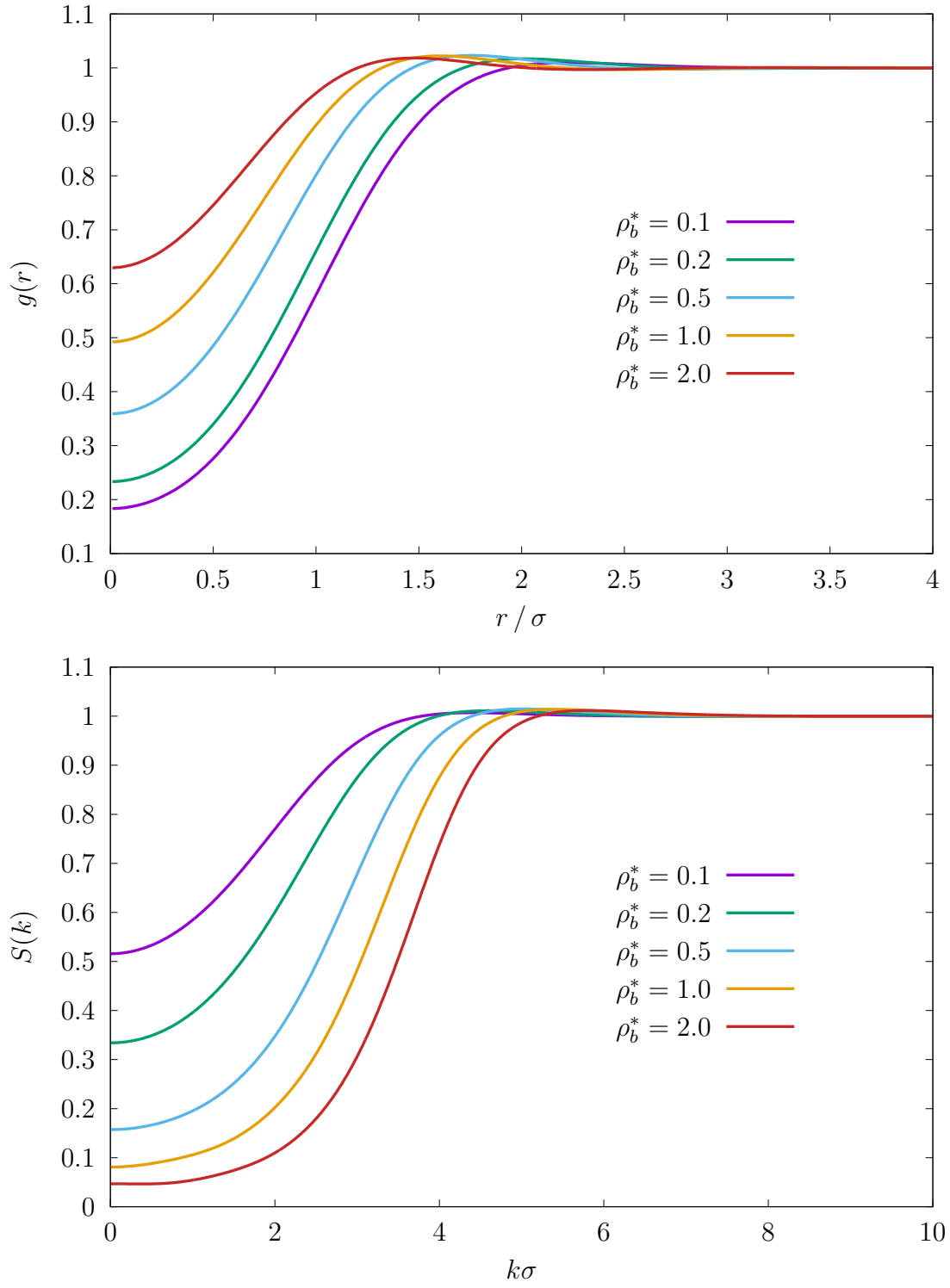

Figure 5.1: The radial distribution function $g(r)$ and the structure factor $S(k)$ of a linear polymer solution modeled using the effective Gaussian pair potential (5.9) at reduced temperature $T^* = k_B T/\epsilon = 0.5$ calculated for increasing bulk density $\rho_b^* = \rho_b \sigma^3$.

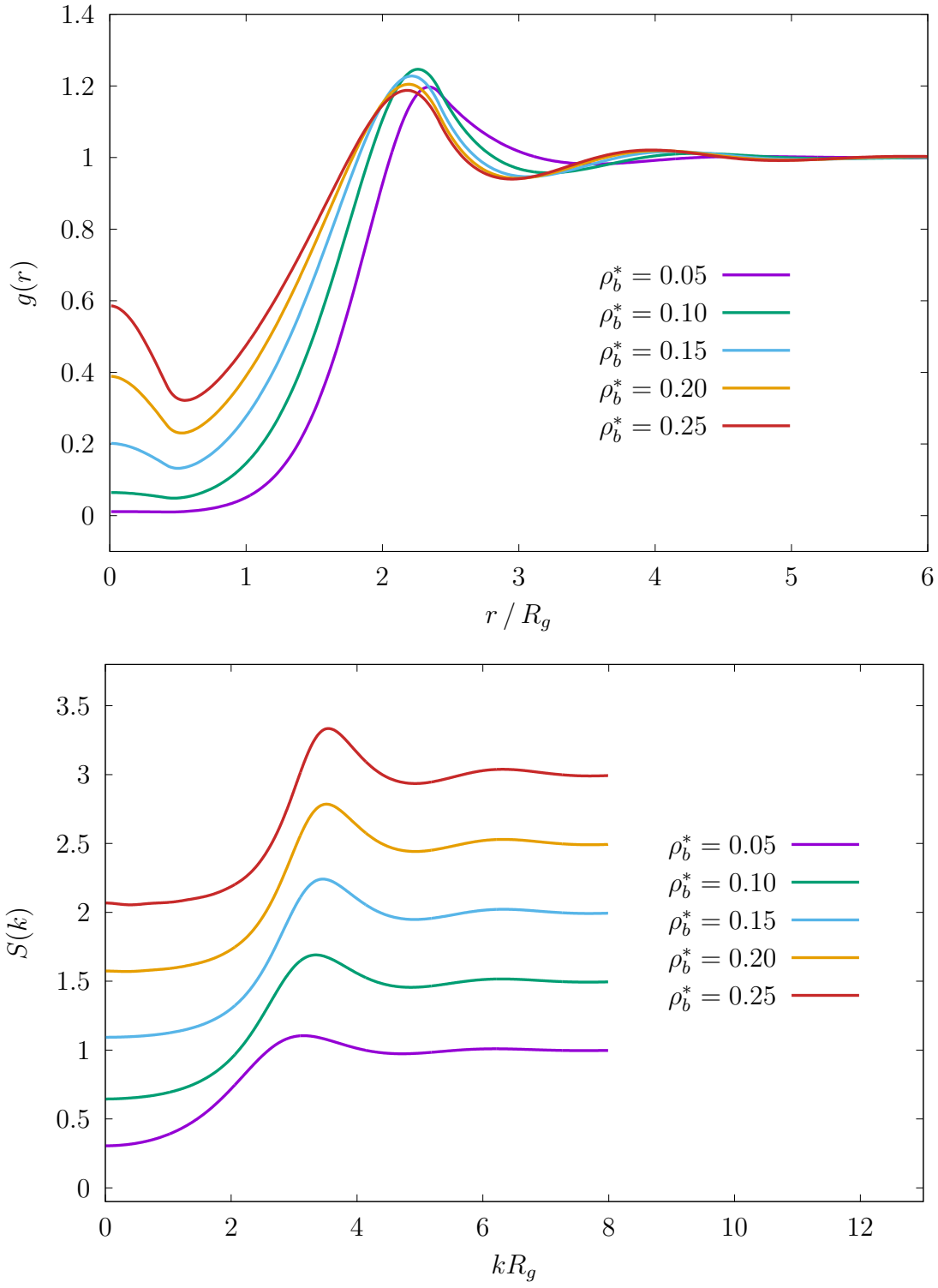

Figure 5.2: The radial distribution function $g(r)$ and the structure factor $S(k)$ of a ring polymer solution modeled using the effective pair potential (5.10) at reduced temperature $T^* = 1$ calculated for increasing bulk density $\rho_b^* = \rho_b R_g^3$. For clarity, the $S(k)$ curves have been shifted vertically by the following constant values indicated in the brackets: $\rho_b^* = 0.05$ [0], $\rho_b^* = 0.10$ [0.5], $\rho_b^* = 0.15$ [1.0], $\rho_b^* = 0.20$ [1.5], $\rho_b^* = 0.25$ [2.0].

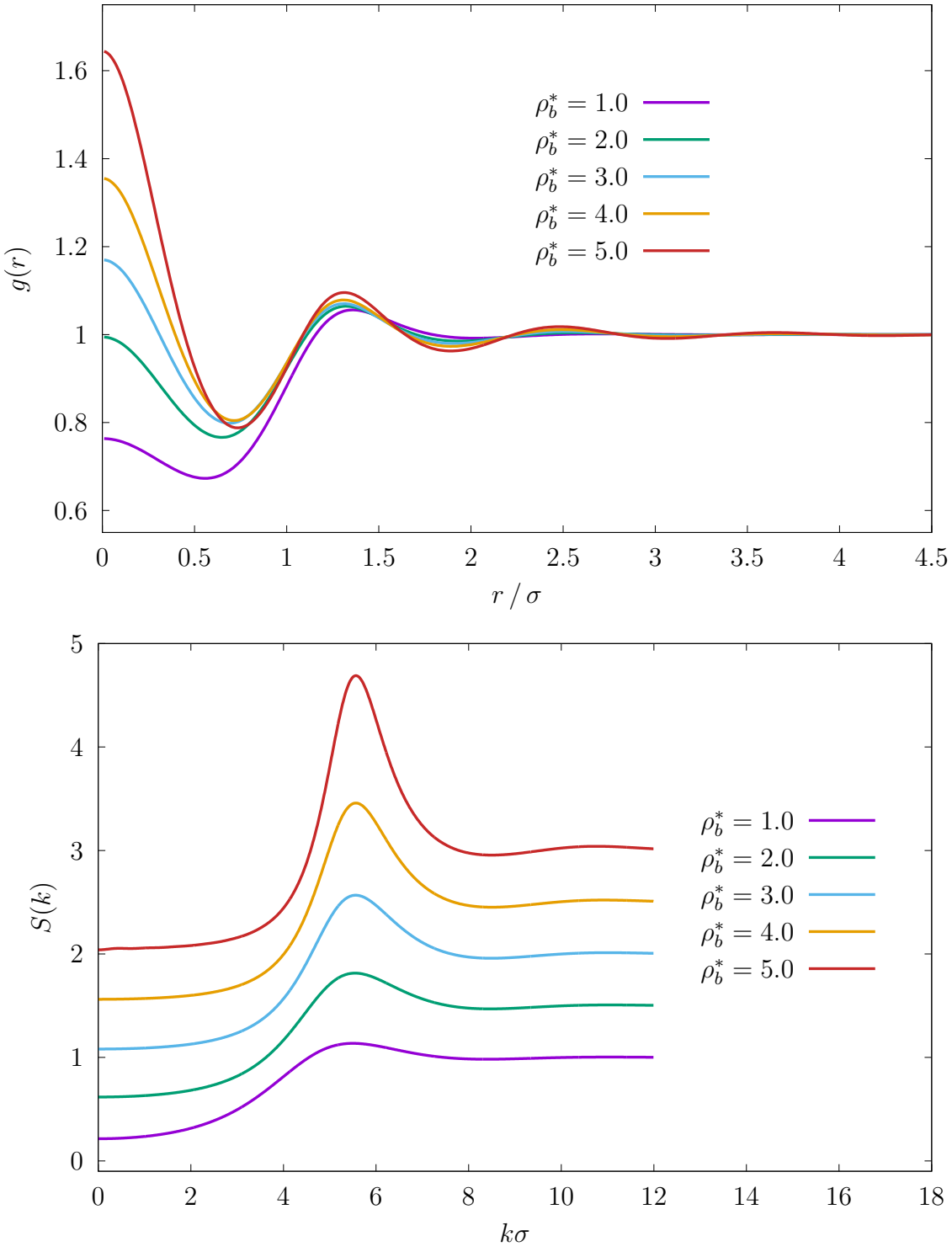

Figure 5.3: The radial distribution function $g(r)$ and the structure factor $S(k)$ of the GEM-4 model at reduced temperature $T^* = 1$ calculated for increasing bulk density $\rho_b^* = \rho_b\sigma^3$. For clarity, the $S(k)$ curves have been shifted vertically by the following constant values indicated in the brackets: $\rho_b^* = 1.0$ [0], $\rho_b^* = 2.0$ [0.5], $\rho_b^* = 3.0$ [1.0], $\rho_b^* = 4.0$ [1.5], $\rho_b^* = 5.0$ [2.0].

5.2 Ring polymer solutions in contact with a planar, hard wall

5.2.1 Structure of the equilibrium density profiles

Let us consider a ring polymer solution in contact with a planar, hard wall. Without loss of generality we assume that the system is enclosed by a large box with volume L^3 and that the wall is located at $z = 0$ and confines the fluid to a half-space $z \geq 0$ (note that the z-axis is orthogonal to the wall). Therefore, the geometry of our setup implies that $\rho(z) = 0$ for $z < 0$. As we will see, under such conditions, the equilibrium single particle density of the ring polymer fluid will be inhomogeneous due to the interaction with the hard wall, although dependent only on the distance away from it, that is, only on the z-coordinate: $\rho(\mathbf{r}) \equiv \rho(z)$. Finally, we adopt the gyration radius R_g of the polymers as the fundamental length scale of the system.

DFT represents a powerful tool for studying inhomogeneous systems [24]. It hinges on two fundamental theorems, which trace back to the original developments of Hohenberg and Kohn for quantum many-electron systems[56, 57], that in the realm of classical statistical mechanics [58] state:

1. In the grand canonical ensemble (that is, at fixed T, V, μ), the grand potential Ω of a system subject to an external potential $U_{\text{ext}}(\mathbf{r})$ is a *unique functional* of the equilibrium single-particle density $\rho_0(\mathbf{r})$ (from this point onwards we will denote the single-particle density without the superscript $^{(1)}$).

2. Consequently, the equilibrium single-particle density $\rho_0(\mathbf{r})$ can be obtained by minimizing the grand potential functional $\Omega[\rho]$ with respect to $\rho(\mathbf{r})$:

$$\left.\frac{\delta\Omega[\rho]}{\delta\rho(\mathbf{r})}\right|_{\rho(\mathbf{r})=\rho_0(\mathbf{r})} = 0. \tag{5.15}$$

   In order to solve the resulting equation (5.15), an explicit form of the grand potential functional is needed. Nevertheless, in general there exists no exact expression for $\Omega[\rho]$ and quality of our results depends heavily on the approximation employed.

Therefore, the grand potential functional $\Omega[\rho]$ of our model fluids can be written as

$$\Omega[\rho] = F[\rho] + \int d\mathbf{r}\, \rho(\mathbf{r}) U_{\text{ext}}(\mathbf{r}) - \mu \int d\mathbf{r}\, \rho(\mathbf{r}), \tag{5.16}$$

where $F[\rho] = F_{\text{id}}[\rho] + F_{\text{ex}}[\rho]$ is the free energy functional consisting of the ideal $F_{\text{id}}[\rho]$ and the excess, interaction part $F_{\text{ex}}[\rho]$, $\mu = \text{const}$ denotes the fixed value of the chemical

potential of the fluid, and $U_{\text{ext}}(\mathbf{r})$ stands for the external potential to which the fluid is subject (more specifically, in our case this is the effective interaction between the ring polymers and the hard wall obtained numerically in the previous chapter). The ideal free-energy part is given by the well-known functional [24, 59, 58]

$$F_{\text{id}}[\rho] = \beta^{-1} \int d\mathbf{r}\, \rho(\mathbf{r}) \left[\ln\left(\rho(\mathbf{r})\Lambda^3\right) - 1 \right], \tag{5.17}$$

whereas the excess part $F_{\text{ex}}[\rho]$ is modeled using the mean-field approximation (MFA) functional, which has been proven to deliver accurate results for ultrasoft pair potentials [59, 60, 54] (i.e., those that satisfy the integrability condition $\int_0^\infty dr\, r^2 u(r) < \infty$):

$$F_{\text{ex}}[\rho] = \frac{1}{2} \iint d\mathbf{r} d\mathbf{r}'\, \rho(\mathbf{r})\rho(\mathbf{r}') u\left(|\mathbf{r} - \mathbf{r}'|\right), \tag{5.18}$$

where $u\left(|\mathbf{r} - \mathbf{r}'|\right)$ denotes the effective pair potential between two ring polymers given by the expression (3.34).

In order to apply the minimization principle (5.15) to our grand potential functional (5.16), we briefly remind here the basic rule of functional differentiation:

$$\frac{\delta F[\rho]}{\delta \rho(\mathbf{r})} = \lim_{\epsilon \to 0} \left(\frac{F[\rho(\mathbf{r}') + \epsilon\delta(\mathbf{r}' - \mathbf{r}))] - F[\rho(\mathbf{r}')]}{\epsilon} \right) \tag{5.19}$$

As a result, in a straightforward way we obtain the following functional derivatives for each constituent of the grand potential functional (5.16):

$$\frac{\delta}{\delta \rho(\mathbf{r})} \left(\mu \int d\mathbf{r}'\, \rho(\mathbf{r}') \right) = \mu, \tag{5.20}$$

$$\frac{\delta F_{\text{id}}\left[\rho\right]}{\delta \rho(\mathbf{r})} = \beta^{-1} \ln\left(\rho(\mathbf{r})\Lambda^3\right), \tag{5.21}$$

$$\frac{\delta F_{\text{ex}}^{\text{MFA}}\left[\rho\right]}{\delta \rho(\mathbf{r})} = \int d\mathbf{r}'\, \rho(\mathbf{r}') u\left(|\mathbf{r} - \mathbf{r}'|\right). \tag{5.22}$$

$$\frac{\delta}{\delta \rho(\mathbf{r})} \left(\int d\mathbf{r}'\, \rho(\mathbf{r}') U_{\text{ext}}(\mathbf{r}') \right) = U_{\text{ext}}(\mathbf{r}), \tag{5.23}$$

Thus, we end up with the following integral equation for the equilibrium density profile that we will be aiming to solve in this chapter:

$$\beta\mu = \beta U_{\text{ext}}(\mathbf{r}) + \ln\left(\rho(\mathbf{r})\Lambda^3\right) + \int d\mathbf{r}'\, \rho(\mathbf{r}') \beta u\left(|\mathbf{r} - \mathbf{r}'|\right). \tag{5.24}$$

It is important to explore symmetries of the equation (5.24), in order to simply further calculations. First of all, in Chapter 4 we have established that the effective potential between the center of mass of the ring polymer and the hard wall depends only on the z-coordinate: $U_{\text{ext}}(\mathbf{r}) \equiv U_{\text{ext}}(z)$, which means, as expected, that the resulting density

obtained from the equation (5.24) must also depend on the z-coordinate only due to the preservation of the translation symmetry in the x- and y-directions: $\rho(\mathbf{r}) \equiv \rho(z)$. Thus, the equation (5.24) in the thermodynamic limit ($N, L \to \infty$, $N/L^3 = \text{const}$) can be recast as follows:

$$\beta\mu = \beta U_{\text{ext}}(z) + \ln\left(\rho(z)\Lambda^3\right) + \int_{-\infty}^{+\infty} dz'\, \rho(z')\beta\bar{u}\left(|z - z'|\right), \tag{5.25}$$

where we have introduced the following shorthand:

$$\beta\bar{u}\left(|z - z'|\right) = \int_{-\infty}^{+\infty} dx' \int_{-\infty}^{+\infty} dy'\, \beta u\left(\sqrt{|x - x'|^2 + |y - y'|^2 + |z - z'|^2}\right). \tag{5.26}$$

In the case of the effective ring-ring pair potential (5.10), the double integral (5.26) can be evaluated analytically and $\beta\bar{u}\left(|z - z'|\right)$ attains the following functional form:

$$\beta\bar{u}\left(|z - z'|\right) = U_0 \frac{\pi^2}{6} \begin{cases} 8R_<^3\left(R_-^2 - |z - z'|^2\right) + C\left(R_-, R_+\right), & \text{for } 0 \le |z - z'| \le R_-, \\ -\frac{|z-z'|^5}{5} + \left(R_-^2 + R_+^2\right)|z - z'|^3 - \\ \quad R_+\left(R_+^2 + 3R_-^2\right)|z - z'|^2 + \\ \quad 3R_-^2 R_+^2|z - z'| + \frac{R_+^5}{5} - R_-^2 R_+^3, & \text{for } R_- \le |z - z'| \le R_+, \\ 0, & \text{for } |z - z'| \ge 0, \end{cases}$$

with the constant $C\left(R_-, R_+\right) = \frac{R_+^5}{5} + \frac{4R_-^5}{5} - R_- R_+\left(3R_-^3 + 2R_- R_+^2 - 4R_+ R_-^2\right)$.

Secondly, the geometry of our setup ensures that

$$U_{\text{ext}}(z) = \begin{cases} +\infty, & \text{for } z < 0, \\ U_{\text{eff}}(z), & \text{for } z \ge 0, \end{cases} \tag{5.27}$$

where $U_{\text{eff}}(z)$ is the effective potential between the ring polymers and the hard wall. From (5.27) it follows that the density $\rho(z)$ is identically vanishing in the region with $z < 0$ and for $z \ge 0$ we obtain the following integral equation:

$$\beta\mu = \beta U_{\text{eff}}(z) + \ln\left(\rho(z)\Lambda^3\right) + \int_0^{+\infty} dz'\, \rho(z')\beta\bar{u}\left(|z - z'|\right) \tag{5.28}$$

together with the boundary condition

$$\lim_{z \to +\infty} \rho(z) = \rho_b, \tag{5.29}$$

where ρ_b is the bulk density of the fluid (i.e., the density far away from the hard wall).

Thirdly, for practical purposes that will be seen later on we replace the fixed value of the chemical potential μ of the ring polymer fluid with its bulk density $\rho_b = \text{const}$ in the equation (5.28) using the identities

$$F[\rho_b] = N\beta^{-1}\left[\ln\left(\rho_b\Lambda^3\right) - 1\right] + \frac{1}{2}N\rho_b u_0, \quad u_0 = \int d\mathbf{r}\, u(|\mathbf{r}|), \tag{5.30}$$

$$\mu = \left(\frac{\partial F[\rho_b]}{\partial N}\right)_{T,V} = \beta^{-1} \ln\left(\rho_b \Lambda^3\right) + \rho_b u_0. \tag{5.31}$$

As a result, the equation (5.28) can be recast as follows:

$$\rho_b \int_{-\infty}^{+\infty} dz'\, \beta\bar{u}(|z-z'|) = \beta U_{\text{eff}}(z) + \ln\left(\rho(z)/\rho_b\right) + \int_0^{+\infty} dz'\, \rho(z')\beta\bar{u}\left(|z-z'|\right), \tag{5.32}$$

where the integral on the left hand side of the equation above is simply the constant u_0 rewritten with the help of its translational invariance:

$$u_0 = \int d\mathbf{r}\, u(|\mathbf{r}|) = \int_{-\infty}^{+\infty} dz'\, \bar{u}(|z'|) \equiv \int_{-\infty}^{+\infty} dz'\, \bar{u}(|z-z'|). \tag{5.33}$$

Finally, for $z \geq 0$ we write

$$\rho(z) = \rho_b + \Delta\rho(z), \tag{5.34}$$

where the function $\Delta\rho(z)$ goes to zero for large values of z, whereas $\rho(z)$ approaches the constant value ρ_b at the same time. By substituting the relation (5.34) into (5.32), we obtain the final form of the original integral equation (5.24):

$$\begin{aligned} \ln\left(1 + \Delta\rho(z)/\rho_b\right) = -\beta U_{\text{eff}}(z) - \int_0^{+\infty} dz'\, \Delta\rho(z')\beta\bar{u}\left(|z-z'|\right) + \\ + \rho_b \int_z^{+\infty} dz'\, \beta\bar{u}(|z'|). \end{aligned} \tag{5.35}$$

Interestingly, the last term on the right hand side of the equation above acts as an effective attractive external potential between the ring polymer fluid and the hard wall.

Consequently, the equation (5.35) can be formally rewritten as follows:

$$\Delta\rho(z) = G\left[\Delta\rho\right](z), \tag{5.36}$$

where G is a functional of $\Delta\rho$, which has the following explicit form:

$$\begin{aligned} G[\Delta\rho](z) = \rho_b \Bigg(\exp\Bigg[- \beta U_{\text{eff}}(z) - \int_0^{+\infty} dz'\, \Delta\rho(z')\beta\bar{u}\left(|z-z'|\right) + \\ + \rho_b \int_z^{+\infty} dz'\, \beta\bar{u}(|z'|) \Bigg] - 1 \Bigg). \end{aligned} \tag{5.37}$$

We solve the equation (5.36) numerically in a self-consistent manner: we start with an initial guess for $\Delta\rho(z)$ (for instance, $\Delta\rho(z) = 0$) and then generate new iterations from the equation (5.35) until the self-consistency is reached. In order to ensure the convergence of our scheme, every new iteration $\Delta\rho^{(n+1)}$ is computed in the following way:

$$\Delta\rho^{(n+1)} = (1-\delta) \cdot \Delta\rho^{(n)} + \delta \cdot G\left[\Delta\rho^{(n)}\right], \tag{5.38}$$

where δ is a mixing parameter (typically, we use $\delta \approx 0.1$, although at higher bulk densities, close to the liquid-solid phase transition, $\rho(z)$ becomes highly oscillating and we have to use smaller values of δ that are of the order of 10^{-2}). Let us additionally note that the integral equation (5.36) contains only one free parameter which has to be specified at the beginning of each numerical calculation: the bulk density ρ_b.

Last of all, it is important to discuss the efficiency of our iterative algorithm (5.38). Since the term $\exp\left[-\beta U_{\text{eff}}(z) + \rho_b \int_z^{+\infty} dz'\, \beta\bar{u}(|z'|)\right]$ in the functional (5.37) does not depend on the running iteration of $\Delta\rho(z)$, it can be computed and stored once and for all on the given grid. The main difficulty lies in the computation of the convolution term $\int_0^{+\infty} dz'\, \Delta\rho(z')\beta\bar{u}\,(|z - z'|)$, which however can be done efficiently in the Fourier space employing the fast Fourier transform algorithm. Thus, the overall complexity per iteration of our scheme is $\mathcal{O}\,(N_G \log N_G)$, where N_G is the number of grid points.

Figure 5.4 displays the resulting density profiles $\rho(z)$ obtained for increasing bulk density. It is important to point out their crucial feature: the density profiles of the ring polymer solution in contact with the hard wall exhibit oscillatory behavior which intensifies with higher bulk density. As ρ_b approaches the critical value $\rho_\lambda R_g^3 \approx 1.19$, the system becomes highly unstable with the oscillations penetrating deeper into the bulk, which signals a freezing transition of the fluid. The development of instabilities in our system can be actually observed in Figure 5.5.

In addition, it is instructive to calculate the density profiles of a linear polymer solution in contact with the hard wall and to compare them to the ones obtained for the ring polymer solution. For this purpose, we use the same integral equation (5.35), although with an integrated effective Gaussian pair potential (5.9):

$$\beta\bar{u}(z) = 2\pi \exp\left(-(z/\sigma)^2\right) \tag{5.39}$$

and a repulsive Yukawa interaction with the wall [23]:

$$\beta U_{\text{eff}}(z) = \frac{\exp(-z/\sigma)}{z/\sigma}. \tag{5.40}$$

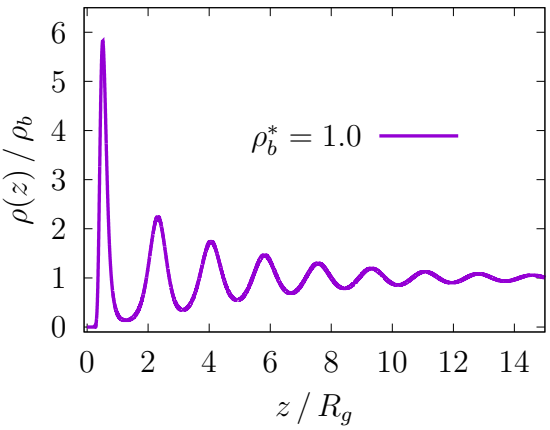

Figure 5.5: The model ring polymer fluid becomes highly unstable as the bulk density increases: even a small external disturbance may cause it to freeze.

The results are shown at the bottom of Figure 5.4: the obtained density profiles, in comparison to the ring polymer case, do not exhibit oscillatory behavior. We observe only a main peak close to the wall that rises sharply with higher density in the bulk.

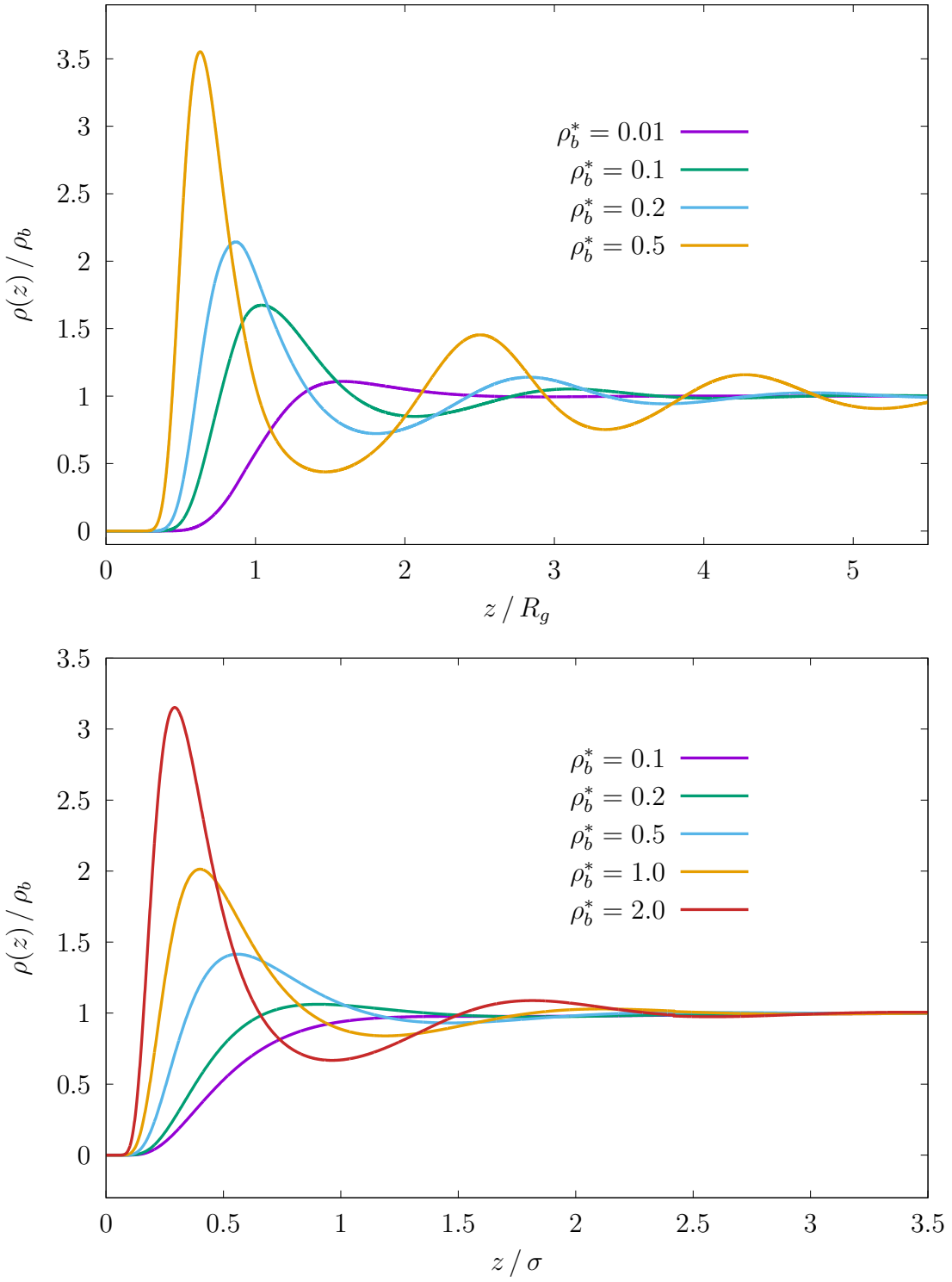

Figure 5.4: The inhomogeneous density profiles of the ring polymer solution (top) in contact with the planar, hard wall in comparison to those of the linear polymer solution (bottom) calculated for increasing reduced bulk density ρ_b^*. In the ring polymer case, the density profiles exhibit oscillatory behavior which intensifies with higher density in the bulk.

Finally, it is very important to emphasize the range of applicability of our calculations. As we have already discussed in Section 3.4, the coarse-grained representation of flexible ring polymers as 'ultrasoft' colloids interacting via the effective pair potential (5.10) breaks at the density $\rho^\star R_g^3 \approx 0.2$ and the clustering effect predicted by the $k^\pm$-class of the effective interaction potential is not reproducible in the monomer-resolved simulations. Nevertheless, as we can see in Figure 5.4, even in the dilute regime below the value $\rho^\star R_g^3 \approx 0.2$, the density profiles of the ring polymer solution in contact with the wall preserve their oscillatory behavior, which means that the depletion force acting between two plates (or two colloidal particles) immersed in the solution might also have a similar oscillatory form. This fact encourages us to study the depletion interaction between two parallel plates immersed in a "sea" of ring polymers.

5.2.2 Surface tension at the wall-liquid interface

The surface tension γ of an interface is defined as the work needed to increase it by unit area [24]. Therefore, an infinitesimal change of the grand potential of a system containing interfaces in thermodynamic equilibrium must include a term proportional to γ:

$$d\Omega = -SdT - PdV - Nd\mu + \gamma dA, \tag{5.41}$$

where dA denotes the change of the interfacial area. The equation (5.41) automatically implies that

$$\gamma = \left(\frac{\partial \Omega}{\partial A}\right)_{T,\,V,\,\mu}. \tag{5.42}$$

Moreover, because of the fact that $\Omega(T, V, A, \mu)$ is a homogeneous function of first order in A and V, the equation (5.41) can be integrated at fixed T and μ and yields the following expression for the grand potential [24]:

$$\Omega = -PV + \gamma A. \tag{5.43}$$

Therefore, the surface tension γ can be calculated through to the surface excess grand potential:

$$\gamma = \frac{\Omega + PV}{A} = \frac{\Omega^{(\mathrm{ex})}}{A}, \tag{5.44}$$

where $-PV$ is the bulk grand potential of the fluid Ω_b. Obviously, the values of the excess grand potential $\Omega^{(\mathrm{ex})}$ can be easily computed using the DFT methods. In particular, using the general expression for the grand potential functional (5.16), we immediately obtain the bulk term Ω_b:

$$\beta\Omega_b = -V\left(\rho_b + \frac{\rho_b^2 u_0}{2}\right), \tag{5.45}$$

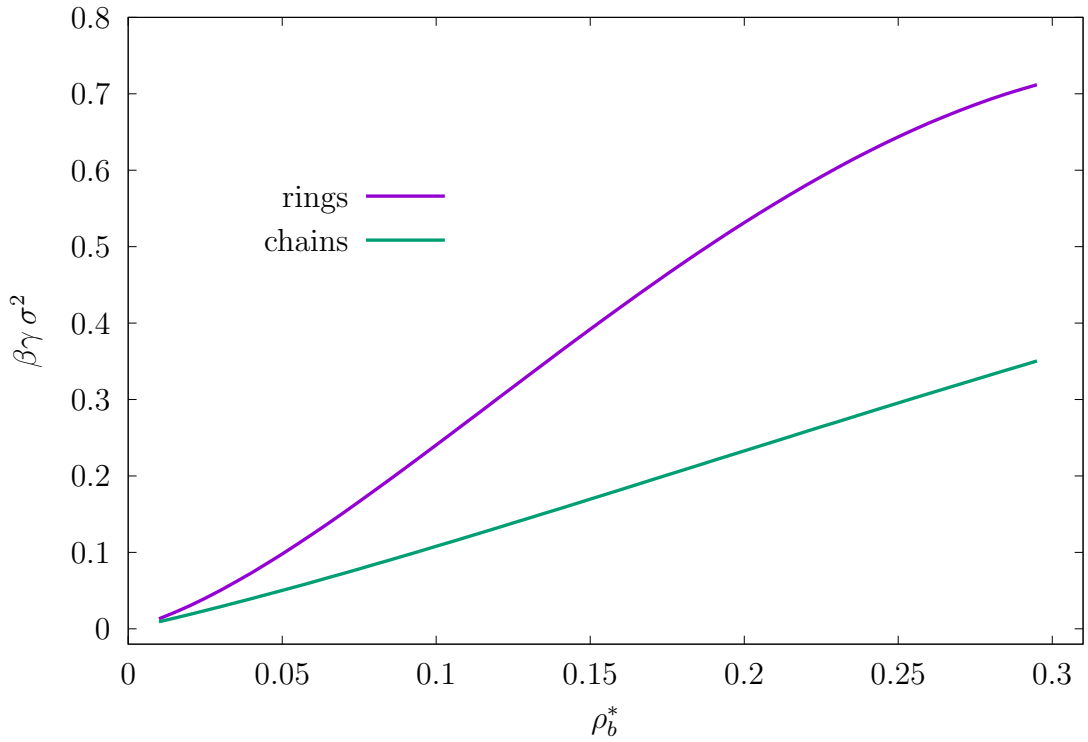

Figure 5.6: The surface tension at the wall-liquid interface in the case of the ring and linear polymer solution (for rings, $\sigma = R_g$) calculated for increasing reduced bulk density ρ_b^*.

where V is the volume of the system and the bulk pressure of the fluid P is given by

$$\beta P = \rho_b + \frac{\rho_b^2 u_0}{2}. \tag{5.46}$$

Accordingly, in the presence of the wall the total grand potential per unit area Ω_1/A of the fluid becomes:

$$\begin{aligned}\beta\Omega_1[\rho]/A = &\int_0^{+\infty} dz\,\rho(z)\left[\ln\left(\rho(z)\Lambda^3\right) - 1\right] - \left[\ln\left(\rho_b\Lambda^3\right) + \rho_b u_0\right]\int_0^{+\infty} dz\,\rho(z) + \\ &+ \int_0^{+\infty} dz\,\rho(z)\beta U_{\text{ext}}(z) + \frac{1}{2}\int_0^{+\infty} dz\,\rho(z)\int_0^{+\infty} dz'\,\rho(z')\beta\bar{u}(|z-z'|),\end{aligned} \tag{5.47}$$

where $\rho(z)$ is the equilibrium density profile. Consequently, the excess grand potential $\Omega_1^{(\text{ex})}$ in the presence of the wall can be directly calculated from the equation (5.47) using the identity $\rho(z) = \rho_b + \Delta\rho(z)$:

$$\begin{aligned}\beta\Omega_1^{(\text{ex})}[\rho]/A = &\int_0^{+\infty} dz\,\rho(z)\ln\left(\rho(z)/\rho_b\right) - (1+\rho_b u_0)\int_0^{+\infty} dz\,\Delta\rho(z) + \\ &+ \int_0^{+\infty} dz\,\rho(z)\beta U_{\text{ext}}(z) + \rho_b\int_0^{+\infty} dz\int_0^{+\infty} dz'\,\Delta\rho(z')\beta\bar{u}(|z-z'|) + \\ &+\frac{1}{2}\int_0^{+\infty} dz\,\Delta\rho(z)\int_0^{+\infty} dz'\,\Delta\rho(z')\beta\bar{u}(|z-z'|) - \\ &-\frac{\rho_b^2}{2}\int_0^{+\infty} dz\int_z^{+\infty} dz'\,\beta\bar{u}(|z'|).\end{aligned} \tag{5.48}$$

The resulting surface tension $\gamma = \Omega_1^{(\mathrm{ex})}/A$ at the wall-liquid interface in the case of the ring and linear polymer solution as a function of the bulk density ρ_b is shown in Figure 5.6.

5.3 Ring polymer fluids confined between two parallel walls

5.3.1 Structure of the equilibrium density profiles

In order to address the problem of the depletion force acting between two plates immersed in the ring polymer solution, let us first calculate the density profiles of the ring polymer fluid confined between two parallel, hard walls. In particular, we consider the following geometry of our setup: the first wall is placed at $z = 0$, whereas the second one is located at the distance $z = d > 0$ away from it. As in the previous problem, symmetry arguments imply that $\rho(\mathbf{r}) \equiv \rho(z)$. Moreover, in this case we expect that the resulting densities are reflection-invariant with respect to the plane $z = d/2$: $\rho(z) = \rho(d - z)$ for $0 \leq z \leq d$.

Since our current task is roughly analogous to the one considered in the previous section, let us start with the general integral equation (5.25):

$$\beta\mu = \beta U_{\mathrm{ext}}(z) + \ln\left(\rho(z)\Lambda^3\right) + \int_{-\infty}^{+\infty} dz'\, \rho(z')\beta\bar{u}\left(|z - z'|\right), \tag{5.49}$$

and let us take into account a modified form of the external potential induced by two hard walls:

$$U_{\mathrm{ext}}(z) = \begin{cases} U_{\mathrm{eff}}(z) + U_{\mathrm{eff}}(d - z), & \text{for } 0 \leq z \leq d, \\ +\infty, & \text{else.} \end{cases} \tag{5.50}$$

The form of the external potential (5.50) ensures that the density profiles are identically vanishing outside the region $0 \leq z \leq d$ and therefore the integral equation (5.49) for $0 \leq z \leq d$ takes the form

$$\begin{aligned} \rho_b \int_{-\infty}^{+\infty} dz'\, \beta\bar{u}(|z - z'|) = \beta U_{\mathrm{eff}}(z) + \beta U_{\mathrm{eff}}(d - z) + \\ + \ln\left(\rho(z)/\rho_b\right) + \int_0^d dz'\, \rho(z')\beta\bar{u}\left(|z - z'|\right), \end{aligned} \tag{5.51}$$

where we have used the fact that $\beta\mu = \ln\left(\rho_b\Lambda^3\right) + \rho_b \int_{-\infty}^{+\infty} dz'\, \beta\bar{u}(|z - z'|)$. This condition simply means that the density $\rho(z)$ attains the bulk value ρ_b at the point $z = d/2$, as the separation between the walls becomes very large.

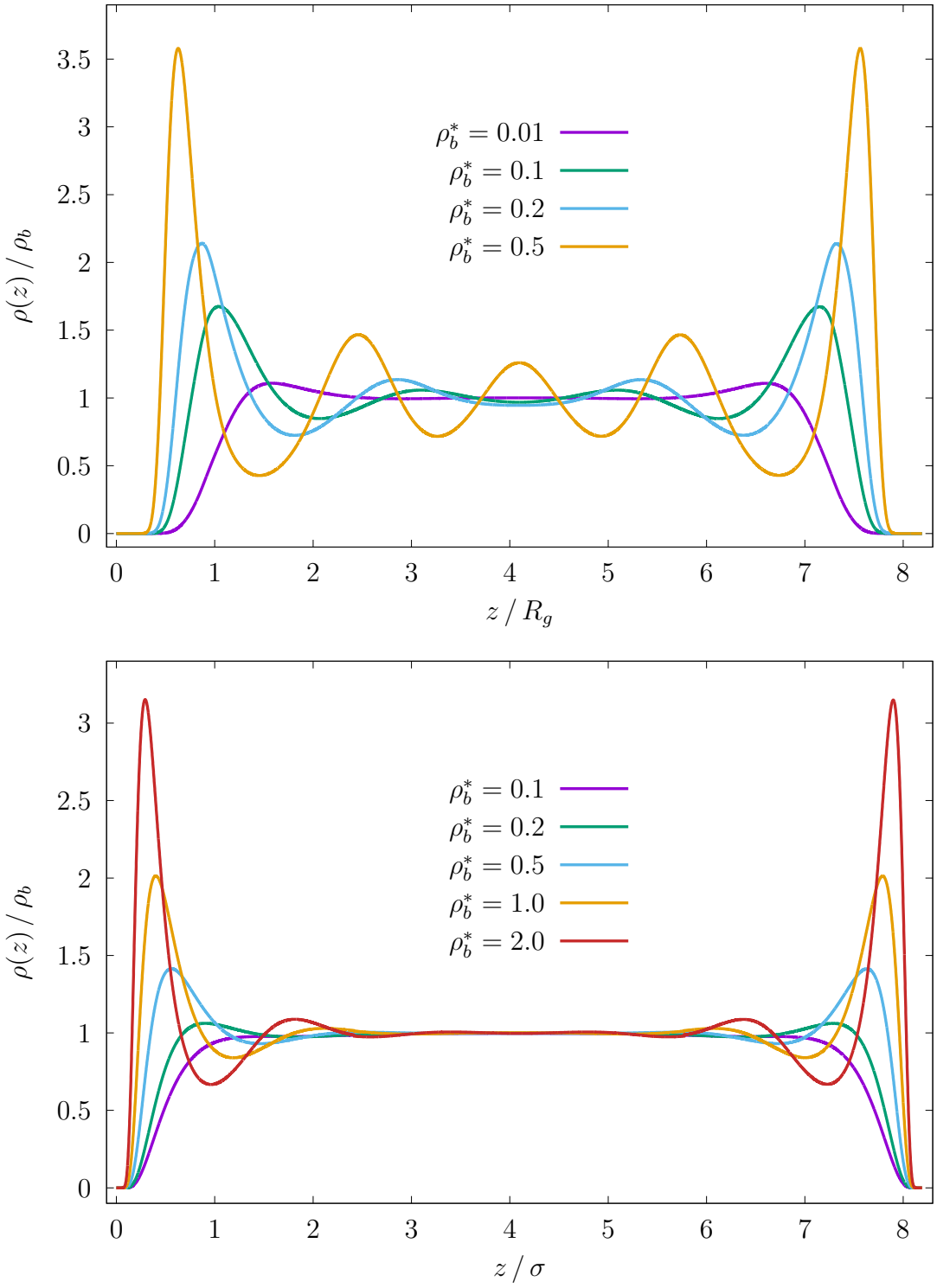

Figure 5.7: The inhomogeneous density profiles of the ring polymer solution (top) confined between two parallel hard walls separated by the fixed distance $d^* = 8.192$ compared to the linear polymer solution (bottom) calculated for increasing reduced bulk density ρ_b^*. As in the previous section, the density profiles that correspond to the ring polymers have an oscillatory shape.

Finally, we separate the bulk contribution ρ_b from the total density $\rho(z)$ by writing for $0 \leq z \leq d$:

$$\rho(z) = \rho_b + \Delta\rho(z). \tag{5.52}$$

As a result, the integral equation (5.51) can be recast in the following way:

$$\begin{aligned}\ln\left(1 + \Delta\rho(z)/\rho_b\right) = -\beta U_{\text{eff}}(z) - \beta U_{\text{eff}}(d-z) - \int_0^d dz'\, \Delta\rho(z')\beta\bar{u}\left(|z-z'|\right) + \\ + \rho_b \int_z^{+\infty} dz'\, \beta\bar{u}(|z'|) + \rho_b \int_{d-z}^{+\infty} dz'\, \beta\bar{u}(|z'|).\end{aligned} \tag{5.53}$$

Obviously, the only difference between the equation (5.53) and (5.35) is the appearance of the term $-\beta U_{\text{eff}}(d-z) + \rho_b \int_{d-z}^{+\infty} dz'\, \beta\bar{u}(|z'|)$ responsible for the interaction with the second wall located at $z = d$. Consequently, the equation (5.53) takes the form:

$$\Delta\rho(z) = G\left[\Delta\rho\right](z), \tag{5.54}$$

where G is a functional of $\Delta\rho$, which in this case becomes

$$\begin{aligned}G[\Delta\rho](z) = \rho_b \Bigg(\exp\Bigg[- \beta U_{\text{eff}}(z) - \beta U_{\text{eff}}(d-z) - \int_0^d dz'\, \Delta\rho(z')\beta\bar{u}\left(|z-z'|\right) + \\ + \rho_b \int_z^{+\infty} dz'\, \beta\bar{u}(|z'|) + \rho_b \int_{d-z}^{+\infty} dz'\, \beta\bar{u}(|z'|)\Bigg] - 1\Bigg).\end{aligned} \tag{5.55}$$

As explained in the previous section, the equation (5.53) can be solved numerically in a self-consistent manner. The only term that leads to difficulties is the convolution $\int_0^d dz'\, \Delta\rho(z')\beta\bar{u}\left(|z-z'|\right)$, which however can be computed efficiently in the Fourier space.

Consequently, Figure 5.7 contains the resulting density profiles of the ring polymer solution at various bulk densities ρ_b obtained for a fixed distance between the walls. As in the case of a single wall, for high enough ρ_b (or, equivalently, for small enough d) densities exhibit oscillatory behavior remaining still within the range of applicability of our effective potential. The corresponding density profiles of the linear polymer solution confined between two hard walls are provided at the bottom of Figure 5.7: as in the case of a single, hard wall, they are not oscillatory.

5.3.2 The Attard's superposition approximation

Another method of determining the inhomogeneous density profiles of a fluid confined between two hard walls is provided by the Attard's *superposition approximation* (SA) [61]. In the SA, the total density profiles generated by two walls are written as a product

$$\rho_2(z;\, d) \approx \rho_b\, g_1(z) g_1(d-z), \tag{5.56}$$

where d is the distance between the walls and ρ_b is the bulk density of the fluid. Furthermore, g_1 denotes the pair distribution function calculated in the case of just one hard wall and it is simply given by

$$g_1(z) = \rho_1(z) \,/\, \rho_b. \tag{5.57}$$

Obviously, this method will provide good results as long as $g_1(z)$ will not deviate much from unity for z approaching d. Such a behavior can be actually seen in Figure 5.8.

Lastly, it is worth mentioning that although this method yields only an approximate solution, it might be very useful in the case of complex geometries [62], where simple self-consistent equations cannot be formulated at all.

5.3.3 The depletion potential

Following the ideas developed in Chapter 2 and in particular the equation (2.37) , the depletion potential between two hard walls can be calculated as the difference in the excess grand potential of the system at finite and infinite separation between the walls [1, 63]:

$$V_{\text{dep}}(d, \mu, T) = \Omega^{(\text{ex})}(d, \mu, T) - \Omega^{(\text{ex})}(d \to \infty, \mu, T), \tag{5.58}$$

where $\Omega(d, \mu, T)$ can be calculated using the DFT methods applied in Subsection (5.3.1). More specifically, the grand potential functional (5.16) $\Omega_2(d)/A$ per unit area for the two wall case becomes

$$\begin{aligned} \beta\Omega_2\left([\rho];\, d\right)/A = &\int_0^d dz\, \rho(z) \left[\ln\left(\rho(z)\Lambda^3\right) - 1\right] - \left[\ln\left(\rho_b\Lambda^3\right) + \rho_b u_0\right] \int_0^d dz\, \rho(z) + \\ &+ \int_0^d dz\, \beta U_{\text{ext}}(z)\rho(z) + \frac{1}{2}\int_0^d dz\rho(z) \int_0^d dz'\, \rho(z')\beta\bar{u}(|z - z'|). \end{aligned} \tag{5.59}$$

By separating the bulk contribution from the total density (i.e., $\rho(z) = \rho_b + \Delta\rho(z)$), the grand potential functional (5.59) can be rewritten as follows:

$$\begin{aligned} \beta\Omega_2\left([\rho];\, d\right)/A = &\int_0^d dz\, \rho(z) \ln\left(\rho(z)/\rho_b\right) - (1 + \rho_b u_0) \int_0^d dz\, \Delta\rho(z) + \\ &+ \int_0^d dz\, \beta U_{\text{ext}}(z)\rho(z) + \rho_b \int_0^d dz \int_0^d dz'\, \Delta\rho(z')\beta\bar{u}(|z - z'|) + \\ &+ \frac{1}{2}\int_0^d dz \Delta\rho(z) \int_0^d dz'\, \Delta\rho(z')\beta\bar{u}(|z - z'|) - \\ &- \frac{\rho_b^2}{2}\int_0^d dz \left[\int_z^{+\infty} dz'\, \beta\bar{u}(|z'|) + \int_{d-z}^{+\infty} dz'\, \beta\bar{u}(|z'|)\right] + \beta\Omega_b\left(d\right)/A, \end{aligned} \tag{5.60}$$

where the last term $\Omega_b\left(d\right)$ corresponds to the grand potential contribution of the bulk given by

$$\beta\Omega_b\left(d\right)/A = -d \cdot \left(\rho_b + \frac{\rho_b^2 u_0}{2}\right). \tag{5.61}$$

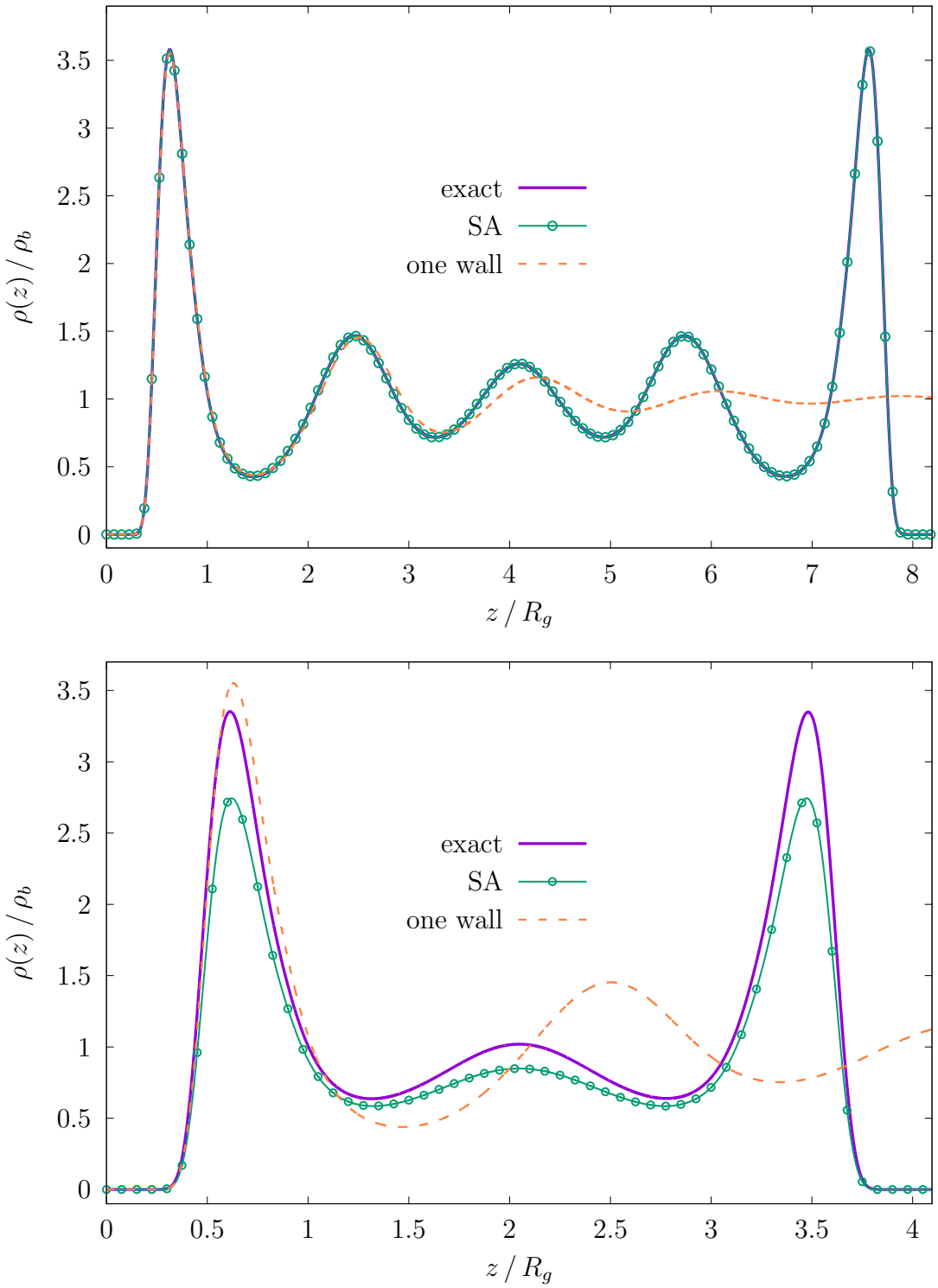

Figure 5.8: The inhomogeneous density profiles of the ring polymer solution confined between two parallel hard walls separated by the distances $d_1^* = 8.192$ (top) and $d_2^* = 4.096$ (bottom) calculated using the exact integral equation (5.53) and the SA (5.56) at the bulk density $\rho_b^* = 0.5$. Obviously, $\rho_{\mathrm{SA}}(z)$ deviates significantly from the exact solution in the figure at the bottom, since $g_1(z)$ does not approach unity for $z \to d$.

Therefore, the first term in the equation (5.58) becomes:

$$\Omega^{(\mathrm{ex})}(d, \mu, T) = \Omega_2\left([\rho];\, d\right) - \Omega_b\left(d\right). \tag{5.62}$$

Furthermore, in the limit $d \to \infty$ the excess grand potential $\Omega^{(\mathrm{ex})}(d \to \infty, \mu, T)$ reduces to the excess grand potential in the one hard wall case $\Omega_1^{(\mathrm{ex})}[\rho]$. which is given by the expression (5.48).

Figure 5.9 depicts the depletion potential between two hard walls immersed in the ring and linear polymer solution as a function of the bulk density ρ_b. As expected, even in the dilute regime the deletion potential in the ring polymer case preserves its oscillatory shape.

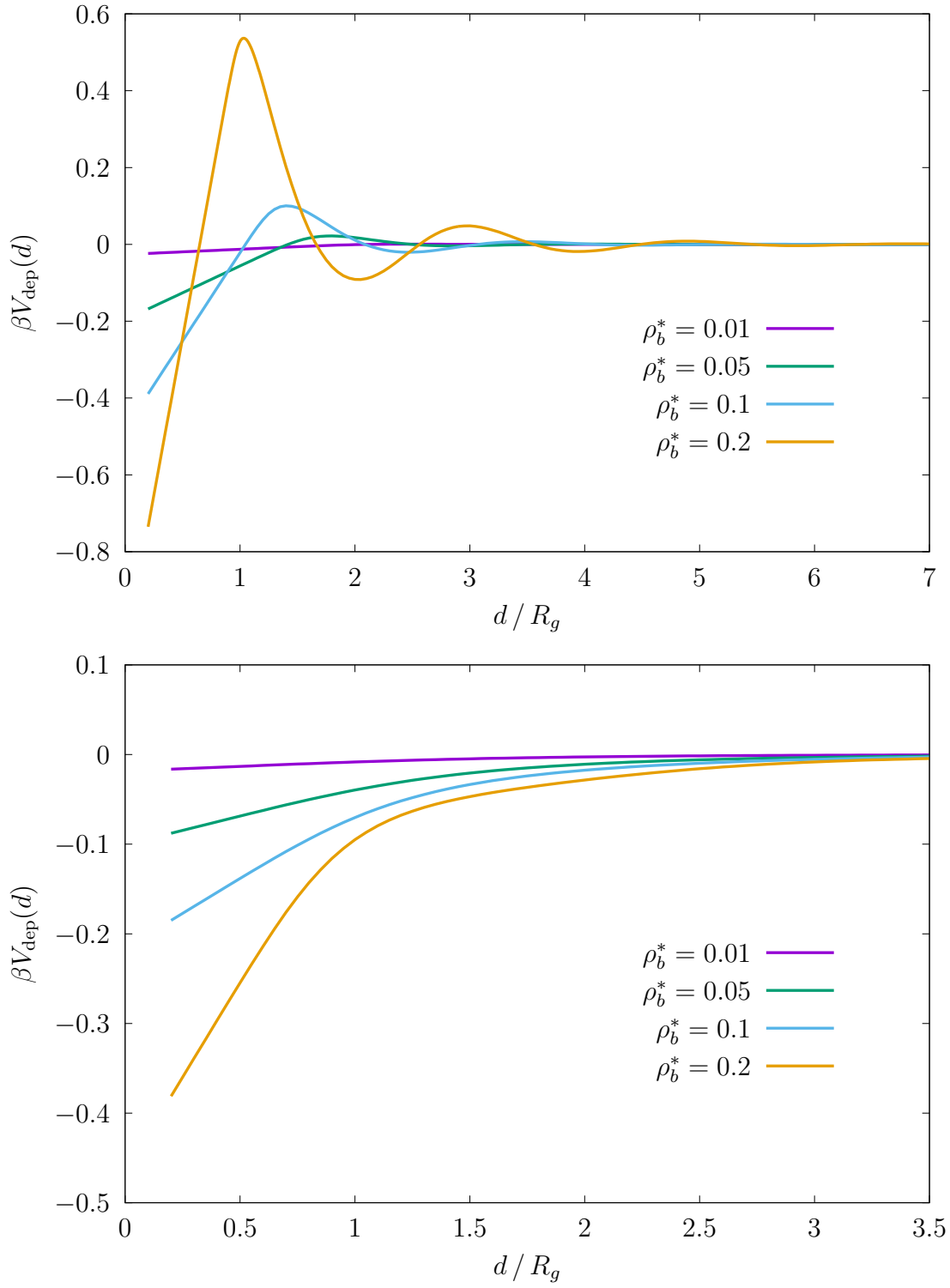

Figure 5.9: The depletion potential between two hard walls immersed in the ring (top) and linear (bottom) polymer solution for increasing reduced bulk density ρ_b^*. In the ring polymer case, the potential has an oscillatory form which intensifies with higher values of ρ_b^*.

Chapter 6

Discussion

In this thesis, we first obtained, by means of MC simulations, the effective interaction potential between the center of mass of a flexible, unknotted ring polymer and a hard wall 4.10. This effective potential was shown to attain a universal shape for relatively big rings with the polymerization degree $N > 200$. In contrast, in the linear polymer case, this effective interaction reaches the scaling regime already for $N > 100$ 4.11. Interestingly, energy of the rings in the presence of the hard wall not only considerably exceeds that of the linear chains, but also increases steeper with the shorter distance to it. For the ring polymers, we found an analytical form of the effective potential: close to the wall it behaves as a repulsive Yukawa potential, whereas for the distances greater than R_g it decays as a Gaussian 4.14. Finally, we tested the scaling behavior of the gyration radius of the polymers, and we found the Flory exponent ν very close to the numeric value 0.588 when employing a fitting model that accounts for the next-to-leading order corrections in N 4.8.

Next, we used the coarse-grained models of the ring and linear polymers to obtain their structure in solution with the help of the mean-field density functional theory. More specifically, we calculated the equilibrium density profiles for our effective fluids in contact with one and two planar, hard walls and used them to obtain the surface tension at the wall-liquid interface 5.6 and the depletion potential between two hard walls 5.9. As a result, the surface tension in the ring polymer case is approximately twice as large as for the linear chains. Moreover, the depletion potential for the rings, even within the range of applicability of the effective models, features an oscillatory form which intensifies with increasing bulk density of the fluid. This form of the depletion potential can be used to control the self-assembly process of crystals. Finally, we should stress that the oscillatory depletion interactions are not inherent in the linear polymer case.

Some interesting questions concerning ring polymer solutions remained beyond the

scope of this thesis, and they represent a possibility for the future work:

- ◇ it is interesting to calculate the depletion interaction between two spherical colloidal particles immersed in the ring polymer solution to find out whether it preserves the oscillatory shape, as in the case of two parallel, hard walls;
- ◇ it would be fascinating to investigate the effects of the ring polymer's topology on the form of the depletion interaction between the walls or the colloids. Probably, the knotted rings may develop even higher oscillations of the depletion potential because their interaction energy may in times exceed that of the unknotted rings.
- ◇ finally, the full monomer-resolved simulations would help to understand the depletion interaction even at higher densities of the solution, where the coarse-grained models deliver inaccurate results.

Acknowledgements

I would like to sincerely thank my supervisor, Professor Christos Likos, for giving me the opportunity to work on a fascinating and novel project and for all his permanent support, guidance and enlightening insights into soft matter physics. I am also deeply indebted to Emanuele Locatelli for teaching me all the peculiarities of molecular simulations and for his invaluable help and encouragement throughout this thesis. In addition, I would like to express my gratitude to the whole Computational Physics group for a friendly and open-minded working environment. Finally, I would like to thank my family and, especially, my wife Olesya for always believing in me.

Bibliography

[1] C. N. Likos. "Effective interactions in soft condensed matter physics." In: *Phys. Rep.* 348 (2001), pp. 267–439.

[2] R. Blaak et al. "Accurate coarse-grained potentials for soft matter systems." In: *Computational Trends in Solvation and Transport in Liquids - Lecture Notes*. Ed. by G. Sutmann et al. IAS. Forschungszentrum Jülich, 2015.

[3] M. D. Frank-Kamenetskii, A. V. Lukashin, and A. V. Vologodskii. "Statistical mechanics and topology of polymer chains." In: *Nature* 258 (1975), pp. 398–402.

[4] E. Orlandini and S. G. Whittington. "Statistical topology of closed curves: Some applications in polymer physics." In: *Rev. Mod. Phys.* 79 (2 2007), pp. 611–642.

[5] C. Micheletti, D. Marenduzzo, and E. Orlandini. "Polymers with spatial or topological constraints: theoretical and computational results." In: *Phys. Rep.* 504 (2011).

[6] A. Rosa. "Topological constraints and chromosome organization in eukaryotes: a physical point of view." In: *Biochem. Soc. Trans.* 41 (2013), p. 612.

[7] A. and Rosa. "Structure and dynamics of interphase chromosomes." In: *PLoS Comput. Biol.* 4 (2008), e1000153.

[8] M. Piwecka et al. "Loss of a mammalian circular RNA locus causes miRNA deregulation and affects brain function." In: *Science* (2017).

[9] A. Narros, A. J. Moreno, and Ch. N. Likos. "Architecture-induced size asymmetry and effective interactions of ring polymers: simulation and theory." In: *Macromolecules* 46.23 (2013), pp. 9437–9445.

[10] M. Bohn and D. W. Heermann. "Topological interactions between ring polymers: implications for chromatin loops." In: *J. Chem. Phys.* 132.4 (2010), p. 044904.

[11] A. Narros, A. J. Moreno, and C. N. Likos. "Influence of topology on effective potentials: coarse-graining ring polymers." In: *Soft Matter* 6 (11 2010), pp. 2435–2441.

[12] A. Narros, A. J Moreno, and C. N. Likos. *Effective interactions of knotted ring polymers*. 2013.

[13] S. S. Jang, T. Çağin, and W. A. Goddard III. "Effect of cyclic chain architecture on properties of dilute solutions of polyethylene from molecular dynamics simulations." In: *J. Chem. Phys.* 119.3 (2003), pp. 1843–1854.

[14] A. Narros, A. J. Moreno, and C. N. Likos. "Effects of knots on ring polymers in solvents of varying quality." In: *Macromolecules* 46.9 (2013), pp. 3654–3668.

[15] M. Kapnistos et al. "Unexpected power-law stress relaxation of entangled ring polymers." In: *Nature materials* 7.12 (2008), p. 997.

[16] P.-G. De Gennes. *Scaling concepts in polymer physics*. Cornell university press, 1979.

[17] M. Dijkstra, R. van Roij, and R. Evans. "Phase diagram of highly asymmetric binary hard-sphere mixtures." In: *Phys. Rev. E* 59 (1999), pp. 5744–5771.

[18] R. K. Pathria and Paul D. Beale. *Statistical mechanics*. 3rd ed. Elsevier, 2011, pp. 306–307.

[19] M. Dijkstra, R. van Roij, and R. Evans. "Phase behaviour and structure of model colloid–polymer mixtures." In: *J. Phys. Condens. Matter* 11 (1999), p. 10079.

[20] S. Asakura and F. Oosawa. "Interaction between particles suspended in solutions of macromolecules." In: *J. Polym. Sci.* 33 (1958), pp. 183–192.

[21] G. S. Grest, K. Kremer, and T. A. Witten. "Structure of many arm star polymers: a molecular dynamics simulation." In: *Macromolecules* 20.6 (1987), pp. 1376–1383.

[22] D. Chandler. *Introduction to modern statistical mechanics*. Oxford University Press, 1987, pp. 200–202.

[23] A. A. Louis et al. "Can polymer coils be modeled as "soft colloids"?" In: *Phys. Rev. Lett.* 85 (12 Sept. 2000), pp. 2522–2525.

[24] J.-P. Hansen and I. R. McDonald. *Theory of simple liquids*. Elsevier, 1990, p. 59.

[25] A. A. Louis, P. G. Bolhuis, and J. P. Hansen. "Mean-field fluid behavior of the Gaussian core model." In: *Phys. Rev. E* 62 (2000), pp. 7961–7972.

[26] A. J. Archer and R. Evans. "Wetting in the binary Gaussian core model." In: *J. Phys. Condens. Matter* 14.6 (2002), p. 1131.

[27] A. Jusufi et al. "Effective interactions between star polymers and colloidal particles." In: *J. Phys. Condens. Matter* 13.28 (2001), p. 6177.

[28] M Daoud and J. P. Cotton. "Star shaped polymers: a model for the conformation and its concentration dependence." In: *Journal de Physique* 43.3 (1982), pp. 531–538.

[29] O. F. Olaj, W. Lantschbauer, and K. H. Pelinka. "Dimension and shape of model chains as a function of their intermolecular separation." In: *Macromolecules* 13.2 (1980), pp. 299–302.

[30] V. Krakoviack, J.-P. Hansen, and A. A. Louis. "Influence of solvent quality on effective pair potentials between polymers in solution." In: *Phys. Rev. E* 67 (4 Apr. 2003), p. 041801.

[31] P. G. Bolhuis et al. "Accurate effective pair potentials for polymer solutions." In: *J. Chem. Phys.* 114.9 (2001), pp. 4296–4311.

[32] B. Kruger, L. Schäfer, and A. Baumgärtner. "Correlations among interpenetrating polymer coils: the probing of a fractal." In: *Journal de Physique* 50.21 (1989), pp. 3191–3222.

[33] A. Narros et al. "Multi-blob coarse graining for ring polymer solutions." In: *Soft Matter* 10 (48 2014), pp. 9601–9614.

[34] C. N. Likos et al. "Why do ultrasoft repulsive particles cluster and crystallize? Analytical results from density functional theory." In: *J. Chem. Phys.* 126.22 (2007), p. 224502.

[35] M. Bernabei et al. "Fluids of semiflexible ring polymers: effective potentials and clustering." In: *Soft Matter* 9 (4 2013), pp. 1287–1300.

[36] M.Z. Slimani et al. "Cluster glasses of semiflexible ring polymers." In: *ACS Macro Lett.* 3.7 (2014), pp. 611–616.

[37] P. Poier et al. "An anisotropic effective Model for the simulation of semiflexible ring polymers." In: *Macromolecules* 48.14 (2015), pp. 4983–4997.

[38] R. H. Colby and M. Rubinstein. *Polymer physics*. Oxford University Press, 2003, p. 101.

[39] G. S. Grest and K. Kremer. "Molecular dynamics simulation for polymers in the presence of a heat bath." In: *Phys. Rev. A* 33 (5 1986), pp. 3628–3631.

[40] J. O'Rourke. *Computational geometry in C*. Cambridge University Press, 1998, pp. 226–238.

[41] D. Sunday. *Intersections of rays and triangles*. URL: `http://geomalgorithms.com/a06-_intersect-2.html`.

[42] N. Metropolis and S. Ulam. "The Monte Carlo method." In: *JASA* 44.247 (1949), pp. 335–341.

[43] G. M. Torrie and J. P. Valleau. "Nonphysical sampling distributions in Monte Carlo free-energy estimation: Umbrella sampling." In: *J. Comp. Phys.* 23 (1977), pp. 187–199.

[44] B. M. Mladek, G. Kahl, and C. N. Likos. "Computer assembly of cluster-forming amphiphilic dendrimers." In: *Phys. Rev. Lett.* 100 (2 2008), p. 028301.

[45] C. N Likos et al. "Why do ultrasoft repulsive particles cluster and crystallize? Analytical results from density-functional theory." In: *J. Chem. Phys.* 126.22 (2007), p. 224502.

[46] P. Poier et al. "Concentration-induced planar-to-homeotropic anchoring transition of stiff ring polymers on hard walls." In: *Soft Matter* 12 (38 2016), pp. 7983–7994.

[47] R. Kubo. "The fluctuation-dissipation theorem." In: *Rep. Prog. Phys.* 29.1 (1966), p. 255.

[48] L. Verlet. "Computer "experiments" on classical fluids. I. Thermodynamical properties of Lennard-Jones molecules." In: *Phys. Rev.* 159 (1 1967), pp. 98–103.

[49] B. Widom. "Some topics in the theory of fluids." In: *J. Chem. Phys.* 39.11 (1963), pp. 2808–2812.

[50] R. Guida and J. Zinn-Justin. "Critical exponents of the N -vector model." In: *J. Phys. A* 31.40 (1998), p. 8103.

[51] B. Li, N. Madras, and A. D. Sokal. "Critical exponents, hyperscaling, and universal amplitude ratios for two- and three-dimensional self-avoiding walks." In: *J. Stat. Phys.* 80.3 (1995), pp. 661–754.

[52] J.-P. Hansen and L. Verlet. "Phase transitions of the Lennard-Jones system." In: *Phys. Rev.* 184 (1 Aug. 1969), pp. 151–161. DOI: 10.1103/PhysRev.184.151.

[53] J.-P. Hansen and D. Schiff. "Influence of interatomic repulsion on the structure of liquids at melting." In: *Mol. Phys.* 25.6 (1973), pp. 1281–1290.

[54] C.N. Likos et al. "Criterion for determining clustering versus reentrant melting behavior for bounded interaction potentials." In: *Phys. Rev. E* 63.3 (2001), p. 031206.

[55] A. J. Archer, C. N. Likos, and R. Evans. "Soft-core binary fluid exhibiting a λ-line and freezing to a highly delocalized crystal." In: *J. Phys. Condens. Matter* 16.23 (2004), p. L297.

[56] P. Hohenberg and W. Kohn. "Inhomogeneous electron gas." In: *Phys. Rev.* 136 (1964), B864–B871.

[57] W. Kohn and L. Sham. "Self-consistent equations including exchange and correlation effects." In: *Phys. Rev.* 140 (1965), A1133–A1138.

[58] R. Evans. "The nature of the liquid-vapour interface and other topics in the statistical mechanics of non-uniform, classical fluids." In: *Adv. Phys.* 28.2 (1979), pp. 143–200.

[59] C. N Likos. "Colloidal interactions: From effective potentials to structure." In: *Physics of Complex Colloids* 184 (2013), p. 1.

[60] A. Lang et al. "Fluid and solid phases of the Gaussian core model." In: *J. Phys. Condens. Matter* 12.24 (2000), p. 5087.

[61] P. Attard. "Spherically inhomogeneous fluids. II. Hard-sphere solute in a hard-sphere solvent." In: *J. Chem. Phys.* 91.5 (1989), pp. 3083–3089.

[62] J. Dzubiella, C. N. Likos, and H. Löwen. "Phase behavior and structure of star-polymer–colloid mixtures." In: *J. Chem. Phys.* 116.21 (2002), pp. 9518–9530.

[63] R. Roth, R. Evans, and S. Dietrich. "Depletion potential in hard-sphere mixtures: theory and applications." In: *Phys. Rev. E* 62.4 (2000), p. 5360.